EPRI-NP--1709

DE83 900534

Reactor-Transient Tests at ANO-2

EPRI NP-1709
Research Project 1385-1

Final Report, October 1982

Prepared by

COMBUSTION ENGINEERING, INC.
C-E Power Systems
1000 Prospect Hill Road
Windsor, Connecticut 06095

Principal Investigators
M. L. Kantrowitz
J. P. Thompson

Prepared for

Electric Power Research Institute
3412 Hillview Avenue
Palo Alto, California 94304

EPRI Project Managers
J. A. Naser
R. N. Whitesel

Analysis and Testing Program
Nuclear Power Division

ORDERING INFORMATION

Requests for copies of this report should be directed to Research Reports Center (RRC), Box 50490, Palo Alto, CA 94303, (415) 965-4081. There is no charge for reports requested by EPRI member utilities and affiliates, contributing nonmembers, U.S. utility associations, U.S. government agencies (federal, state, and local), media, and foreign organizations with which EPRI has an information exchange agreement. On request, RRC will send a catalog of EPRI reports.

Prepared by
Combustion Engineering, Inc.
Windsor, Connecticut

EPRI PERSPECTIVE

PROJECT DESCRIPTION

This report, together with two companion reports, documents a series of tests run at Arkansas Nuclear One, Unit-2 (ANO-2). The companion reports are EPRI Final Reports NP-1707, NSSS Design and Cycle 1 Operating History Data for Arkansas Nuclear One, Unit-2, and NP-1708, NSSS Transient Tests at ANO-2. These transient tests consisted of (1) complete loss of forced circulation from an operating level near 80% of rated power, (2) drops of part-length and full-length control element assemblies from operating power levels near 50% of rated power, and (3) a turbine trip from an operating power level near 100% of rated power.

PROJECT OBJECTIVE

The objective of these transient tests conducted under RP1385-1 was to gather high-quality data from an operating nuclear power plant for use in qualifying reactor system transient analysis computer codes such as RETRAN and MEKIN. Since ANO-2 is a PWR, these tests are complementary to the turbine trip and plant stability tests performed at the Peach Bottom-2 BWR in 1977 and 1978 (EPRI Topical Reports NP-563 and NP-564 and EPRI Final Reports NP-971 and NP-972). The purpose of these activities was to provide a basis for increased confidence in the ability of RETRAN, MEKIN, and other industry computer codes to predict the course of various operating transients.

PROJECT RESULTS

In addition to these three reports, the data from each of the four tests have been organized in files on magnetic tape. This information will be useful for utility engineers who wish to model the ANO-2 system and to test the ability of some particular transient analysis computer code to predict the measured data.

Joseph A. Naser, Project Manager
Robert N. Whitesel, Project Manager
Nuclear Power Division

ABSTRACT

This report documents experimental data generated from a series of reactor transient tests performed at Arkansas Nuclear One - Unit 2 (ANO-2) during December 1979 and January 1980. Four tests were conducted: complete loss of forced primary coolant flow, full-length control element assembly (CEA) drop, part-length CEA drop and turbine trip. These tests are part of a program to obtain plant transient test data which will be used for simulation code qualification. Two companion reports, "ANO-2 Design and Cycle One Operating History Data" and "NSSS Transient Tests at ANO-2", provide plant design data and NSSS test data which may be used in conjunction with this report.

CONTENTS

CONTENTS (Cont.)

ILLUSTRATIONS

ILLUSTRATIONS (Cont.)

ILLUSTRATIONS (Cont.)

ILLUSTRATIONS (Cont.)

TABLES

SUMMARY

Four transient tests were conducted at Arkansas Nuclear One - Unit 2 (ANO-2) as part of the initial power ascension test program. The tests were (1) a complete loss of forced primary coolant flow, (2) a full-length CEA drop (FLCEAD), (3) a part-length CEA drop (PLCEAD) and (4) a turbine trip. The principal objective in performing these tests is to add to the data base used by the electric power industry for the qualification of computer codes which are used in the design and safety analysis of Pressurized Water Reactors (PWRs). In addition, an evaluation of the feasibility of using rhodium self-powered neutron detectors in plant tests designed for qualification of space-time core models was performed. The tests chosen represent a range of typical but diverse transients, so that code qualification may be made in a more comprehensive manner than was possible with previously available data.

Raw signal data from rhodium self-powered neutron detectors, background detectors and CEA position indicators were recorded on magnetic tape at the plant site for three of the four tests (all except the turbine trip). Self-powered neutron detector, background detector and CEA position indicator signals were not recorded for the turbine trip since the core response to a turbine trip is very similar to that following a loss of flow.

The tape-recorded data were reproduced and digitized by a PDP-11/15 minicomputer system and stored on disk as discrete numerical sequences. The stored data were then processed by a FORTRAN program to obtain graphic time histories of the local neutron flux and CEA positions during each of the three transients.

The data provided in this report establish a comprehensive data base of integral reactor test data which can be used for the qualification of space-dependent reactor kinetics simulation codes. In addition, the analytical studies and experimental data provided demonstrate the feasibility of using dynamically-compensated rhodium detector signals to discern small variations in the time-dependent behavior of the local neutron flux, thus establishing rhodium self-powered neutron detectors as a useful tool in obtaining in-core data for the qualification of space-time core models.

Section 1

INTRODUCTION

OBJECTIVES

This report documents the results of a series of reactor transient tests performed at Arkansas Nuclear One - Unit 2 (ANO-2) during December, 1979 and January, 1980. The objective of these tests is to add to the data base used by the electric power industry for qualifying computer codes which are used in the design and safety analysis of Pressurized Water Reactors. The tests chosen represent a range of typical but diverse reactor transients, so that code qualification may be made in a more comprehensive manner than was possible with previously available data.

The results presented in this report are in-core detector data from the reactor transient tests. Plant design data and nuclear steam supply system (NSSS) data from the tests are provided in two companion reports (1) - (2).

BACKGROUND

The process of designing a nuclear reactor includes the use of simulation codes to evaluate reactor behavior during design basis events. The design basis events include a broad range of transients, ranging from anticipated transients to highly unlikely events (referred to as postulated accidents). The acceptability of a design is judged by comparing the predicted reactor behavior to acceptance criteria. Acceptance criteria are limits on calculated parameters, such as the departure from nucleate boiling ratio, energy deposition in the fuel and maximum clad surface temperature. The acceptance criteria are set so as to provide a high degree of confidence that unacceptable consequences will not result from the relevant design basis event when these limits are met.

To meet the requirements of the design process, reactor simulation codes must accurately represent the neutronic and thermal-hydraulic phenomena associated with reactor transients. These requirements have led to the development of space-time reactor kinetics codes such as MEKIN (3) and HERMITE (4).

Simulation code qualification is important to verify and/or reduce calculative uncertainties or biases in predicated parameters in the simulation codes and to meet regulatory requirements. Separate effects tests, such as static power distribution measurements and reactivity measurements, are necessary parts of code qualification. However, a complete qualification process requires integral tests. The data provided herein extend the existing base of integral test data that may be used for comparison with space-time neutronics codes for the purpose of code qualification.

The neutron flux transients presented in this report have been measured with in-core rhodium self-powered neutron detectors. At this time, the measurement of fast transients with rhodium detectors is still in the developmental stage. This is due to the fact that some aspects of the response characteristics of rhodium detectors are not yet completely understood. Since the dominant part of the rhodium detector signal is delayed, the raw detector signal must be dynamically compensated to reconstruct the real-time neutron flux transient. (The dynamic compensation process is discussed in the Appendix). The coefficients used in the dynamic compensation procedure are calculated from the parameters used to model the rhodium detector response. These parameters in turn depend on knowledge of the rhodium detector response characteristics. Therefore, the uncertainty in the neutron flux transient as derived from measured rhodium detector signals is determined for the most part by uncertainties in the rhodium detector response characteristics.

The neutron flux transients presented in this report are constructed from the measured rhodium detector signals using best-estimate values of rhodium detector model parameters obtained from test reactor data and the data taken at ANO-2. The uncertainities associated with these parameters result in uncertainties in the neutron flux transients which are larger than the 2-3 percent typically desired for code qualification. However, these uncertainties are, for the most part, not so large as to preclude meaningful comparison with calculations made using space-time neutronics codes. Further discussion of experimental uncertainties are presented in Sections 2 and 5.

TEST PLAN

Four transient tests were conducted at ANO-2 as a part of the initial power ascension test program. The three tests for which in-core detector data were recorded were: (1) a complete loss of forced primary coolant flow (LOF), (2) a full-length control element assembly (CEA) drop (FLCEAD) and (3) a part-length CEA drop (PLCEAD). This combination of tests provides a diverse set of reactor transient conditions suitable for simulation code qualification.

The LOF was initiated from approximately 80 percent power by simultaneously tripping all four reactor coolant pumps. The test is aimed at measuring the neutron flux transient at various locations in the core. The test is principally a measure of how rapidly the local reactor power decreases during a scram. Precise measurement and simulation of the LOF is important since this transient is a design basis event which causes a significant power cooling mismatch and may approach the acceptance criterion on the departure from nucleate boiling ratio.

The FLCEAD and PLCEAD were initiated from approximately 50 percent power by opening the disconnect circuit breaker providing power to the appropriate control element drive mechanism. These tests are aimed at measuring the detailed neutron flux transient and associated power distribution distortions resulting from a single CEA drop. Precise measurement and simulation of these transients is important since CEA drops are anticipated operational occurrences in PWRs and may cause power density changes which approach acceptance criteria. The FLCEAD and PLCEAD differ in that the part-length CEA is a lower-worth CEA which induces significant axial power distortions in addition to radial power distortions.

In-core detector and CEA position signals were recorded on magnetic tape. The in-core detector signals were recorded using a Honeywell Model 5600 tape recorder with servo tape speed control to minimize time base uncertainties. The CEA position signals were recorded using a Honeywell Model 101 tape recorder. Specially-designed low-pass Bessel filters were employed to condition the in-core detector signals.

Section 2

PRE-TEST PREPARATIONS

TEST EQUIPMENT

All in-core data taken at the ANO-2 site were recorded on two 14-track analog tape recorders. One was used to record CEA position indicator signals; the other recorded in-core self-powered neutron detector (SPND) signals and background detector signals.

In-Core Detector System

The fixed in-core detector system in the ANO-2 reactor is comprised of 44 detector assemblies located within the core as shown in Figure 2-1. Each assembly is composed of 5 SPNDs, each 40 centimeters in active length, with centers located at 10, 30, 50, 70, and 90 percent of the active core height, respectively, as shown in Figure 2-2. The axial position nearest the bottom of the core is referred to as level 1; that nearest the top of the core is referred to as level 5. In addition, 12 of the 44 detector assemblies contain background detectors, with core locations also shown in Figure 2-1. At each of these radial positions, there are 2 background detectors, with cable lengths corresponding to those of the level 1 and level 4 rhodium detectors. These are referred to as the long and short background detectors, respectively.

SPND Recording

The SPND and background detector signals were recorded with a Frequency-Modulated (FM) multiplex system. This system records 5 channels of data on a single track of the tape recorder. Each of the 5 signals is frequency-modulated at 5 different center frequencies (16, 24, 32, 40, and 48 KHz). Each channel has a deviation of $\pm$ 2 KHz. The 5 frequency-modulated signals and a 60 KHz reference oscillator signal are electrically summed and recorded on a single tape track in the "direct" record mode. At a tape speed of 15 inches per second (ips) the analog tape has a "direct" bandwidth of 75 KHz. Eight of the 14 tracks were allocated to the multiplex format. Five channels were on each of 7 tracks and 4 channels were on the eighth track for a total of 39 multiplexed channels.

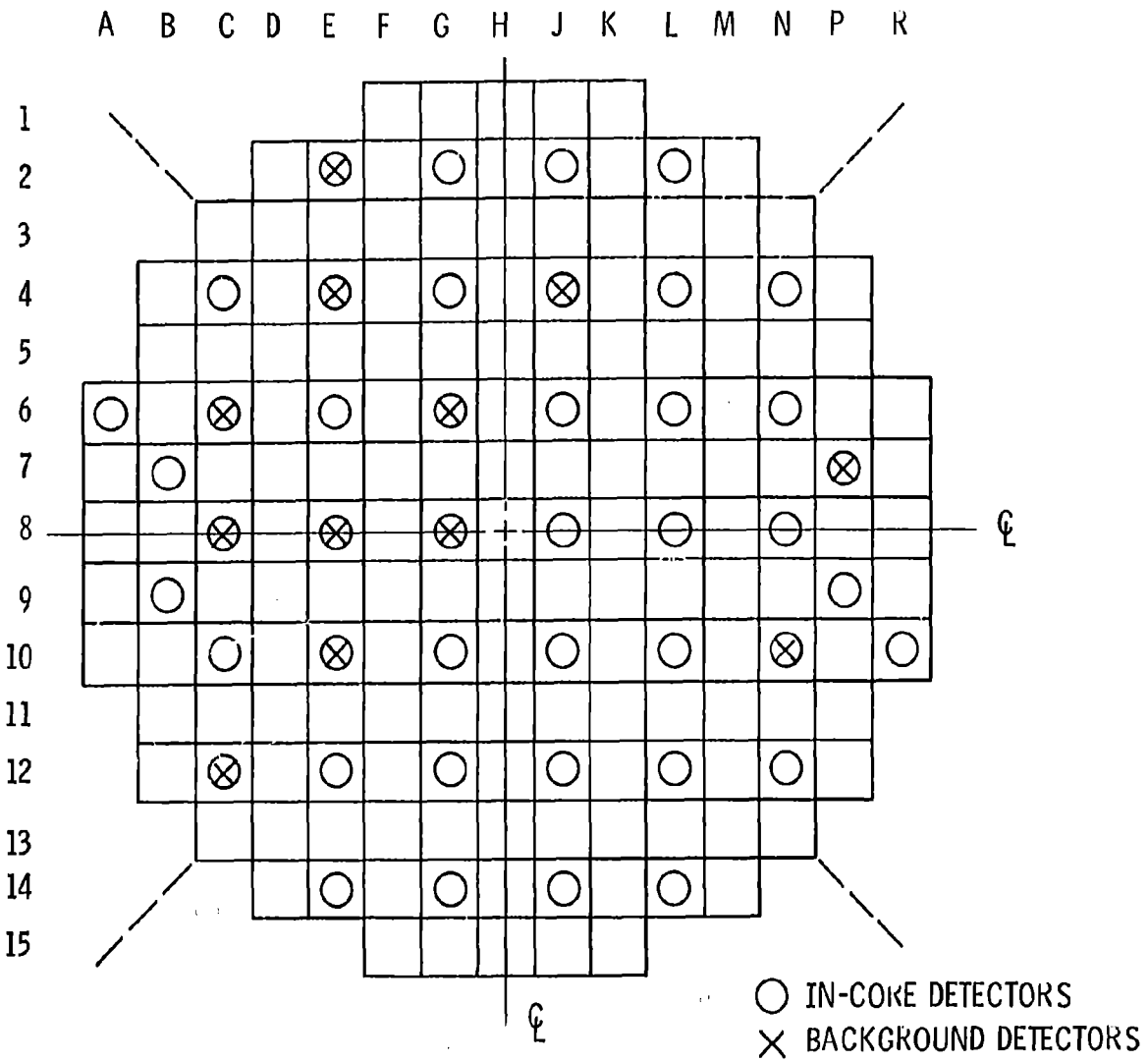

Figure 2-1. In-Core Detector Locations

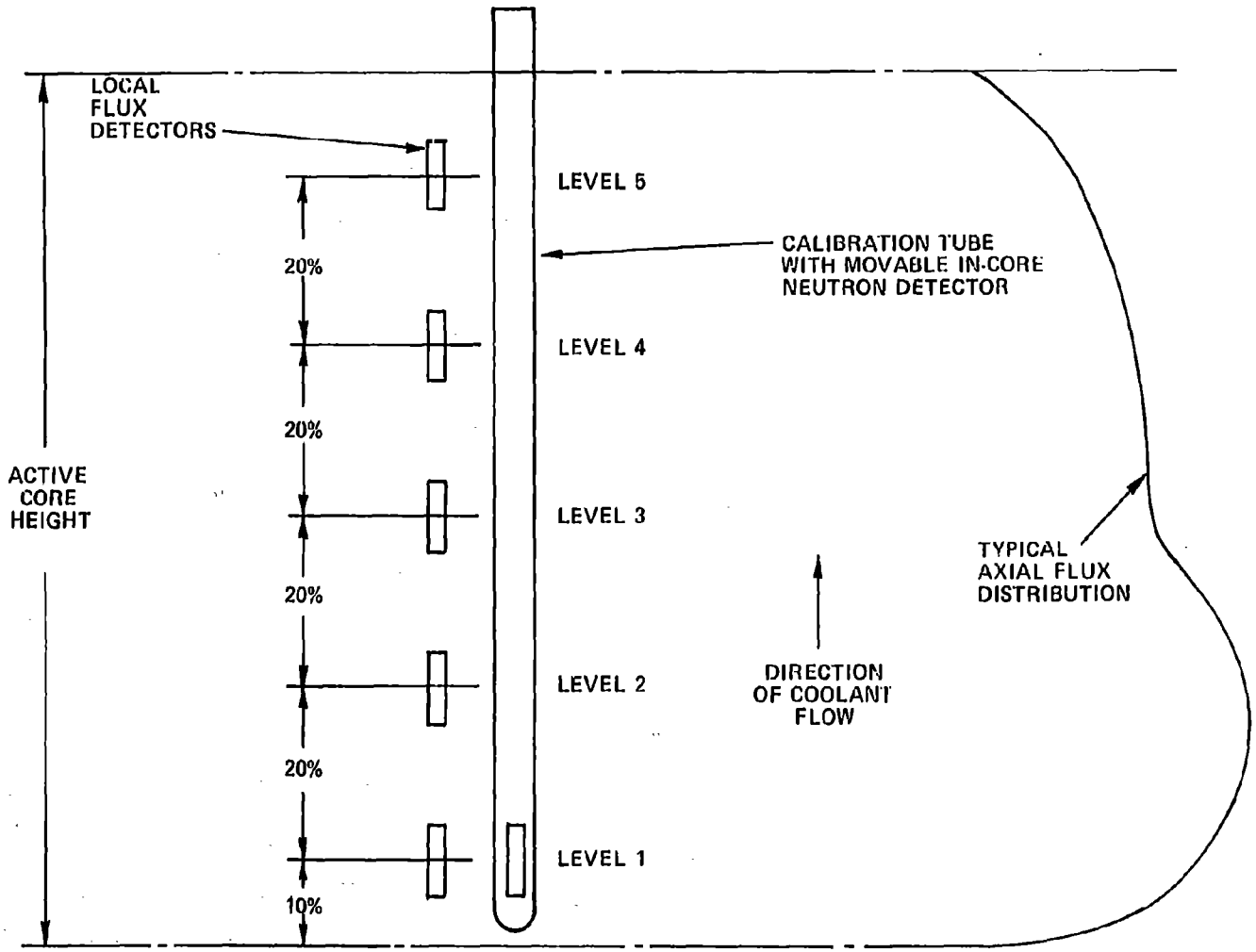

Figure 2-2. In-Core Detector Axial Arrangement

Timing and Synchronization

Three tracks of the analog tape were used for timing and synchronization purposes. A 50 KHz "tape servo" oscillator signal generated by the tape recorder was recorded on one track. This signal was produced by the tape recorder capstan drive and provided a very accurate time base when used to reproduce the data. The accuracy of this time base was determined to be better than 0.1 percent.

A bindary coded decimal (BCD) time-of-day clock was used to generate a serial digital code.

The final data track used recorded a "common timing" signal. This signal was generated by a PDP-11/04 minicomputer located in the control room. It generated a pulse train with a frequency equal to the rate at which it sampled data. This rate was increased just prior to the initiation of each transient. The increase in rate was used as a means for synchronizing data acquired by the PDP-11 and the analog tape recorders. The signal was recorded on one track in the FM mode. At a tape speed of 15 ips, the recorder frequency response in the FM mode is flat to within $\pm$ 1 db over the range 0 to 5 KHz.

A voice annotation was recorded on an edge track. It provides a commentary on the sequence of events as observed by the tape recorder operator.

Signal Conditioning

The SPND and background detector signals were obtained from test points on the printed circuit boards within the in-core detector bin assemblies. The assembly bin provides the signal conditioning for all in-core instrumentation (ICI). The ICI bin assembly has a current-to-voltage converter and low-pass filter for each SPND to condition the signals prior to going to the plant computer or any other monitoring device.

The low-pass filter in the ICI bin has a cut-off frequency o about 1 Hz. Previous feasibility studies had shown this value to be too low for the purposes of these transient tests. Since some filtering was necessary to reduce 60 Hz power line noise, special low-pass Bessel filters were constructed for each SPND and background signal recorded. Each filter has 4 poles at approximately 10 Hz. The amplitude and phase characteristics of each filter were carefully tested to ensure proper time correlation of all channels.

The test points on the ICI printed circuit board provided a signal upstream of the plant 1 Hz low-pass filter. This unfiltered signal was connected to the 10 Hz low-pass filter input. The output of the filter was routed to the FM multiplex system for recording. Figures 2-3 (a) and (b) show a block diagram of the reactor transients recording system.

CEA Position Recording

CEA position signals were recorded on the second 14-track tape recorder in FM mode. The "common timing" signal was also input to this recorder.

RHODIUM NEUTRON DETECTOR FEASIBILITY STUDY

The first part of this program consisted of a study to evaluate the feasibility of using rhodium self-powered neutron detectors in transient tests designed for qualification of space-time core models. The evaluation was based on a review of public literature and analyses of simulated detector response experiments and existing test reactor data. The results of these analyses demonstrated that small variations in a neutron flux transient produce measurable differences in the corresponding rhodium detector signal over the time range of interest. In addition, it was demonstrated that uncertainties in the measurement of a neutron flux transient using rhodium detectors, arising from signal noise, errors due to dynamic compensation and errors introduced by numerical methods, can be maintained at acceptable levels. Therefore, it was concluded that rhodium detectors will be able to provide meaningful data that may be compared with calculations made using space-time neutronics codes.

Public Literature

A number of other investigations have endeavored to use self-powered detectors for transient flux measurements and/or studies of the reactions which give rise to the SPND signal [(5) - (6)]. The current-generating reactions which occur in a rhodium detector under the influence of a neutron flux are discussed in the Appendix. Of the three major rhodium detector signal components, the two Rh-104 decay schemes are well understood; that is, the half-lives of Rh-104 decay are well known. However, the relative magnitude of neutron absorption and inelastic neutron scattering resulting in a prompt rhodium detector signal component is not known precisely.

Values reported for the magnitude of the prompt component of the rhodium detector signal range from 4 to 8.4 percent. These variations are due to differences in test conditions, such as neutron spectrum variations between test reactors and heavy-water power reactors, as well as variations in the detector sensitivity. Based on the

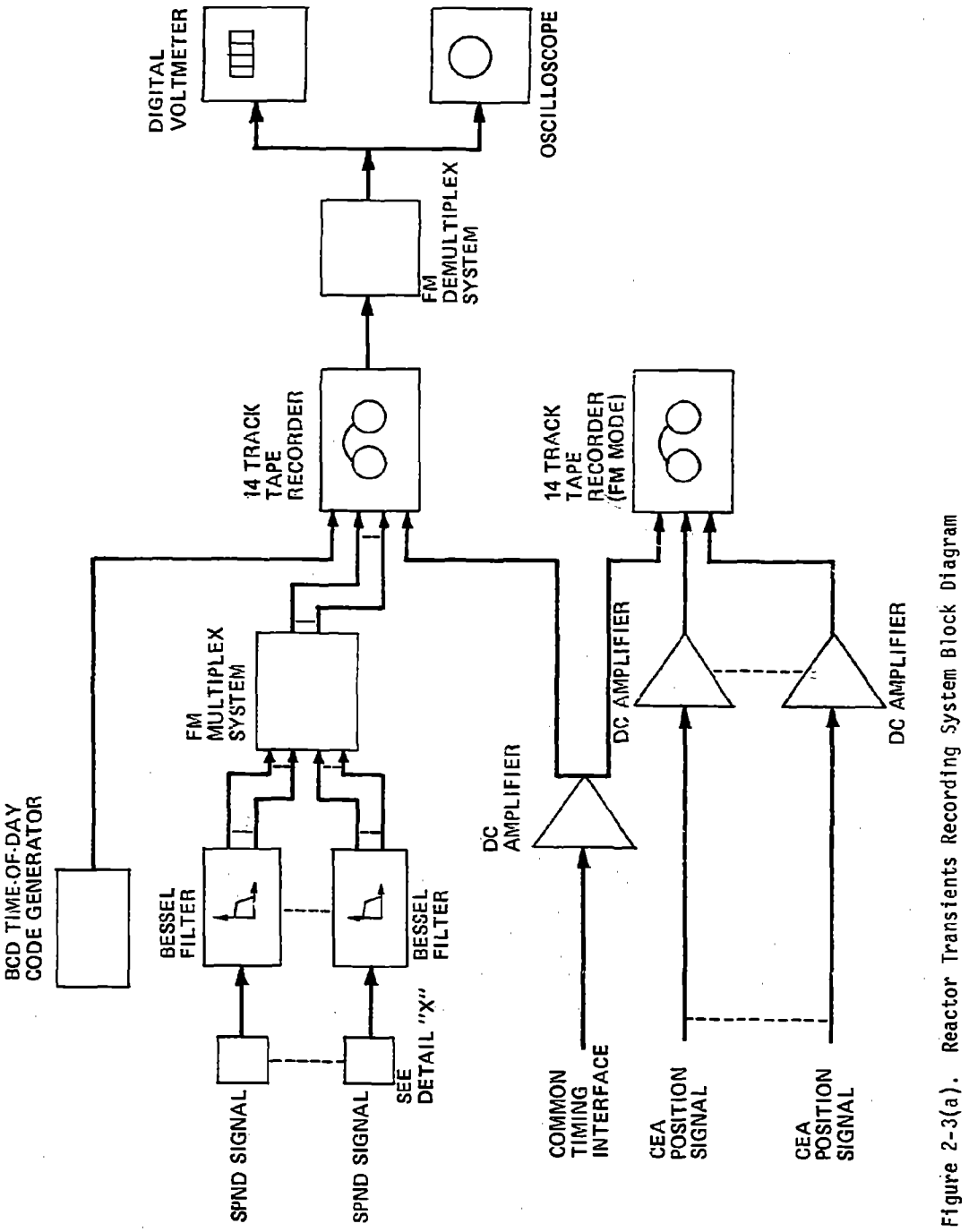

Figure 2-3(a). Reactor Transients Recording System Block Diagram

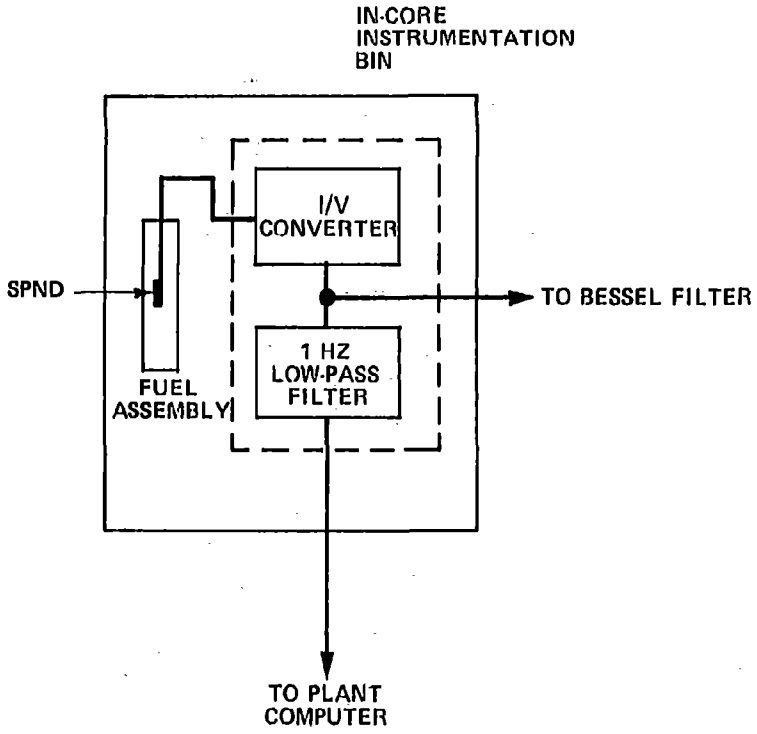

Figure 2-3(b). Detail X of Reactor Transients Recording System Block Diagram

information contained in References (4) and (5) the prompt component can be estimated to be 6 ±2 percent of the total signal. This degree of precision is inadequate to meet the measurement uncertainty objectives of this program. Therefore, additional work, discussed in the Appendix, was performed to obtain a better estimate of the prompt component.

Simulated Detector Response Experiments

A set of simulated detector response experiments was performed to demonstrate the ability of rhodium detectors to measure small variations in a neutron flux transient and to evaluate the magnitude of measurement uncertainties. The methodology used in the simulated experiments is presented as a flow chart in Figure 2-4. First, the flux transient for a Loss of Primary Coolant Flow event was computed using a one-dimensional HERMITE (4) model for a typical C-E reactor. The flow reduction was initiated at zero seconds and the CEAs began to drop at approximately one second. The simulated flux transients at planes centered about the highest detector level and lowest detector level were taken as representative of the type of transients which should occur during the ANO-2 tests. (The simulated flux transient are not, however, meant to represent the actual transients which occurred during the tests). Figures 2-5 and 2-6 show the flux transients for the upper and lower detector levels, respectively. Using a mathematical model of the detector (described in the Appendix) and assuming prompt components of 4, 5, 6, 7 and 8 percent, simulated detector signals are computed from the flux transients. The simulated detectors signals were then dynamically compensated in the same manner as would be done for the measured detector signals using a prompt component value of 6 percent.

Comparison of the simulated input flux transient and the compensated simulated detector signal was then made to obtain an estimate of the measurement uncertainty due to signal processing (dynamic compensation, signal noise, numerical methods).

Small Changes in Flux Transients

The capability of rhodium detectors to measure small variations during a flux transient was demonstrated by comparing (1) the simulated detector signal transient in the upper detector for 10 percent variations in the simulated input flux transient (Figure 2-7), and (2) the simulated detector signal transient in the lower detector for 30 percent variations in the simulated input flux transient (Figure 2-8). It should be noted that the abscissa covers a span of approximately 3 seconds and the ordinate represents approximately 8 percent of the total signal range.

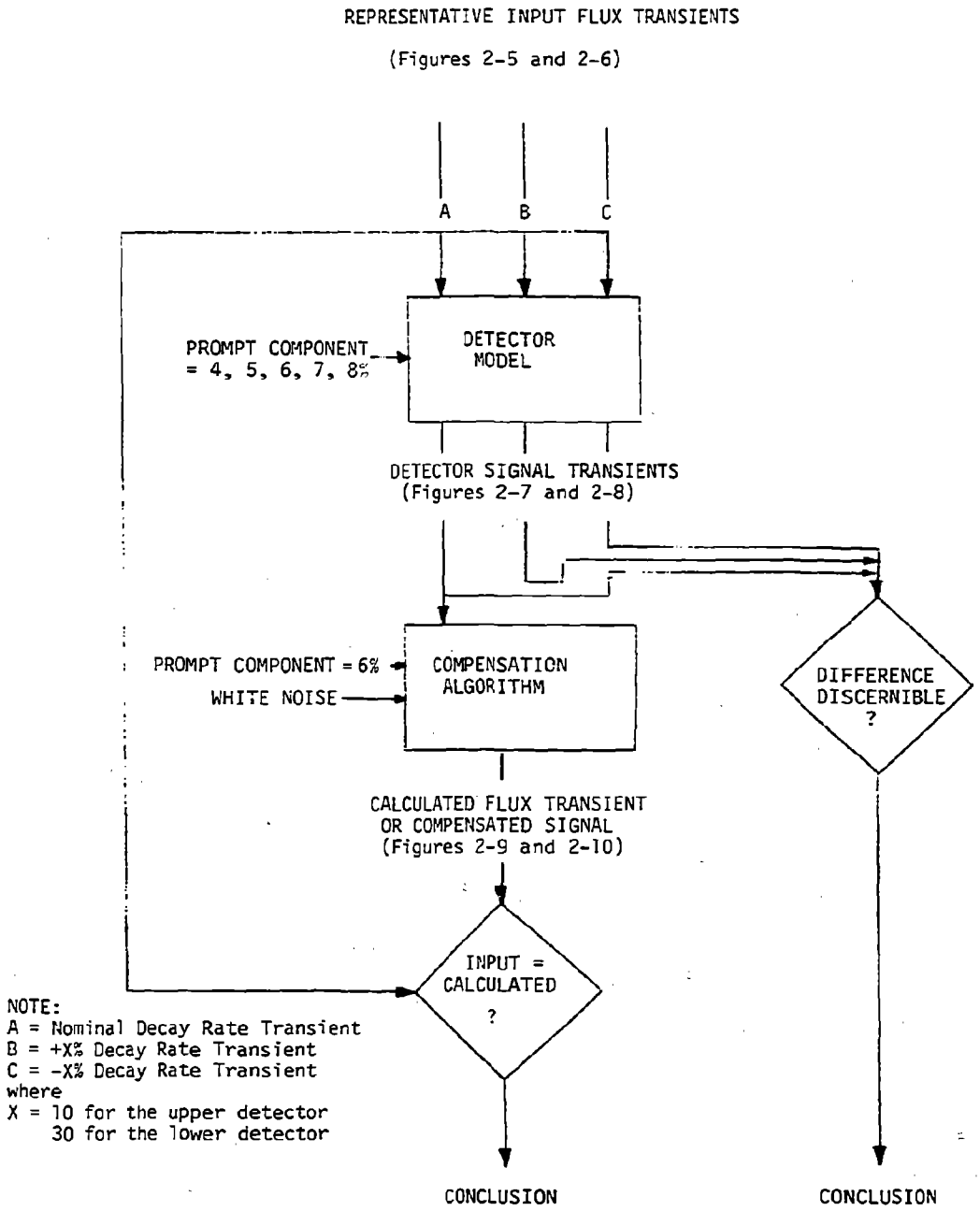

Figure 2-4. Procedure for Simulated Experiments

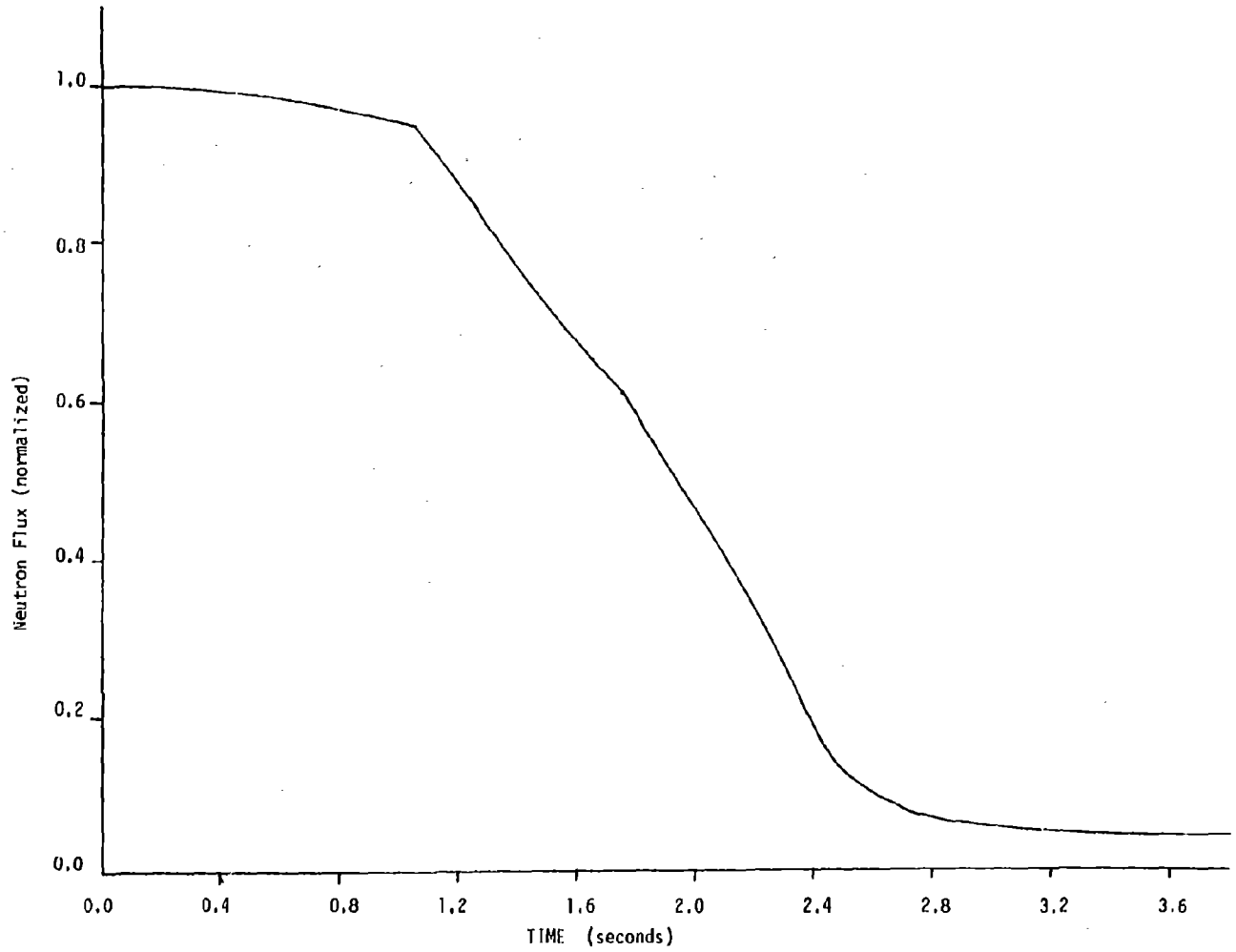

Figure 2-5. Typical Neutron Flux Transient - Upper Detector Level

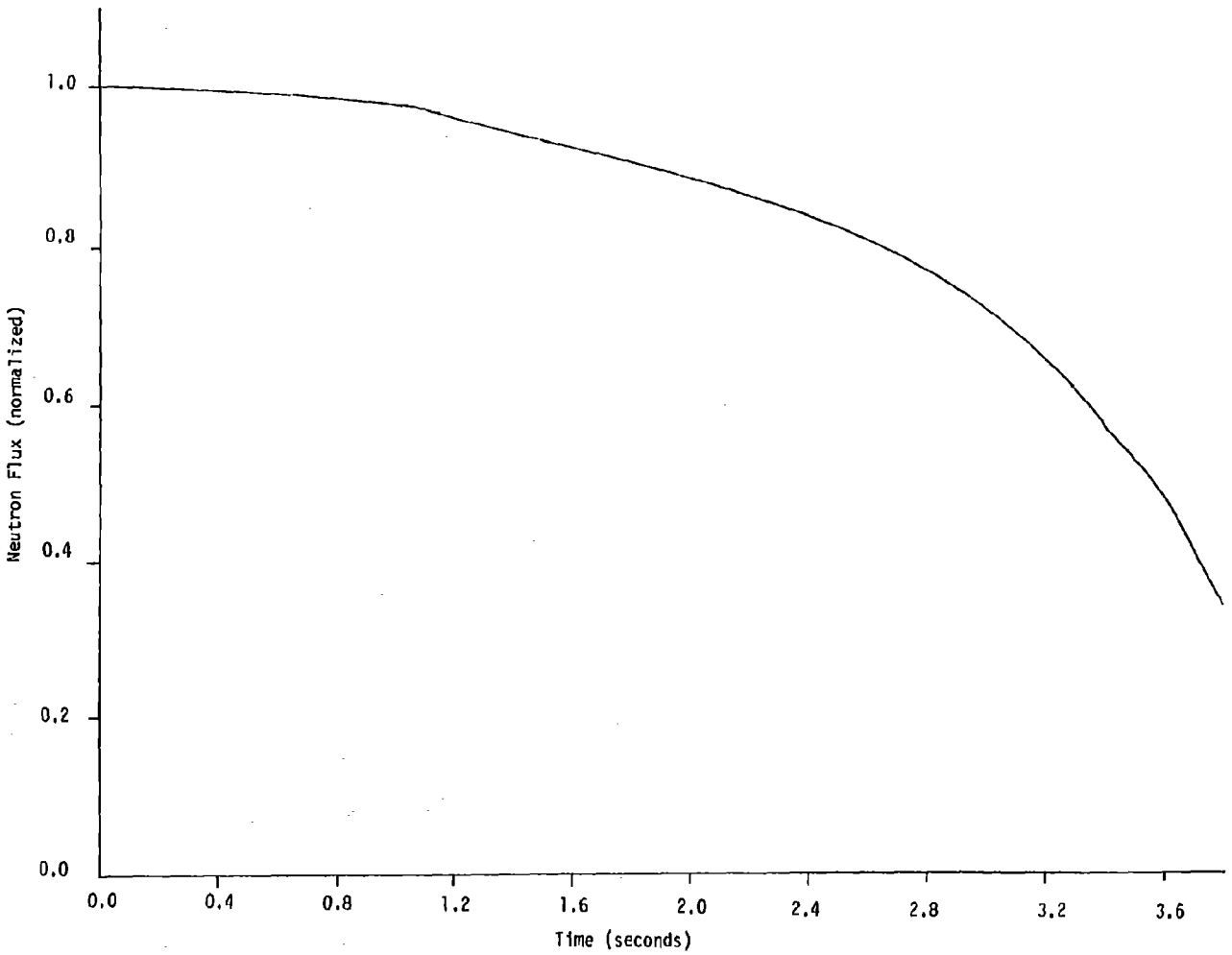

Figure 2-6. Typical Neutron Flux Transient - Lower Detector Level

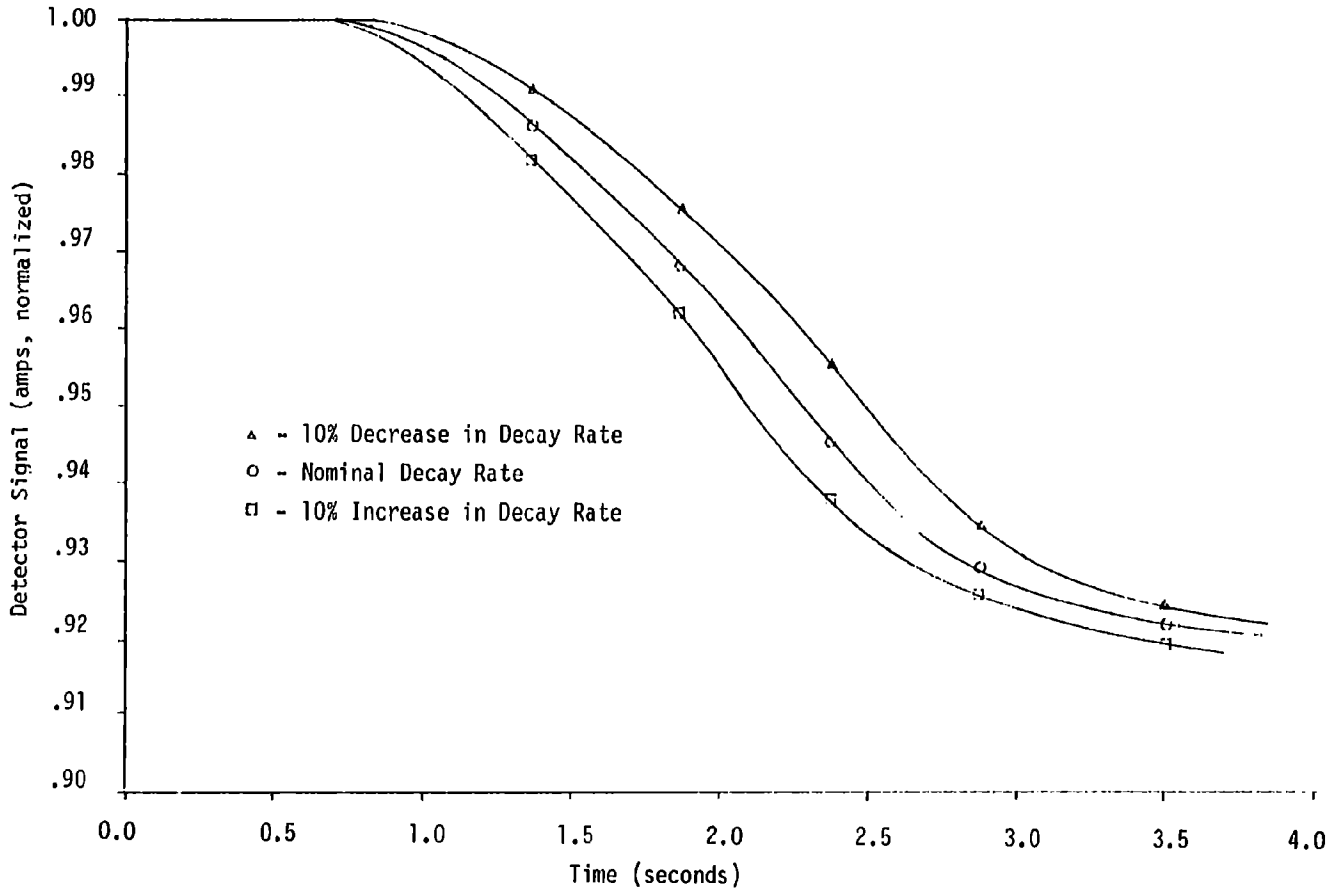

Figure 2-7. Uncompensate Detector Signals With ± 10 Percent Variation in Decay Rate (Upper Detector)

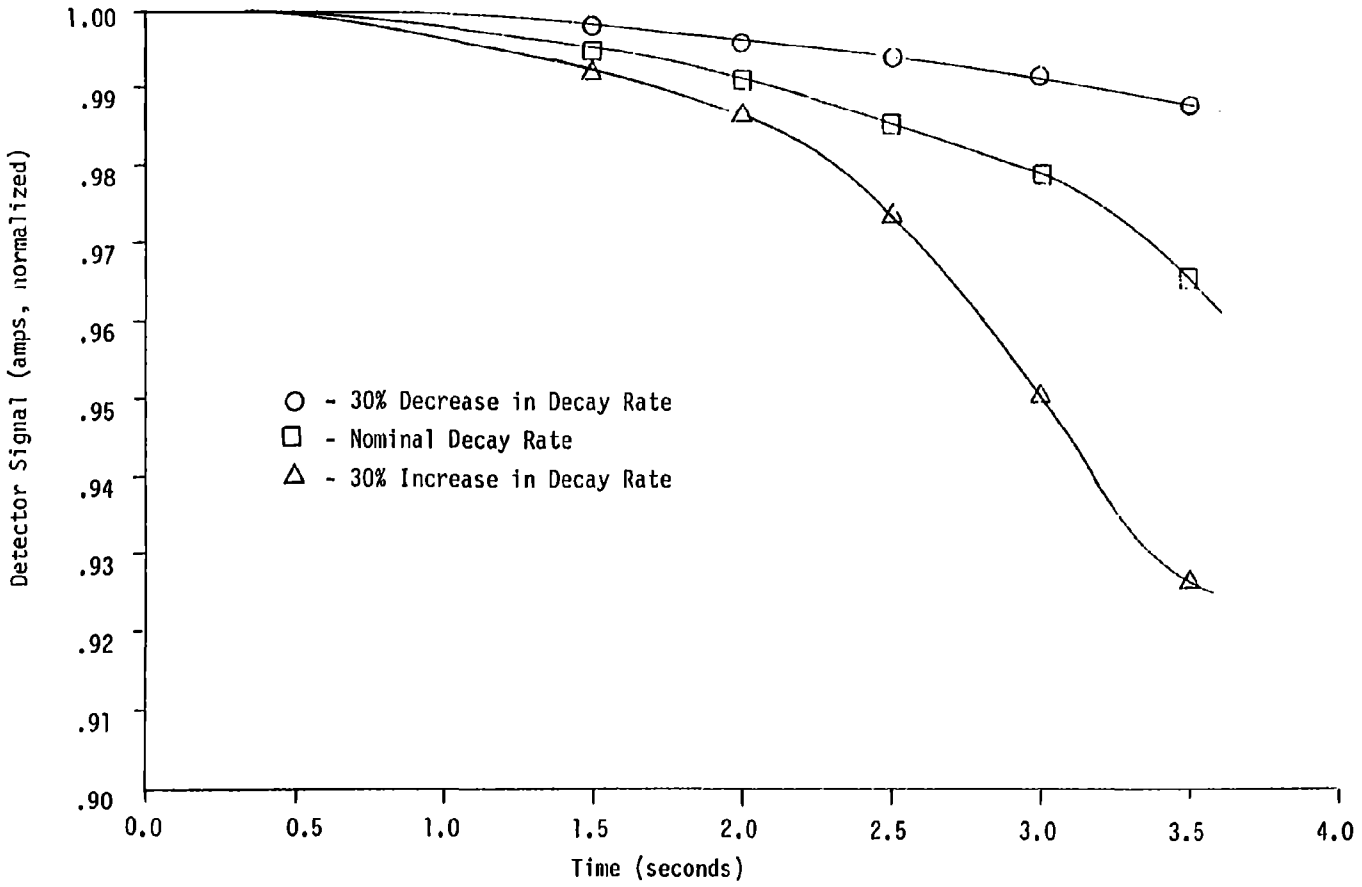

Figure 2-8. Uncompensated Detector Signals With ± 30 Percent Variation in Decay Rate (Lower Detector)

The results contained in Figures 2-7 and 2-8 show that differences in the simulated input flux transient produce significant changes in the simulated detector signal transient. The results also show that 10 percent varations in a flux decay rate produce 0.1 to 0.2 second temporal displacements of the signal transient. These differences are easily discernable using magnetic tape recordings when the time base is known to $\pm$ .05 seconds.

Evaluation of Measurement Uncertainties

Uncertainties in the measurement of a local neutron flux transient using rhodium detectors can arise from signal noise, errors due to compensation and errors introduced through numerical methods. These effects were studied by comparing the compensated simulated detector signal with the simulated input flux transient.

Figures 2-9 and 2-10 show the compensated simulated detector signals for a range of assumed prompt components for the upper and lower detector, respectively. Comparison of the simulated input transient with the compensated simulated detector signal for a prompt component of 6 percent (the same prompt component as that used in the detector simulation) indicates that errors originating from the numerical methods are negligible (<< 1 percent).

Figures 2-9 and 2-10 also demonstrate the sensitivity of the measured flux to errors in the magnitude of the prompt component. By comparing the compensated simulated detector signals for a range of prompt components, it can be seen that over a time of approximately 2.5 seconds, a 1 percent error in the prompt component may yield an error in the compensated detector signal (or calculated flux) of as much as 10 percent. (This result was verified during analysis of the actual measured data).

Another possible source of error is uncertainty associated with the decay rates of Rh-104. However, this potential source contributes a negligible amount of uncertainty to the measurements, since the Rh-104 half-life is long compared to the duration of the transient.

The influence of signal noise on measurement uncertainties has been evaluated for data sampled once per second. White noise with a root mean square (rms) value of 0.1 percent of the dc value of the noise-free detector signal was superimposed on the data samples. Analysis of this data indicates that the error due to 0.1 percent noise is less than 2 percent at a 90 percent confidence level.

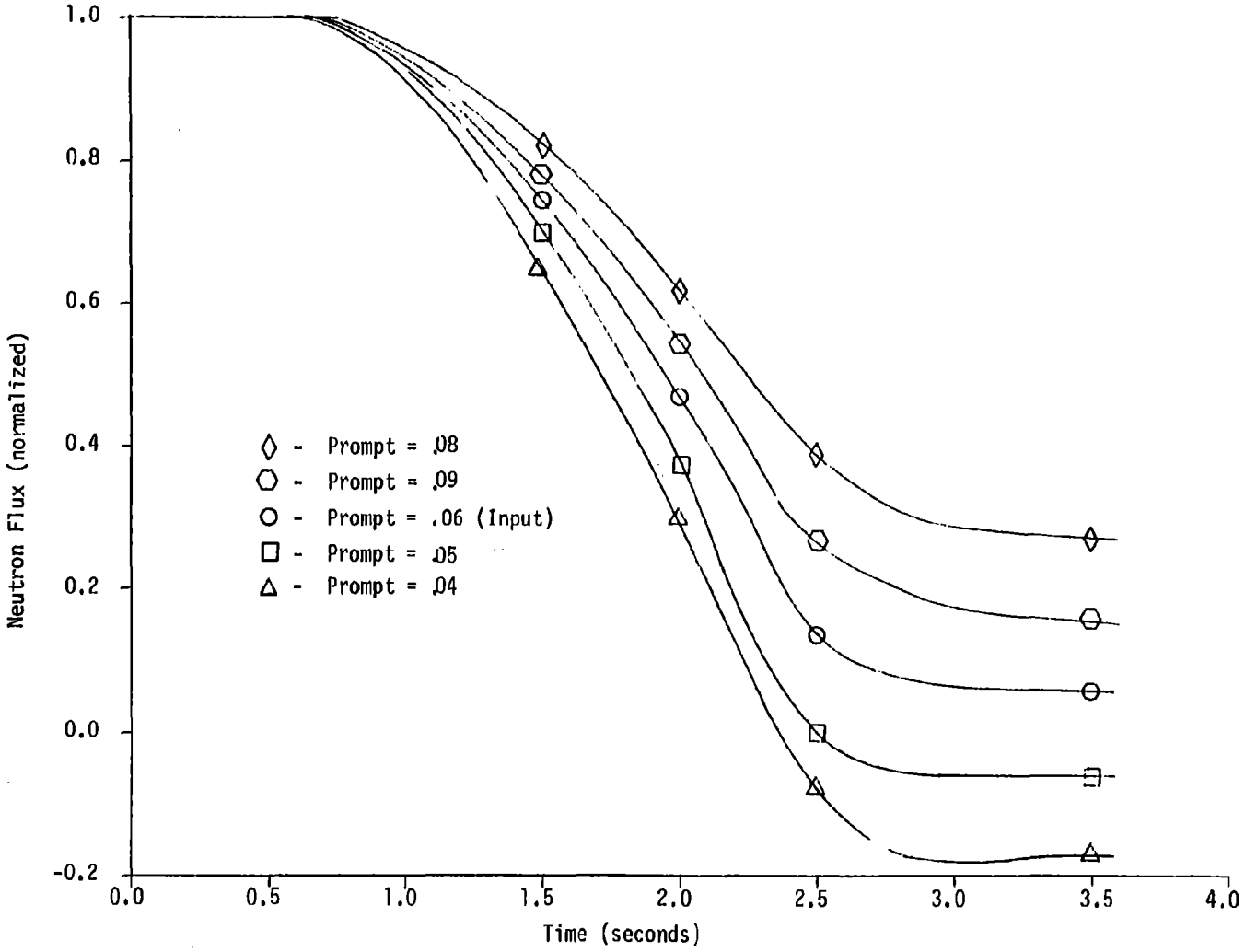

Figure 2-9. Dynamically Compensated Detector Signal Output With Varied Prompt Components (Upper Detector)

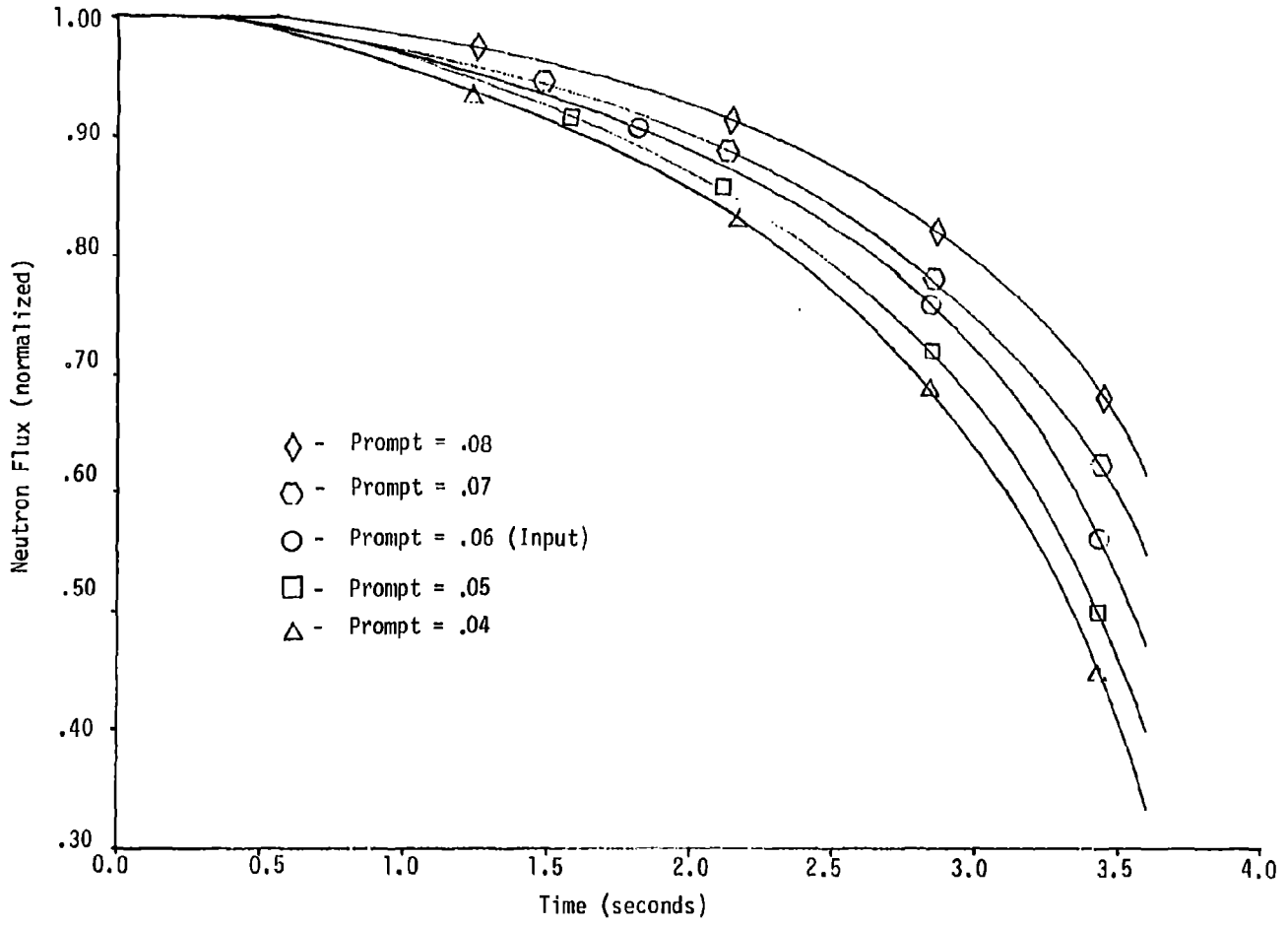

Figure 2-10. Dynamically Compensated Detector Signal Output With Varied Prompt Components (Lower Detector)

The foregoing discussion demonstrates that the largest source of measurement uncertainty originates from uncertainty in the magnitude of the prompt component of the rhodium detector signal. Since each of the uncertainty components (error in the prompt component, error introduced by numerical methods, error arising from signal noise and error associated with uncertainty in the Rh-104 decay rates) is statistically independent, a conservative estimate of the total uncertainty in a neutron flux transient as measured by rhodium detectors is given by

$$E_T = [\varepsilon^2_{\text{prompt component}} + \varepsilon^2_{\text{numerics}} + \varepsilon^2_{\text{noise}} + \varepsilon^2_{\text{Rh decay}}]^{1/2}$$

$$E_T = [(10x)^2 + 1^2 + 2^2 + 1^2]^{1/2}.$$

Here E_T is the total measurement uncertainty due to the uncertainty components described above, x is the absolute error in the rhodium detector prompt component, and 10 is a factor relating the error in the prompt component to the corresponding error in the compensated detector signal.

Section 3

TEST PROCEDURES

OBJECTIVES

The purpose of the transient test procedures was to ensure that the raw data from SPNDs, background detectors and CEA position indicators were properly recorded, calibrated and reduced. The same procedures were followed for all three transient tests for which in-core detector data were recorded. The procedures were specifically designed to meet the following objectives:

1. Ensure the hook-up of the correct SPND to the recording system.
2. Verify the proper wiring and channel identification of the FM multiplex system.
3. Verify that the range of the SPND signal is within the limits of the record/reproduce system.
4. Check the noise level on the SPND signals to ensure that it is not so high as to corrupt the in-core compensation process (S/N > 1000).
5. Ensure that sufficient calibration data is recorded to permit conversion of recorded voltage signals to accurate values of neutron flux (or CEA position).
6. Ensure coordination and synchronization of in-core transient data recordings with data acquired by the plant computer and the PDP-11/04 minicomputer.

METHODOLOGY

Verification of Signal Connections

After installation of the tape recording system, each channel was tested. The test was designed to verify the wiring of the system from the input of the Bessel filters to the output of the FM de-multiplex system. The test was performed by sequentially applying an oscillator signal to each channel input. The output of each channel was then monitored on an oscilloscope to verify correct system wiring and operation.

Electrical diagrams of the plant ICI system were used as the reference for determining the location of the test points for a given SPND or background signal. A test engineer

connected the wiring from the test points to the analog recording system. A second test engineer independently verified this hook-up.

With the NSSS at steady-state power conditions (prior to the transient event) a "core map" printout from the plant computer was obtained. The dc voltage of each in-core detector to be recorded was measured with a digital voltmeter (DVM) and compared to the plant computer readings from the "core map". Variations of 2 percent or less between the plant computer and the DVM readings were accepted as a secondary means of hook-up verification.

The ICI electronics are divided into four independent cabinets. Each cabinet was set to a zero calibration, one at a time, while the signals to the FM multiplex system were monitored to verify that the signals that were supposed to be hooked up to that cabinet went to zero. This provided the third means of independent signal verification.

Signal Noise

The root mean square (rms) value of the signal noise at the output of the Bessel filters was measured with a DVM to verify that it was within 0.1 percent of the dc value of the SPND signal. Feasibility studies made with test reactor data demonstrated that a signal to noise ratio (S/N) of 1000 (1/.001) over a 10 Hz bandwidth provided good results when the signals were later compensated to obtain the dynamic response of the SPNDs. Therefore, SPNDs with substantially lower S/N were examined to either improved the S/N through diagnostic techniques or be dropped from the recording in favor of more acceptable SPNDs.

Calibration

Two methods of calibration were employed in the recording of the SPND data. One was simply an electrical calibration of the recording system. The second used steady-state NSSS conditions and plant computer readings of neutron flux as calibration references.

Electrical Calibrations. Each Bessel filter was calibrated with a signal generator and a DVM. The electrical gain and offset were determined for each filter. The FM multiplex system was calibrated by recording a zero voltage and then a 2.5 volt signal on each channel. The zero calibration from each of the four ICI cabinets was also recorded on tape.

Reference Calibration. For the LOF, plant computer logs before the transient and after the transient (zero flux) provided two reference points for calibration of reproduced data. When compared with the electrical calibration, good agreement was found with gain terms. Offsets obtained with the two methods disagreed. Since the reactor flux may be assumed to be near zero 20 minutes after trip, data from this period of time was used for determining offset calibrations. The offset disagreement was due to two possible causes. One was the inability of the zero calibration in the ICI cabinets to adequately zero the current to the ICI current-to-voltage amplifiers. The other was that although the neutron flux may be zero, there was still considerable gamma radiation in the core. Since the SPND is sensitive to gammas, it is possible for it to have a non-zero output; however, this signal level should correspond to zero neutron flux.

For both the FLCEAD and PLCEAD the calibration gain terms were obtained from electrical calibration. The offsets were obtained from plant computer reference printouts.

Test Coordination

The operator of the tape recorders maintained phone communication with the test supervisor in the control room. In this manner the tape recorder operator was able to start recording well in advance of the plant transients. Time-of-day clocks on the plant computer and PDP-11/04 computer and the tape recorder BCD clock were synchronized to within 1 second.

Data Reduction

The tape-recorded data was reproduced and digitized at Combustion Engineering's Nuclear Development Laboratories. The reduction that followed was conducted on a PDP-11/15 minicomputer system. The Appendix to this report provides the details of the data reduction process.

Section 4

TEST RESULTS

LOSS OF FLOW

Description of Test

The initial core conditions for the 4-pump loss of flow are given in Table 4-1. The core power distribution prior to the test is shown in Figure 4-1.

The loss of flow was initiated by tripping all four reactor coolant pumps simultaneously. The Plant Protective System subsequently tripped the reactor on a low DNBR signal 0.2 seconds after the pumps were tripped. The CEAs began to enter the core immediately after the low DNBR trip. Automatic turbine trip was initiated 0.4 seconds after the pumps were tripped. Both turbine bypass valves received quick-open signals from the Steam Dump and Bypass Control System (SDBCS) and were full-open approximately 2 seconds into the transient. Since the bypass capacity was not sufficient to remove all the core heat, one atmospheric dump valve opened to vent the remaining steam flow to the atmosphere. After 3.0 seconds, the CEAs were fully inserted and the core power reduced to less than 5 percent of full power.

Recorded Signal Locations

The locations of the rhodium in-core and background detector signals recorded during the loss of flow are given in Tables 4-2 and 4-3, respectively. Table 4-4 indicates the locations of the CEAs whose positions were recorded for this test. Data which were judged to be noisy, distorted, or taken from a bad detector are indicated in the legends of Tables 4-2 and 4-4.* These data are not included in the report.

*Visual inspection of the compensated in-core detector signals was used to determine those signals which could provide meaningful data for code qualification.

Table 4-1

INITIAL CORE CONDITIONS FOR TOTAL LOSS OF FLOW FROM 80 PERCENT POWER

Core Power, MWt	2295 (81%)
Axial Shape Index (SIU)	~ 0.0
Boron Concentration, PPM	684
Core Mass Flow Rate, 10^6 lbm/hr	113.0
Pressurizer Pressure, psia	2240
Core Inlet Coolant Temperature, °F	552
Core Outlet Coolant Temperature, °F	596
CEA Position	ARO*

*ARO - all CEAs fully withdrawn

LEGEND:

Box Number - Instrument Number
Integrated Assembly Power, MWTH
Assembly Axial Shape Index, SIU
Assembly Relative Power Fraction

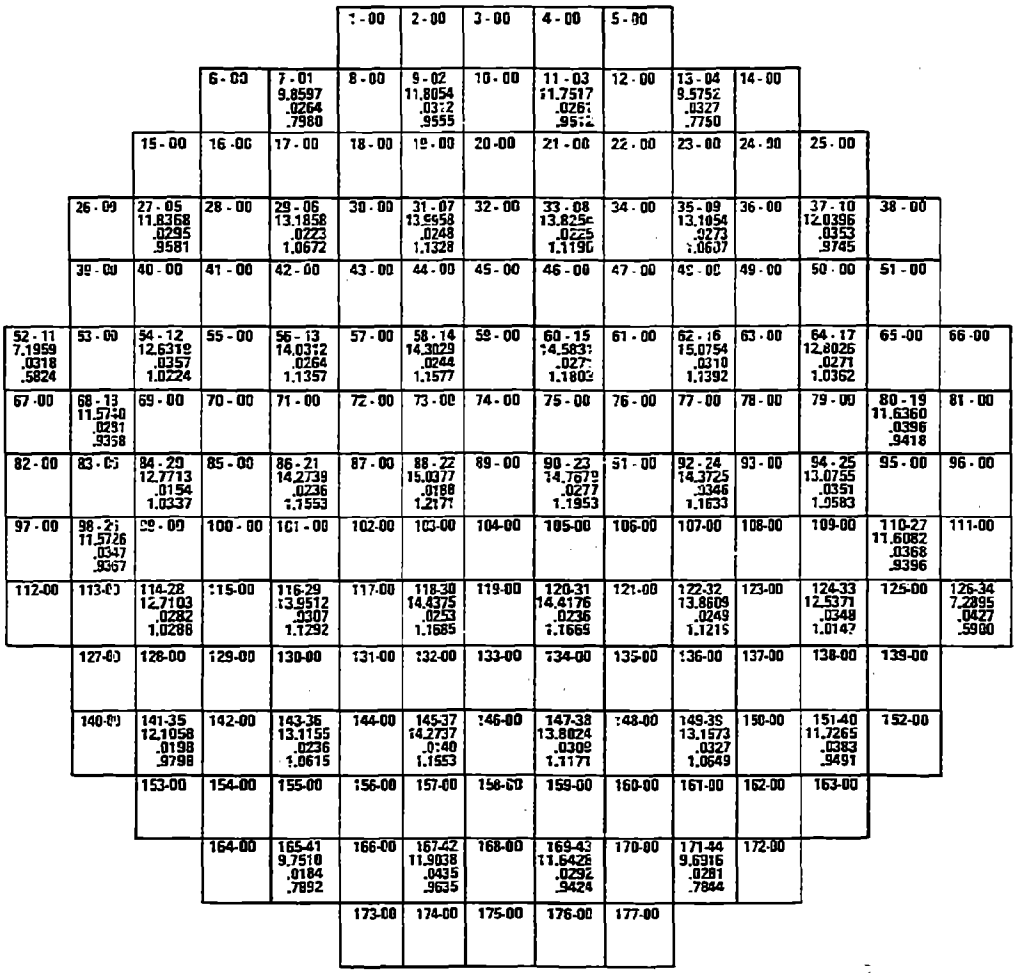

Figure 4-1. Core Power Distribution Prior to Loss of Flow - 12/30/79, 9:47:00

Table 4-2

RECORDED RHODIUM IN-CORE DETECTOR LOCATIONS FOR LOSS OF FLOW

Rh In-Core Detector Location	Level 1	2	3	4	5
E-2		X		X	
G-2	X	X	X	X	X
G-4		D		D	
G-6		X		X	
G-8	N	X	X	X	X
N-10		X	X		B
C-12	X		X		X
G-14		X		X	

X = recorded in-core detector with good signal

N = recorded in-core detector with noisy signal

D = recorded in-core detector with distorted signal

B = bad in-core detector

Table 4-3

RECORDED BACKGROUND DETECTOR LOCATIONS FOR LOSS OF FLOW

Background Detector Location	Level	
	Long	Short
E-2	X	X
E-4	X	X
G-6	X	X
P-7	X	X
G-8	X	X
N-10	X	X
C-12	X	X

X = recorded background detector with good signal

Table 4-4

RECORDED CEAs FOR LOSS OF FLOW

CEA Number	Core Location
3	G-7*
17	G-5
27	E-5
33	F-4*
41	G-3
65	F-2
75	G-1

* = distorted signal

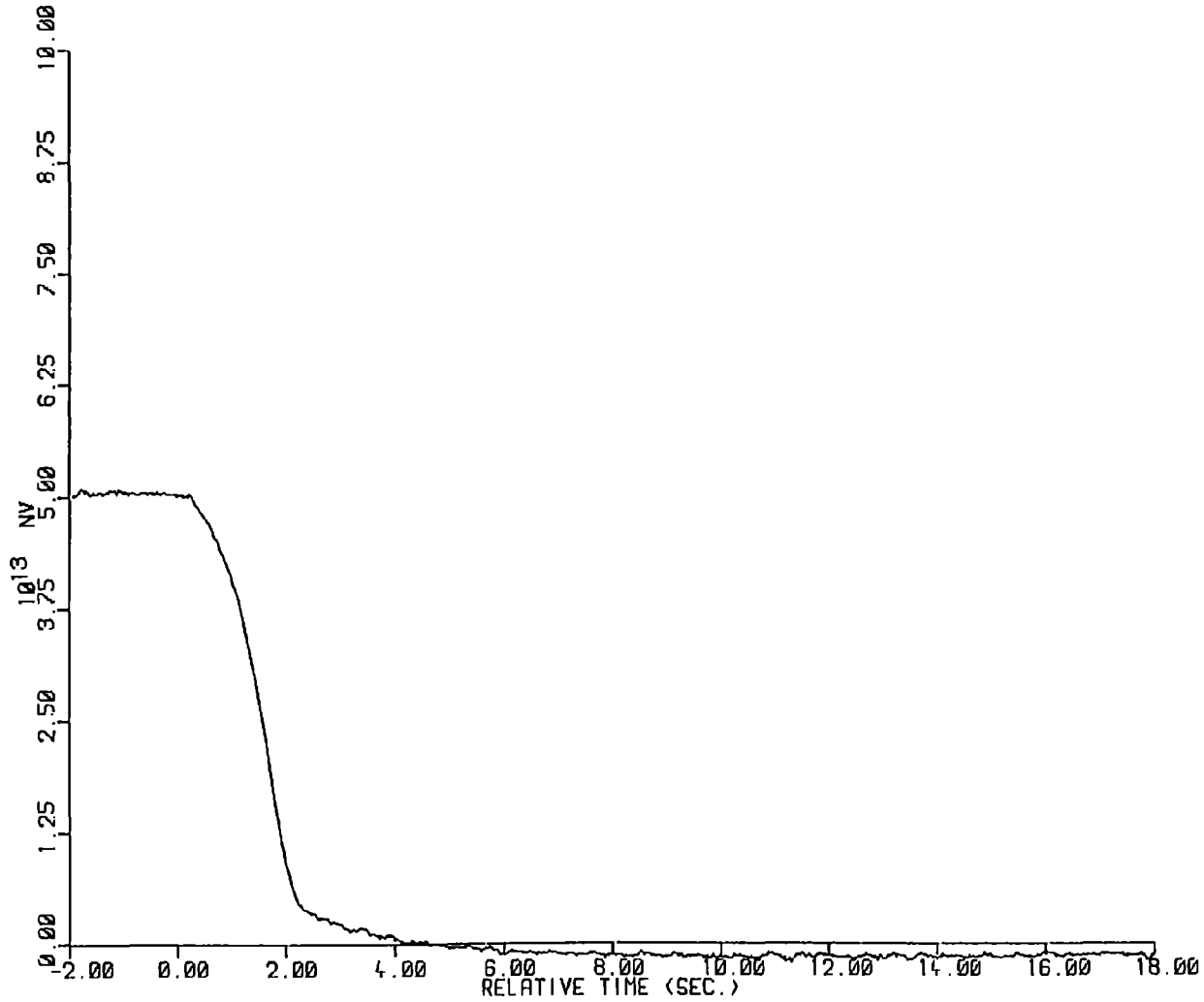

Figure 4-2. Compensated In-Core Flux - Loss of Flow - SPND E2 Level 2

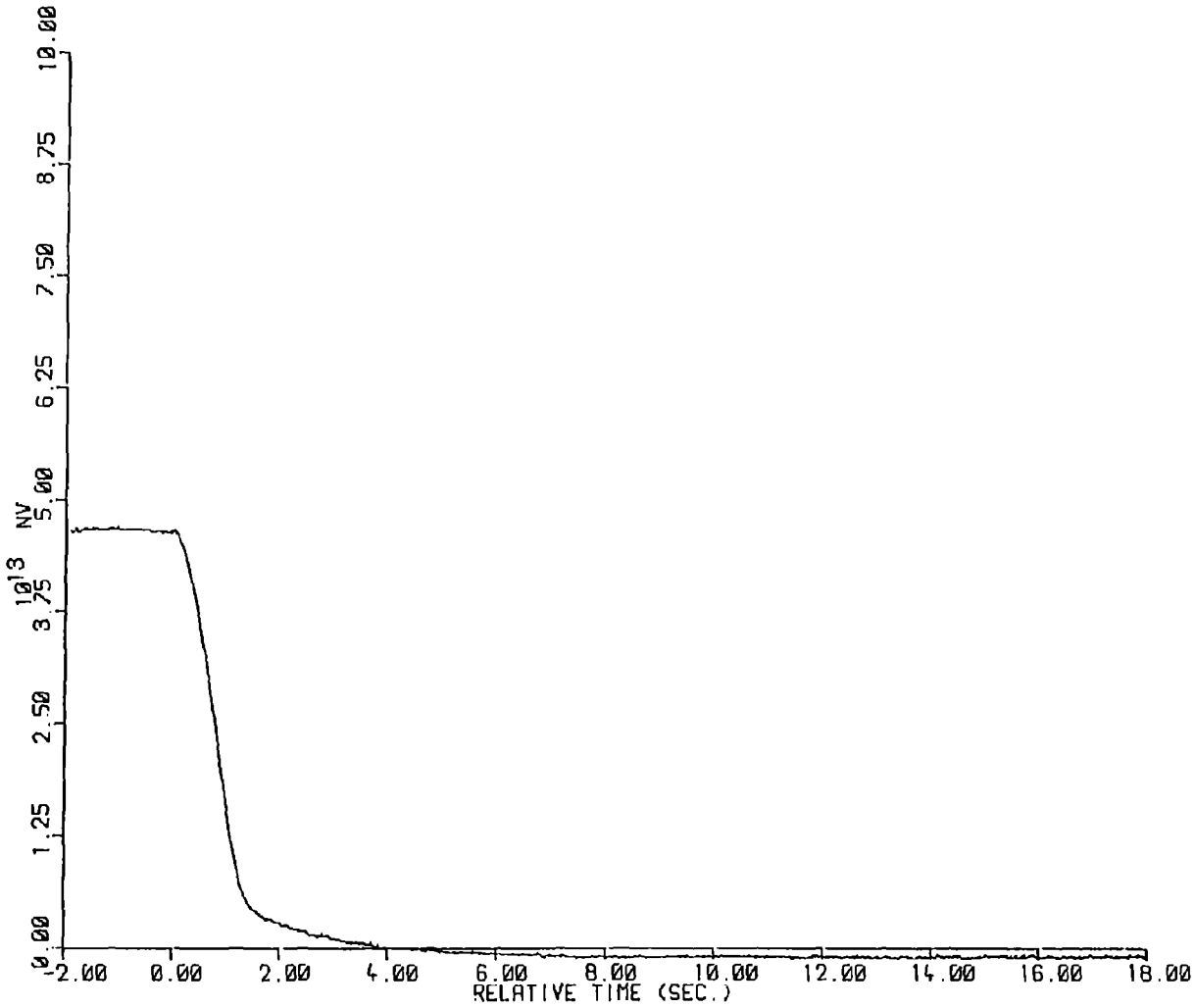

Figure 4-3. Compensated In-Core Flux - Loss of Flow - SPND E2 Level 4

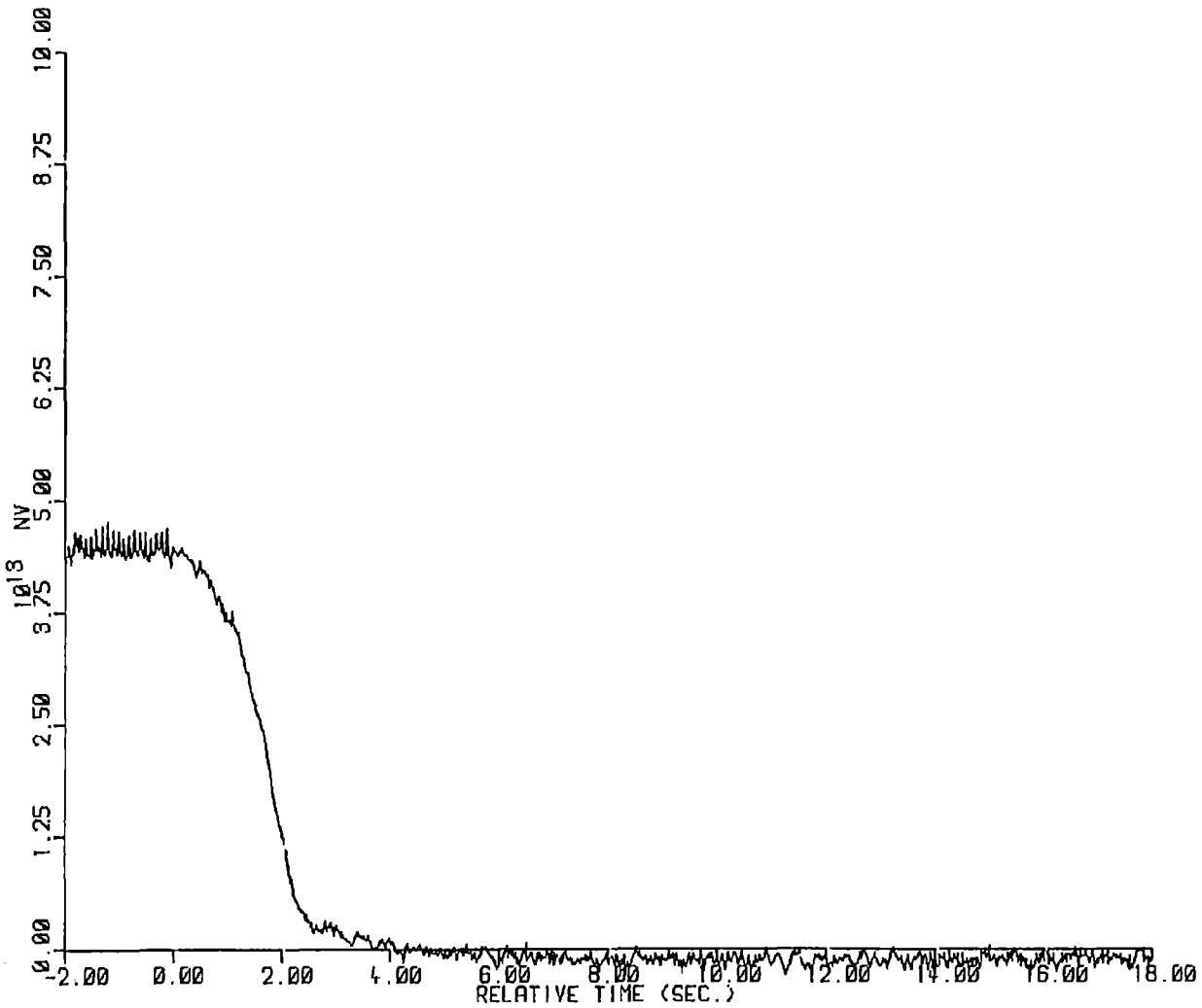

Figure 4-4. Compensated In-Core Flux - Loss of Flow - SPND G2 Level 1

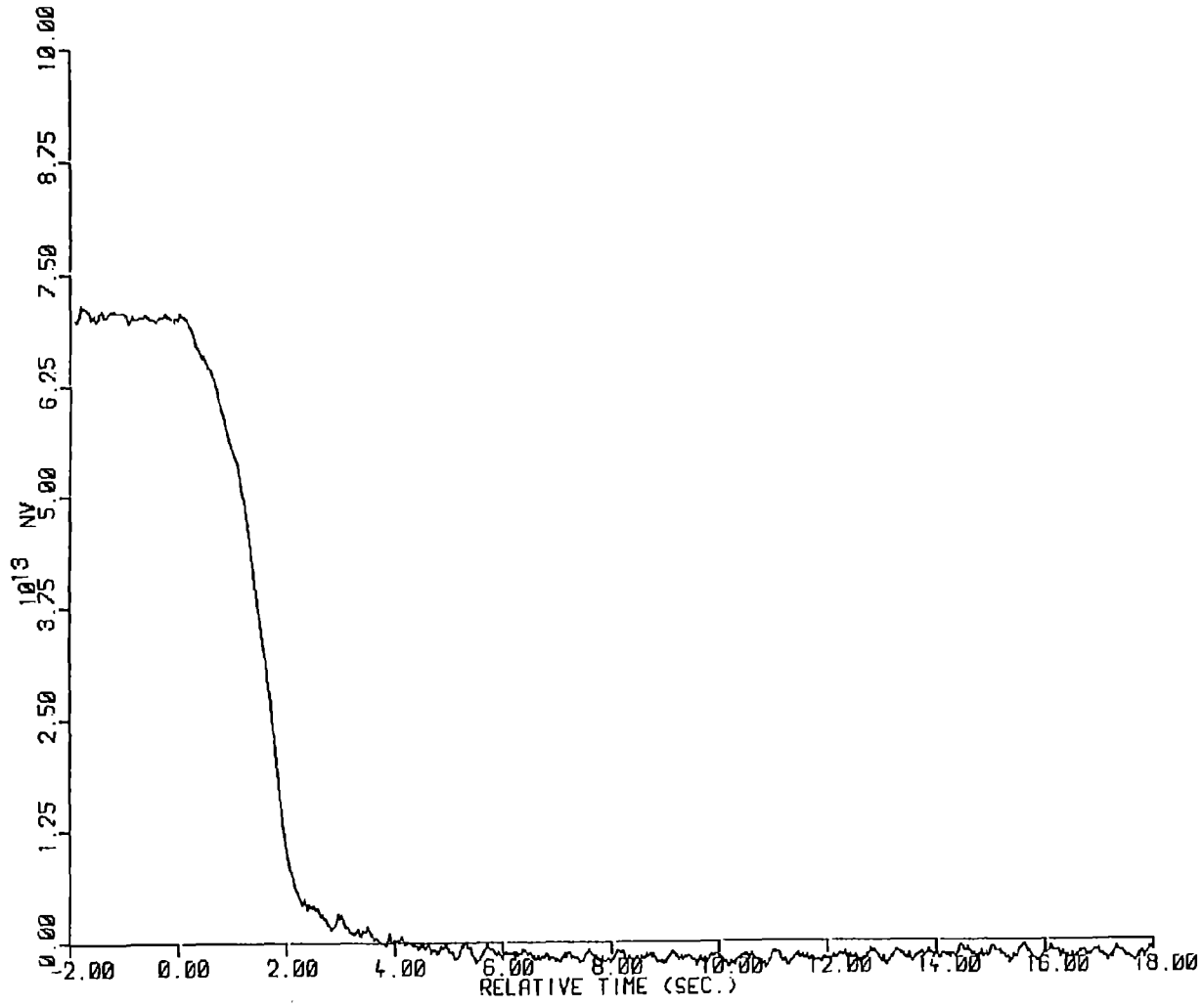

Figure 4-5. Compensated In-Core Flux - Loss of Flow - SPND G2 Level 2

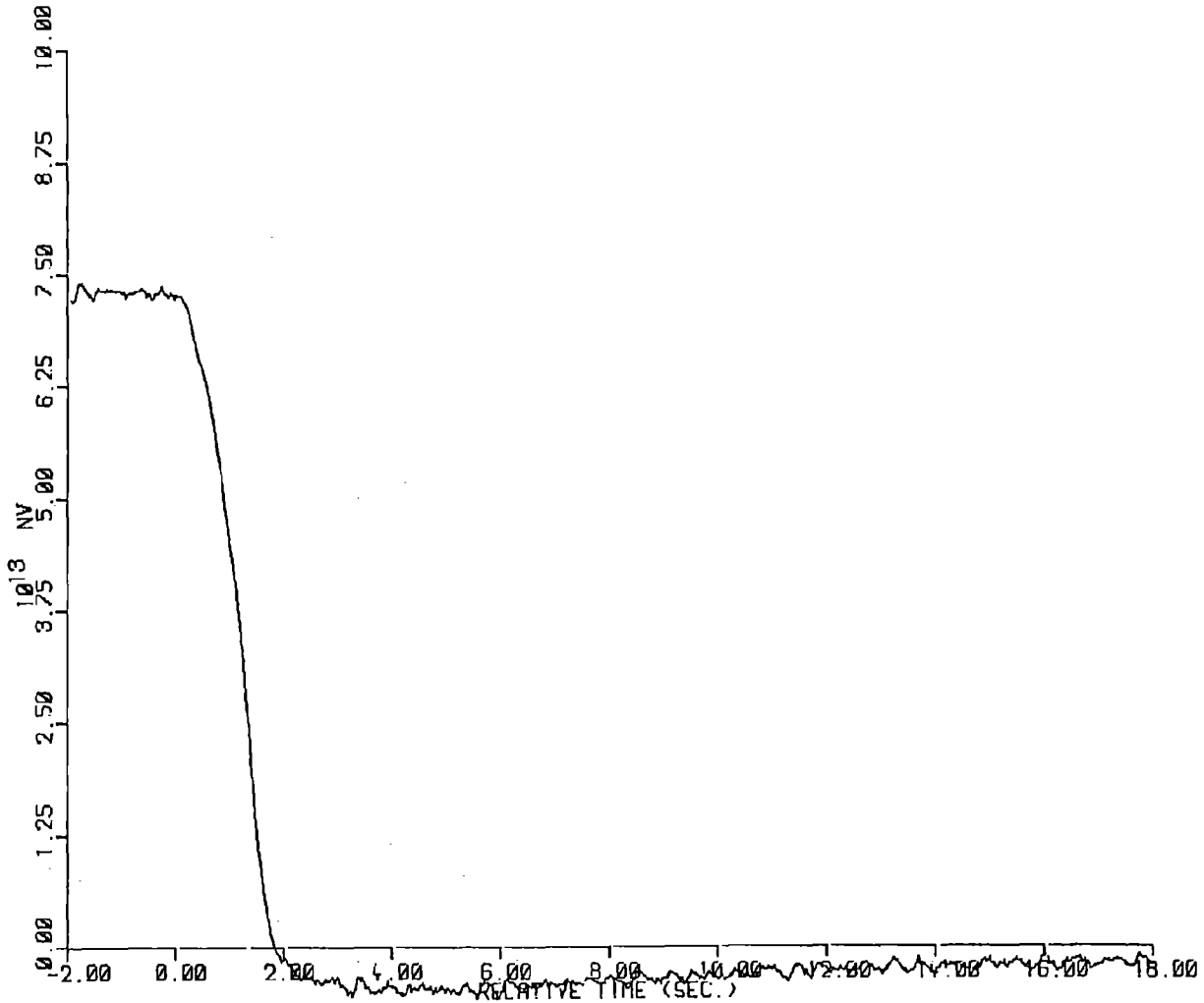

Figure 4-6. Compensated In-Core Flux - Loss of Flow - SPND G2 Level 3

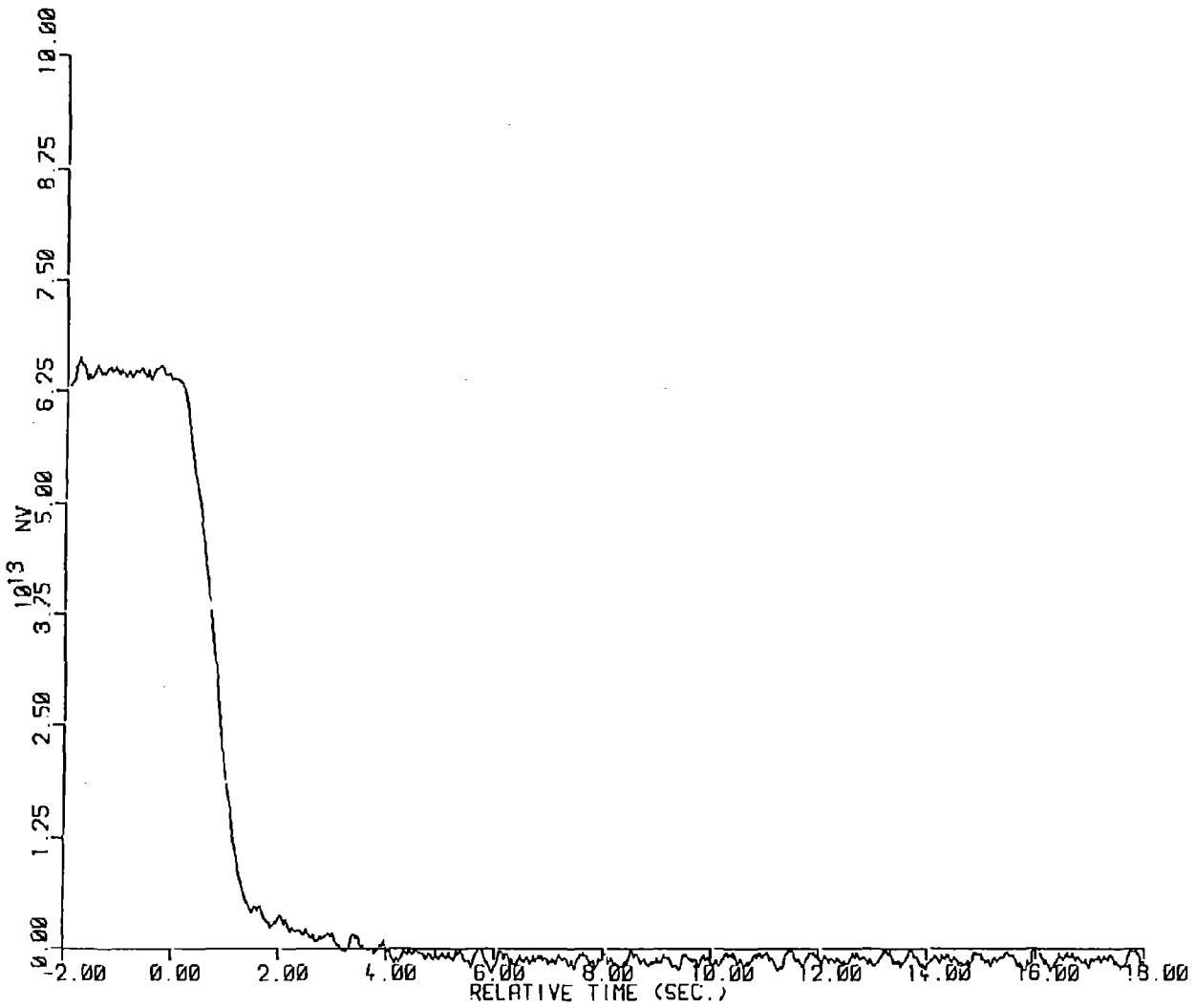

Figure 4-7. Compensated In-Core Flux - Loss of Flow - SPND G2 Level 4

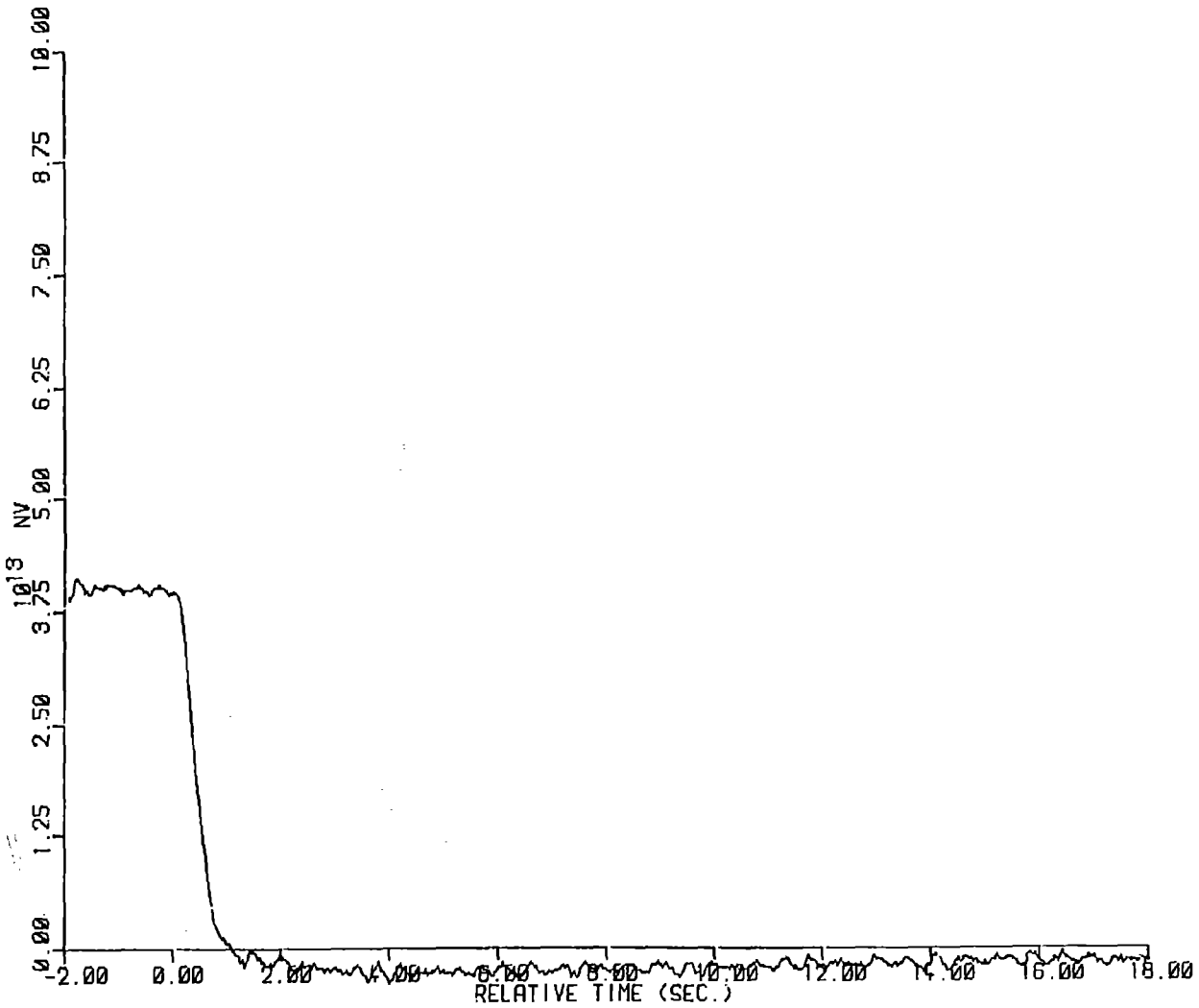

Figure 4-8. Compensated In-Core Flux - Loss of Flow - SPND G2 Level 5

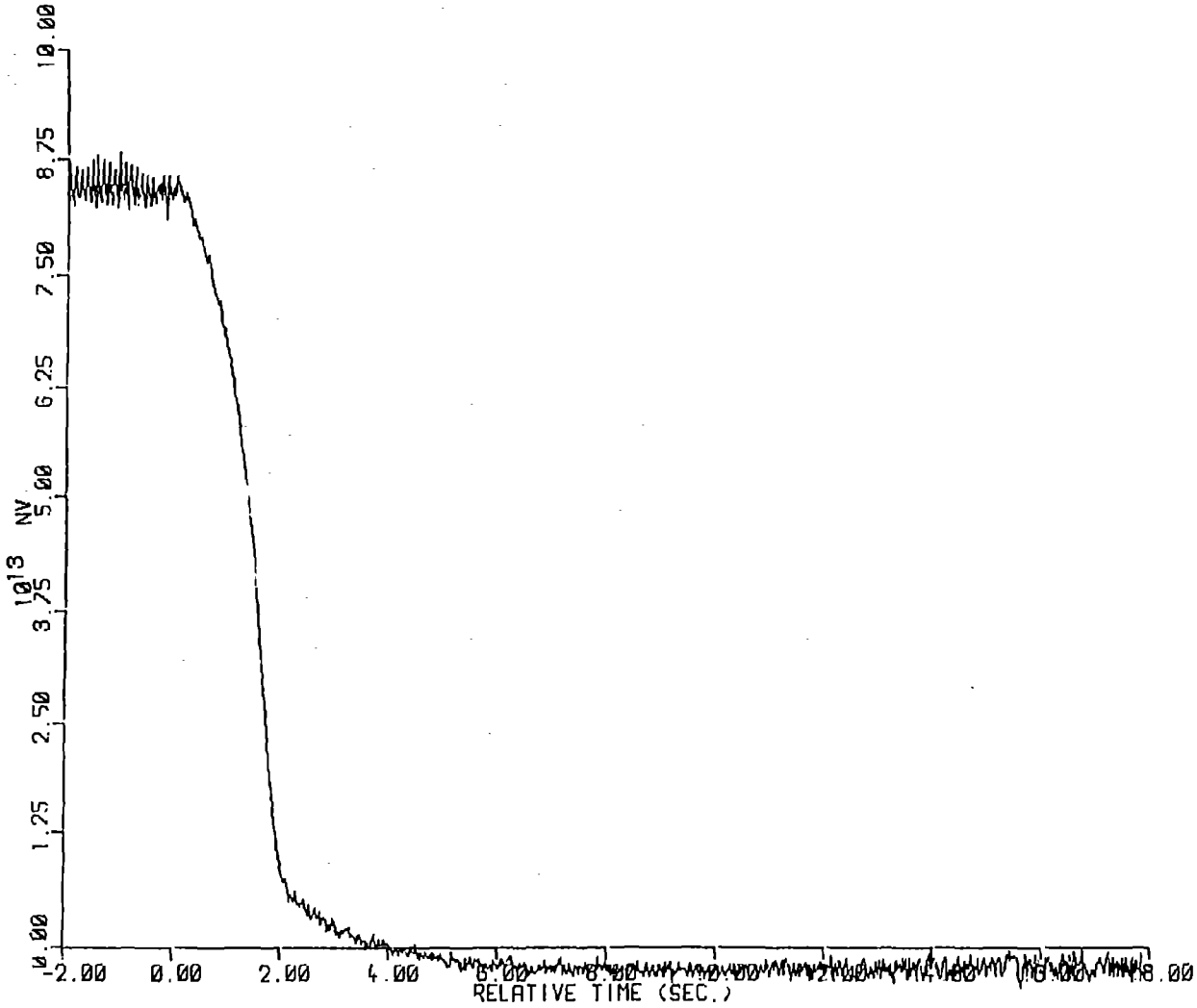

Figure 4-9. Compensated In-Core Flux - Loss of Flow - SPND G6 Level 2

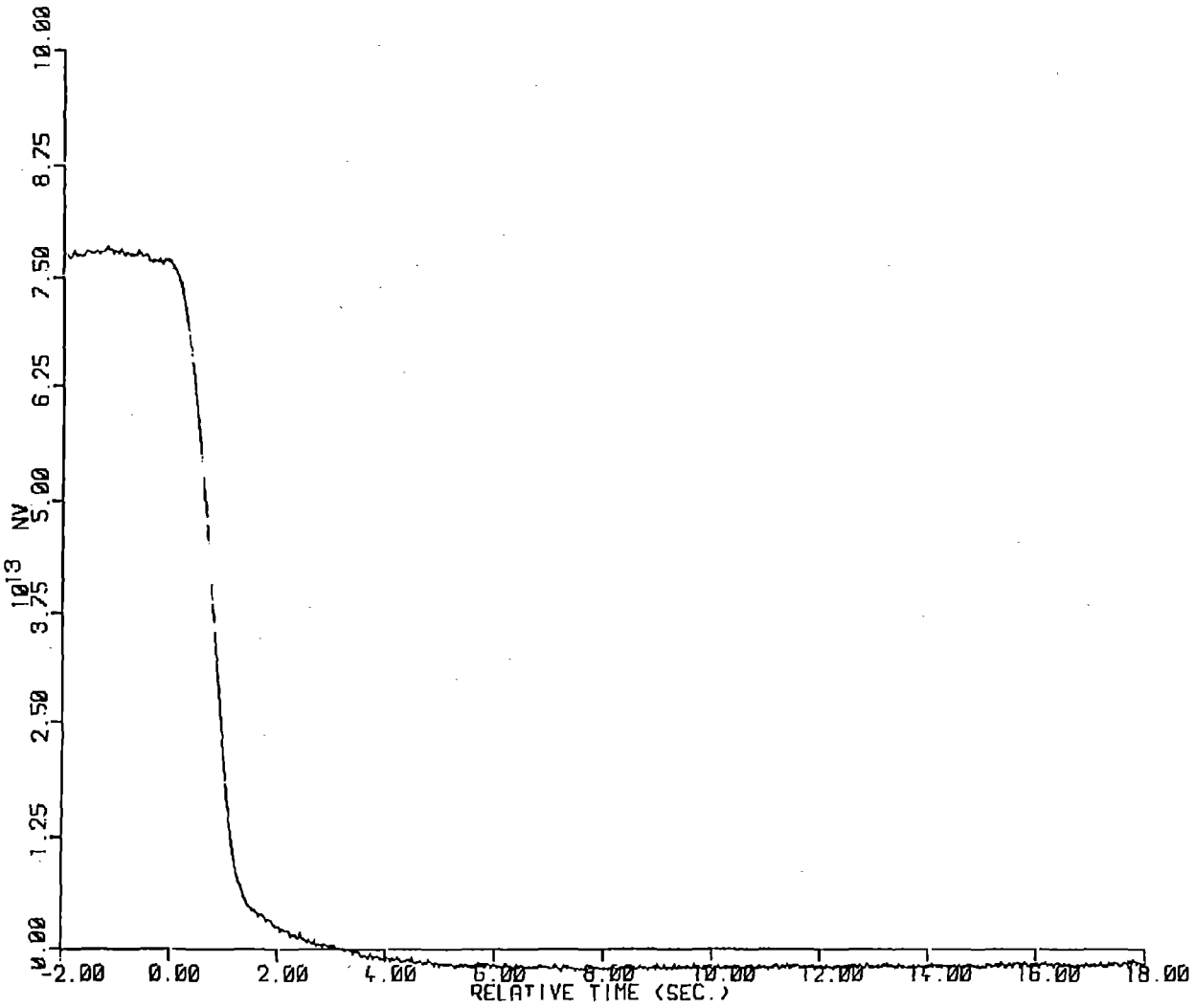

Figure 4-10. Compensated In-Core Flux - Loss of Flow - SPND G6 Level 4

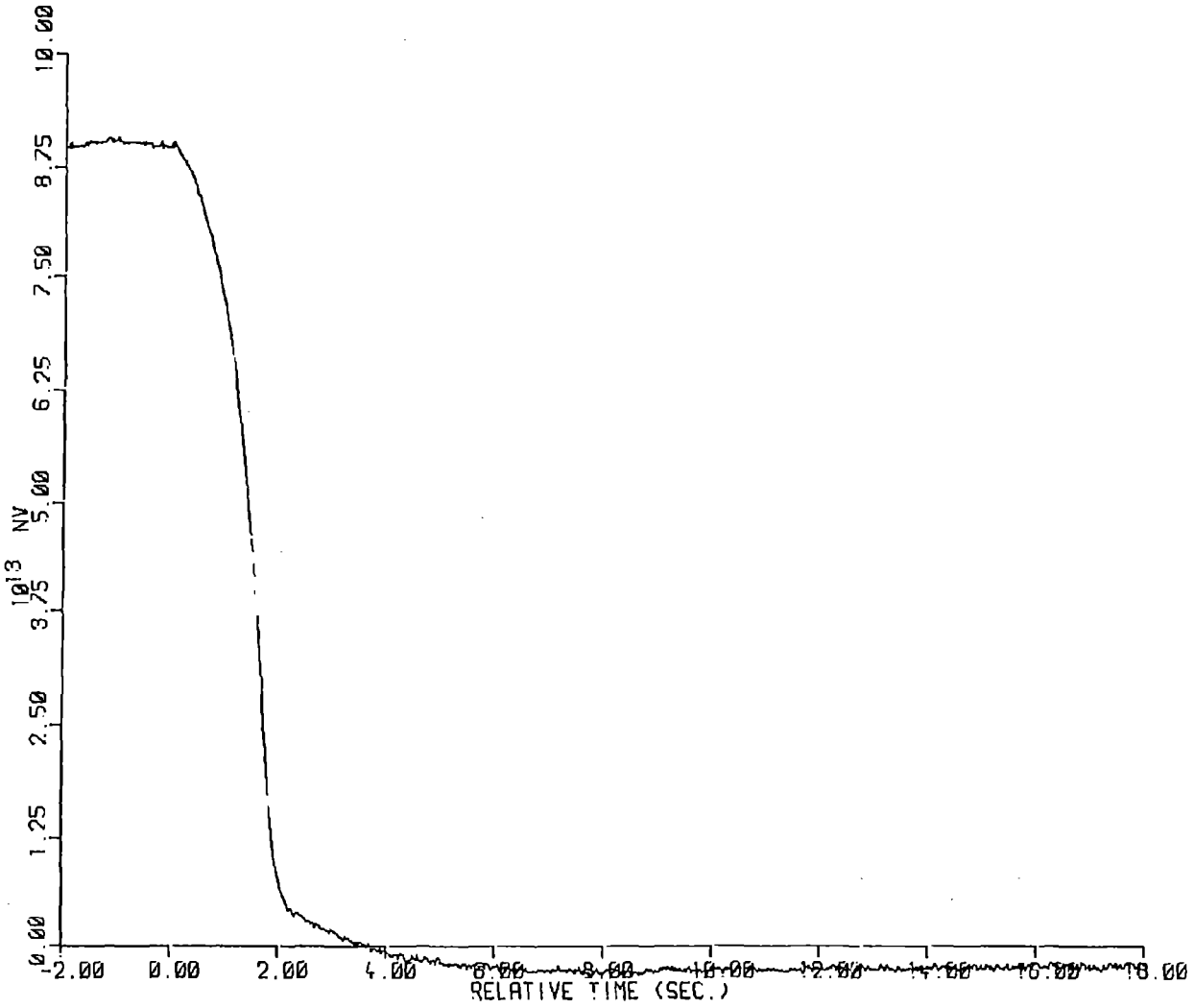

Figure 4-11. Compensated In-Core Flux - Loss of Flow - SPND G8 Level 2

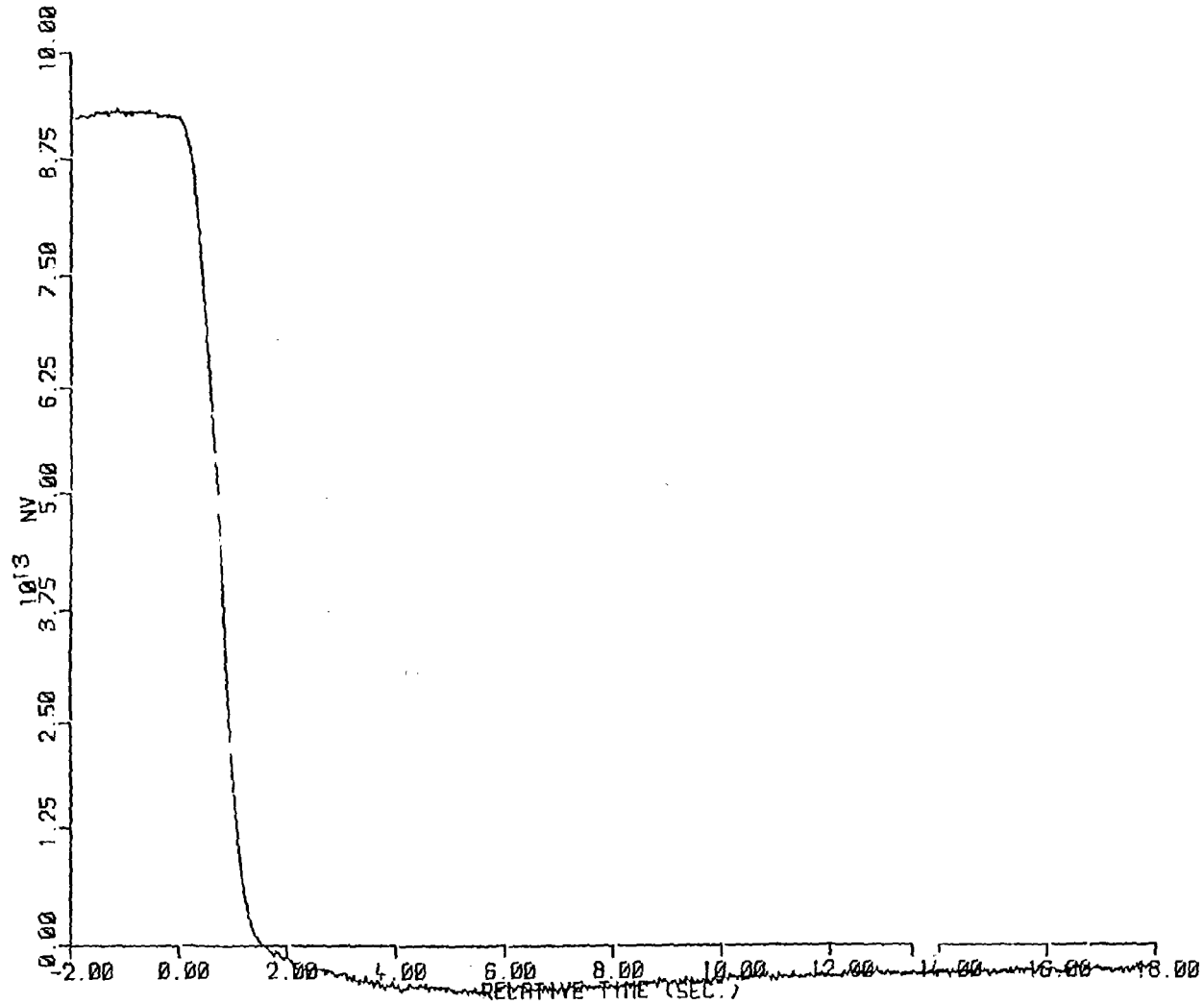

Figure 4-12. Compensated In-Core Flux - Loss of Flow - SPND G8 Level 3

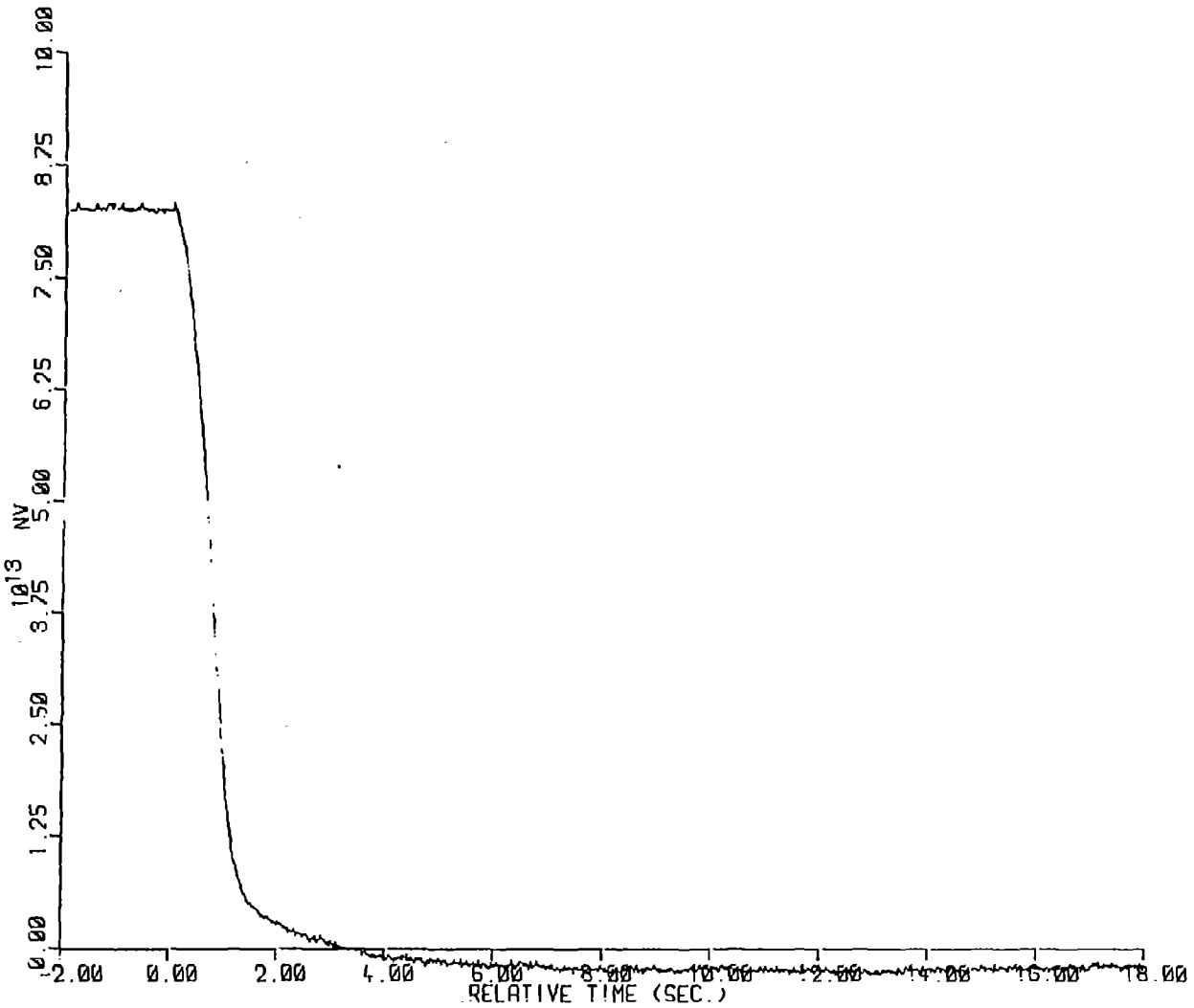

Figure 4-13. Compensated In-Core Flux - Loss of Flow - SPND G8 Level 4

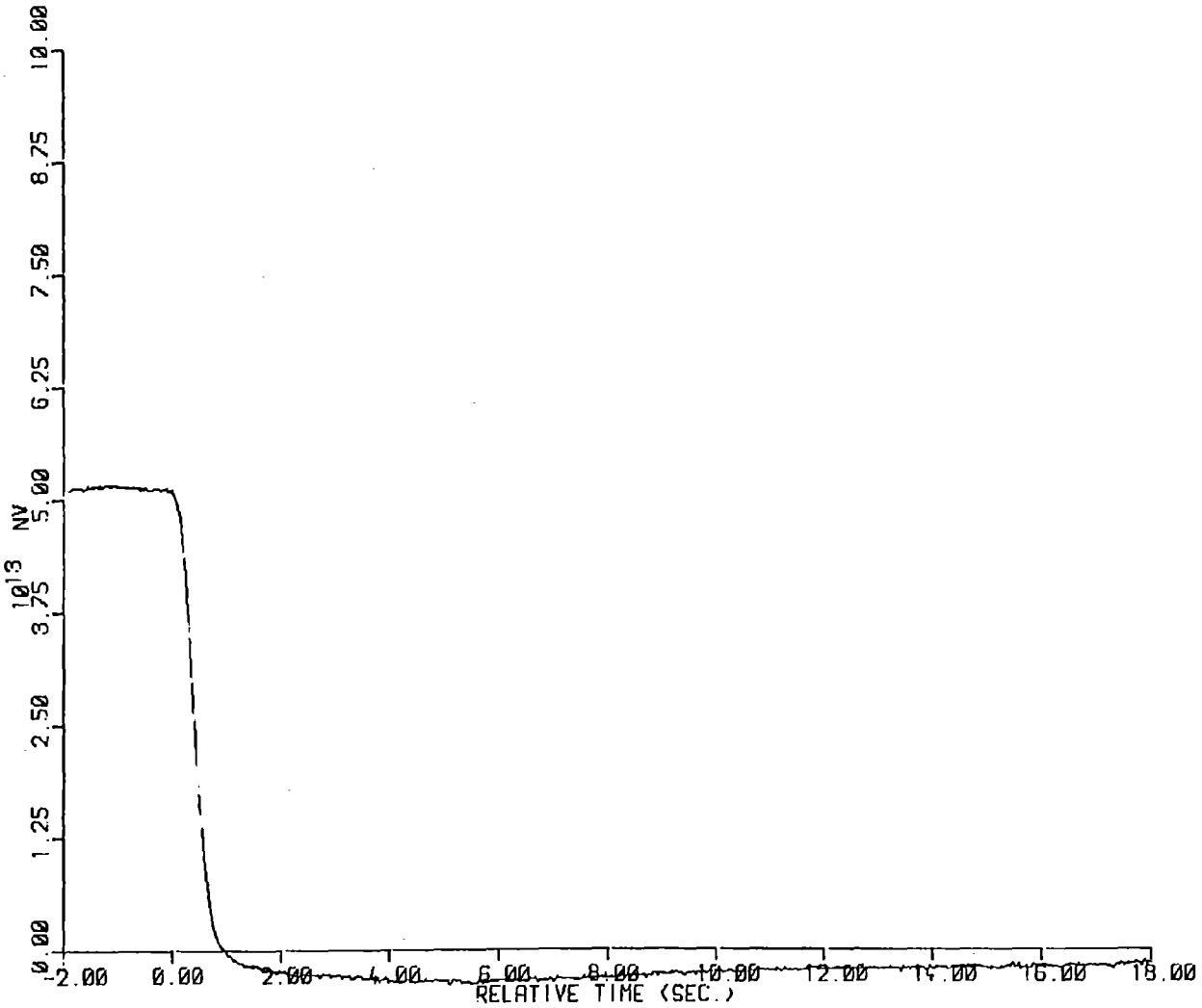

Figure 4-14. Compensated In-Core Flux - Loss of Flow - SPND G8 Level 5

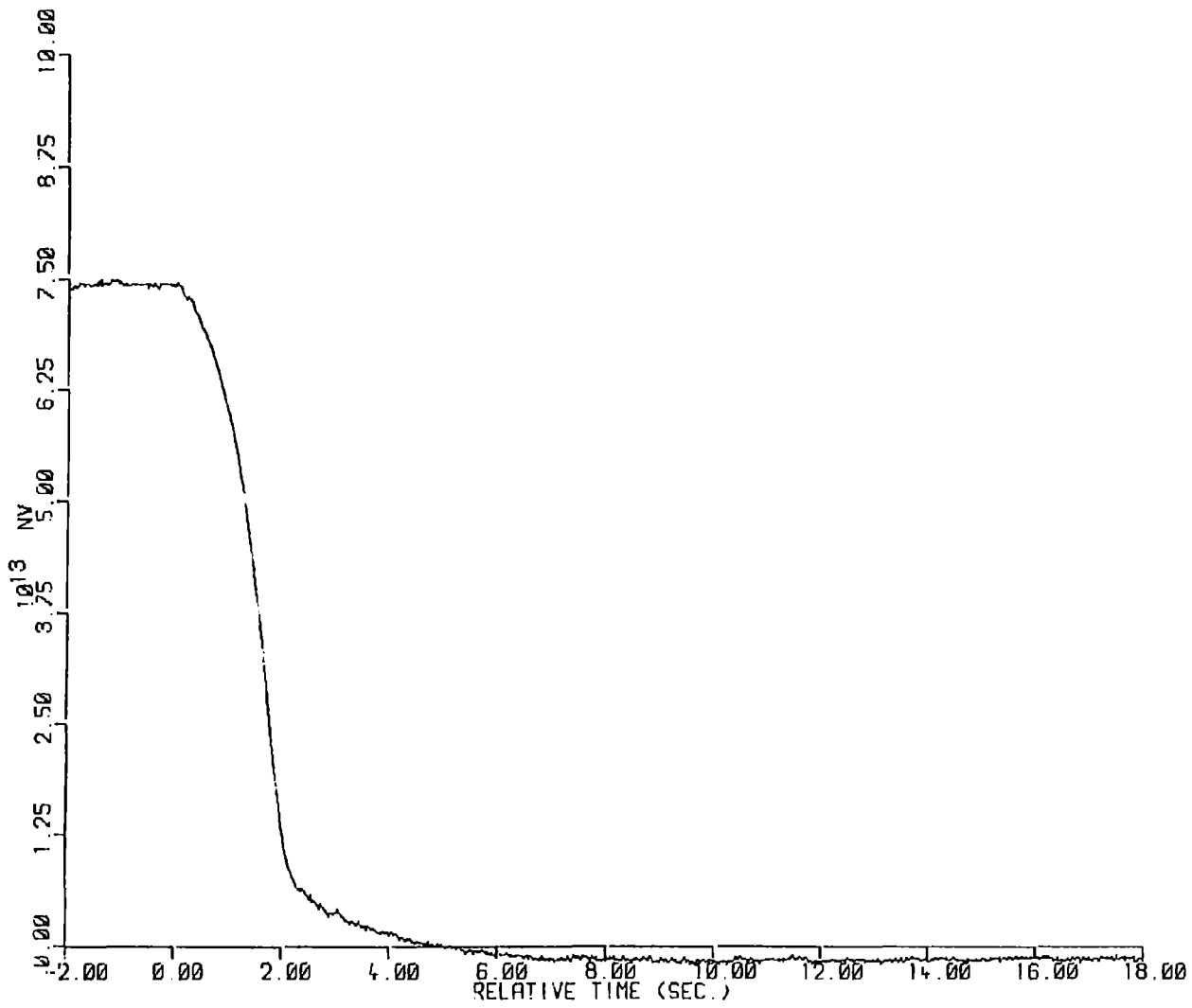

Figure 4-15. Compensated In-Core Flux - Loss of Flow - SPND N10 Level 2

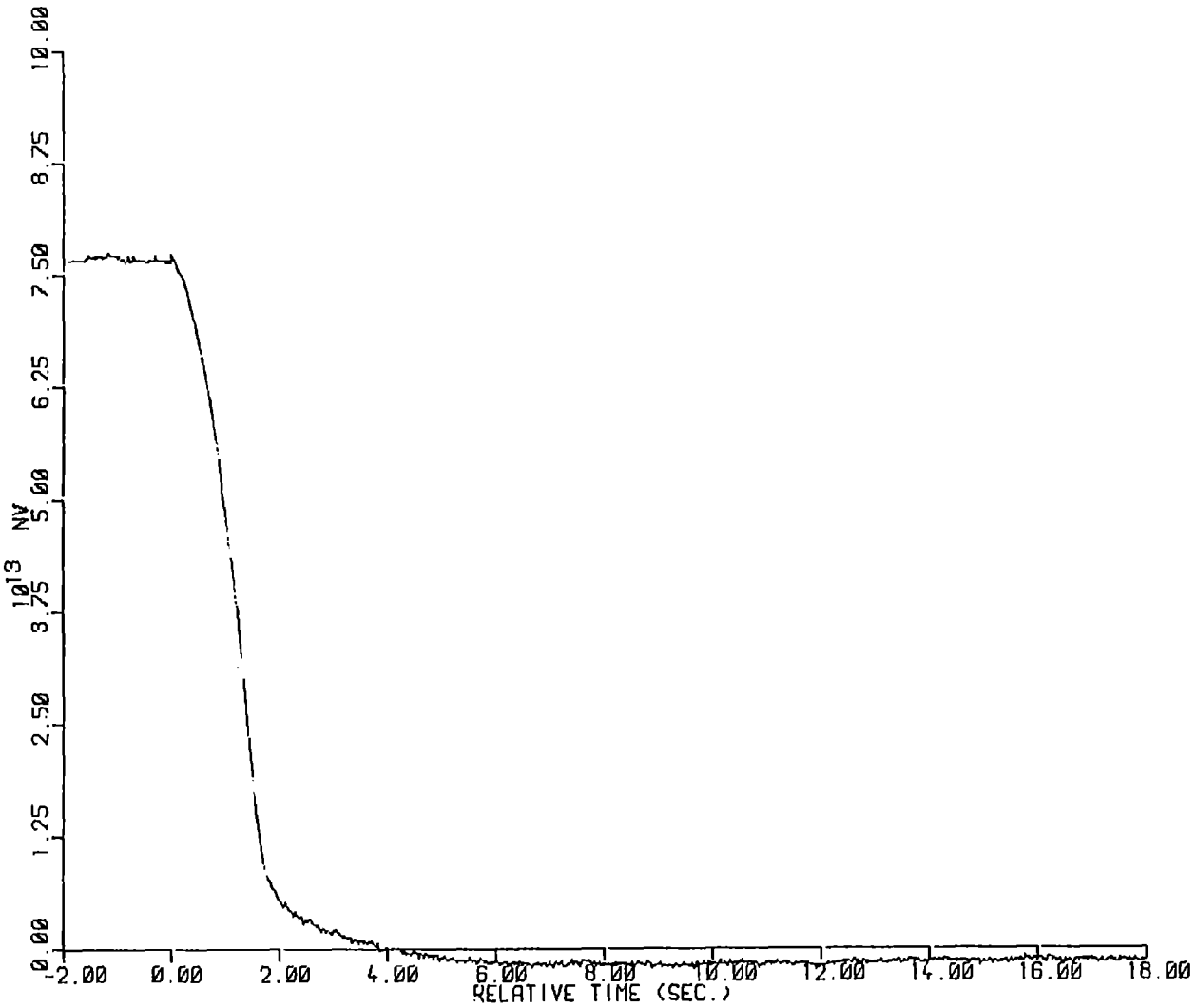

Figure 4-16. Compensated In-Core Flux - Loss of Flow - SPND N10 Level 3

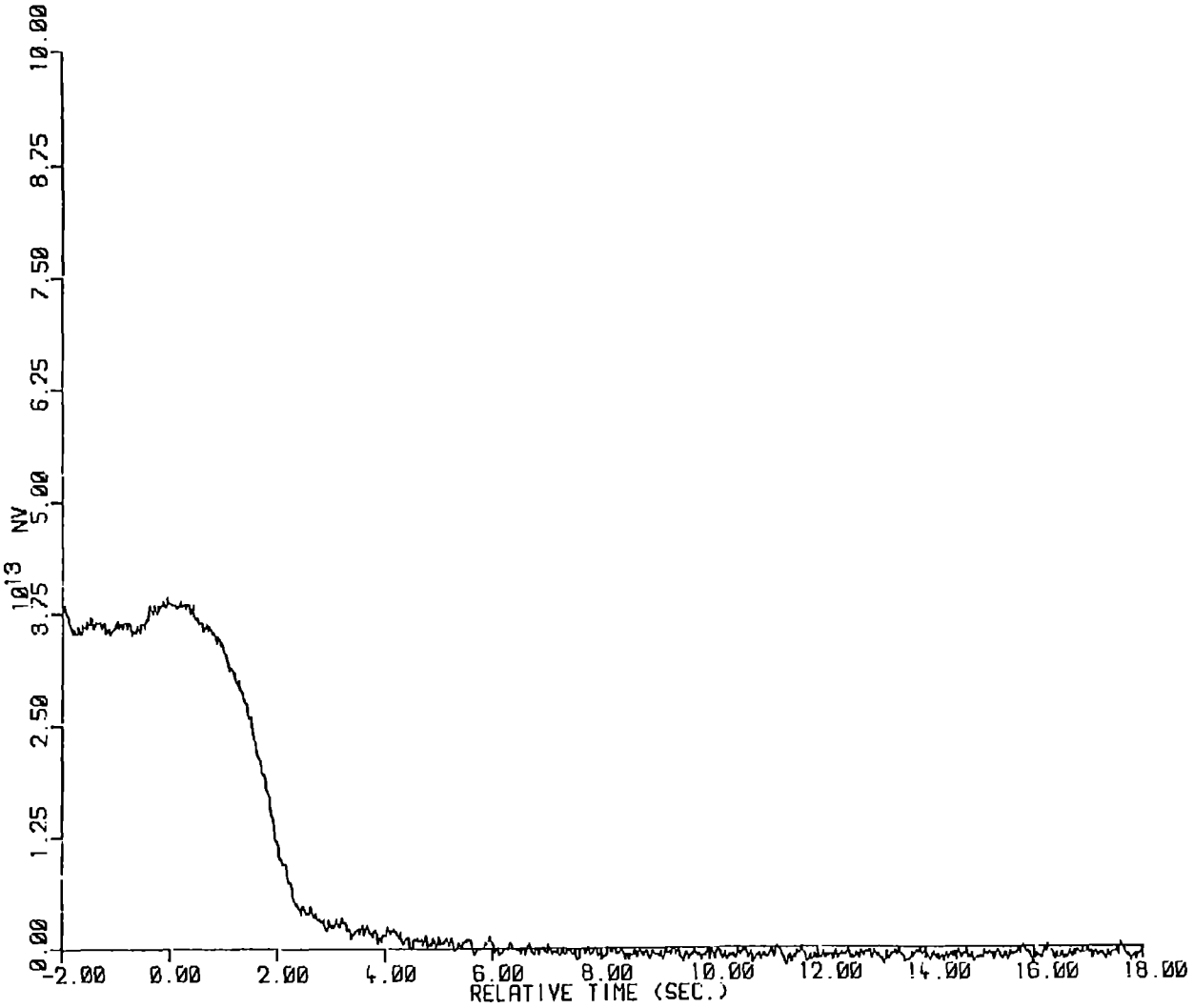

Figure 4-17. Compensated In-Core Flux - Loss of Flow - SPND C12 Level 1

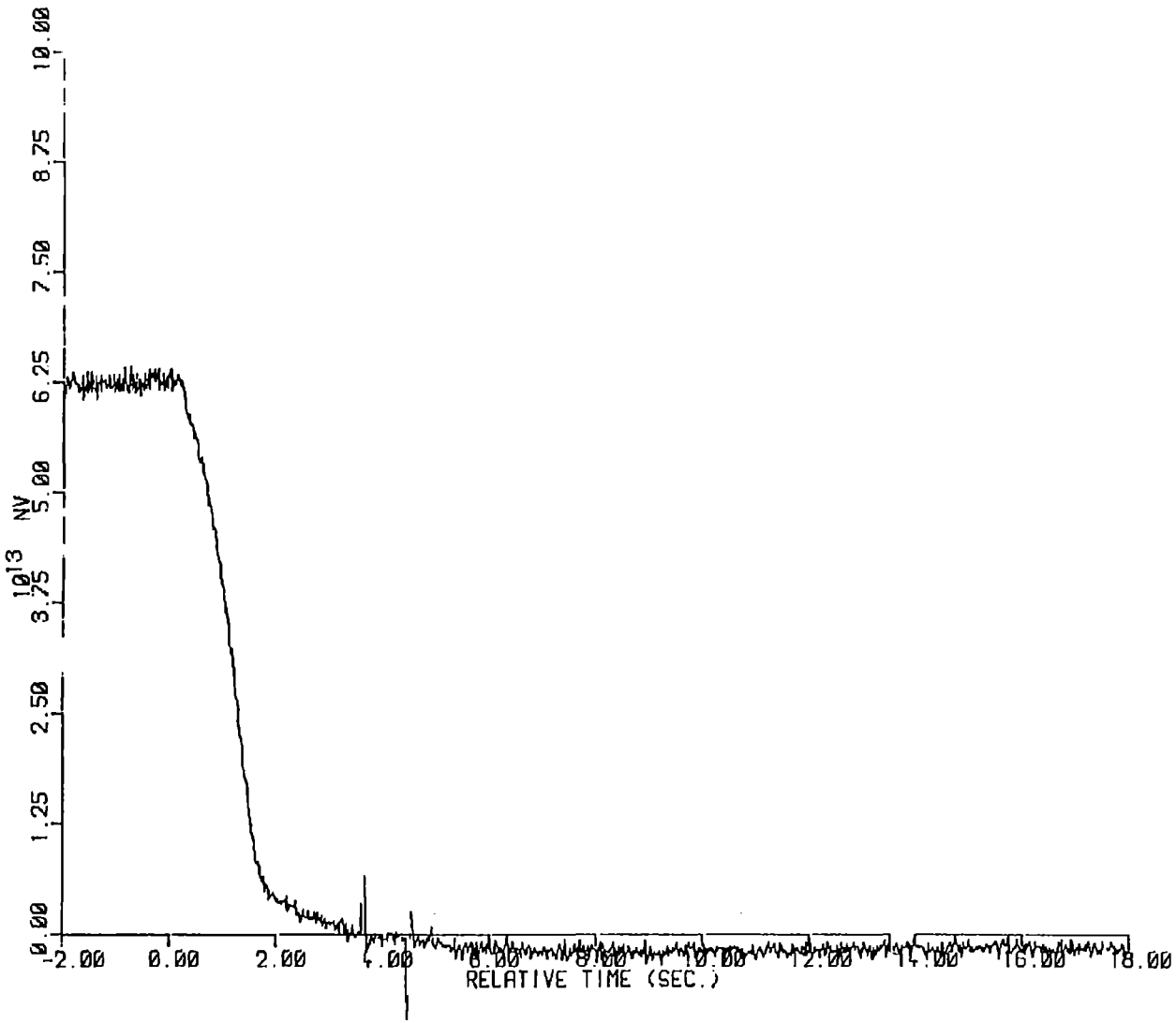

Figure 4-18. Compensated In-Core Flux - Loss of Flow - SPND C12 Level 3

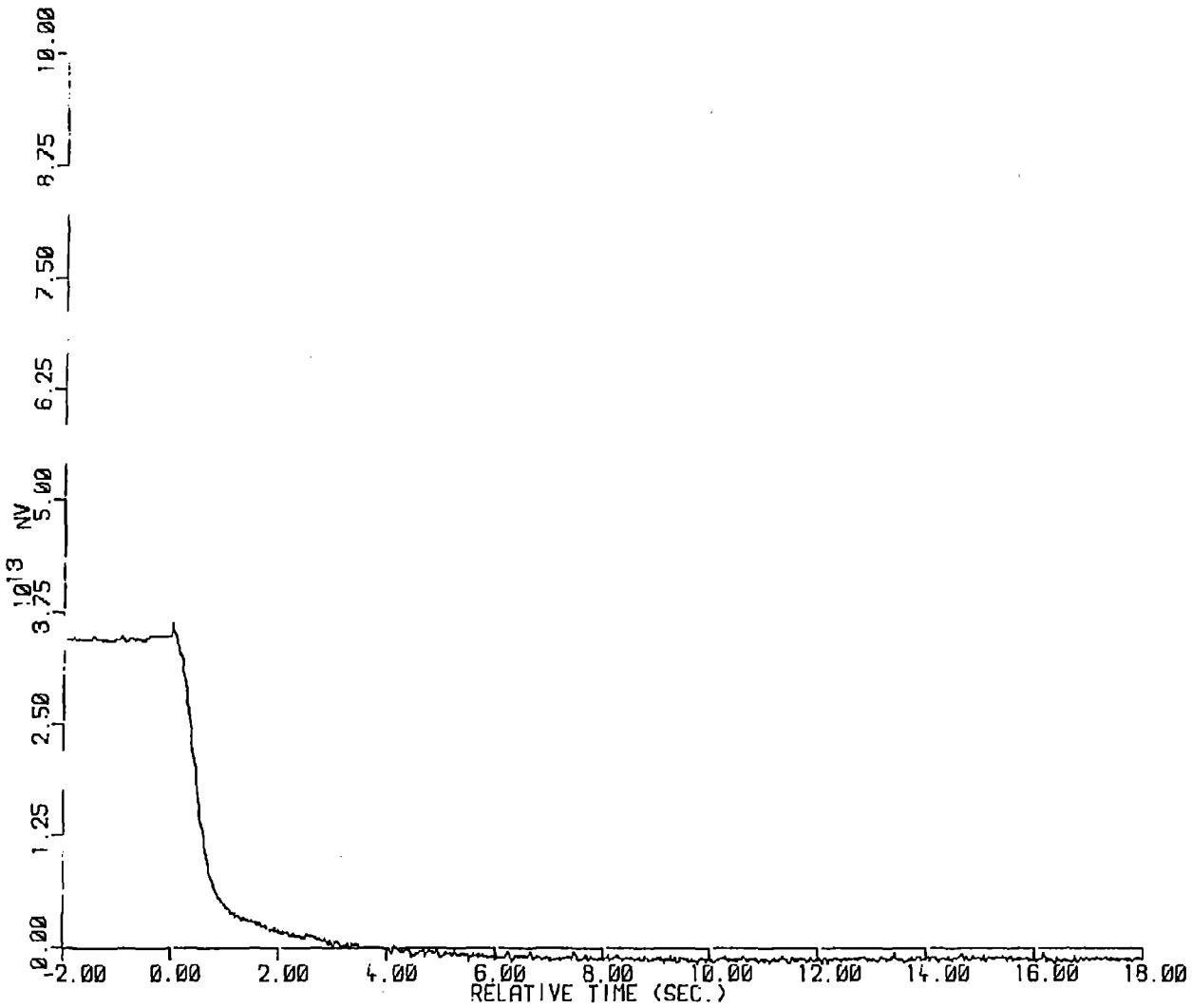

Figure 4-19. Compensated In-Core Flux - Loss of Flow - SPND C12 Level 5

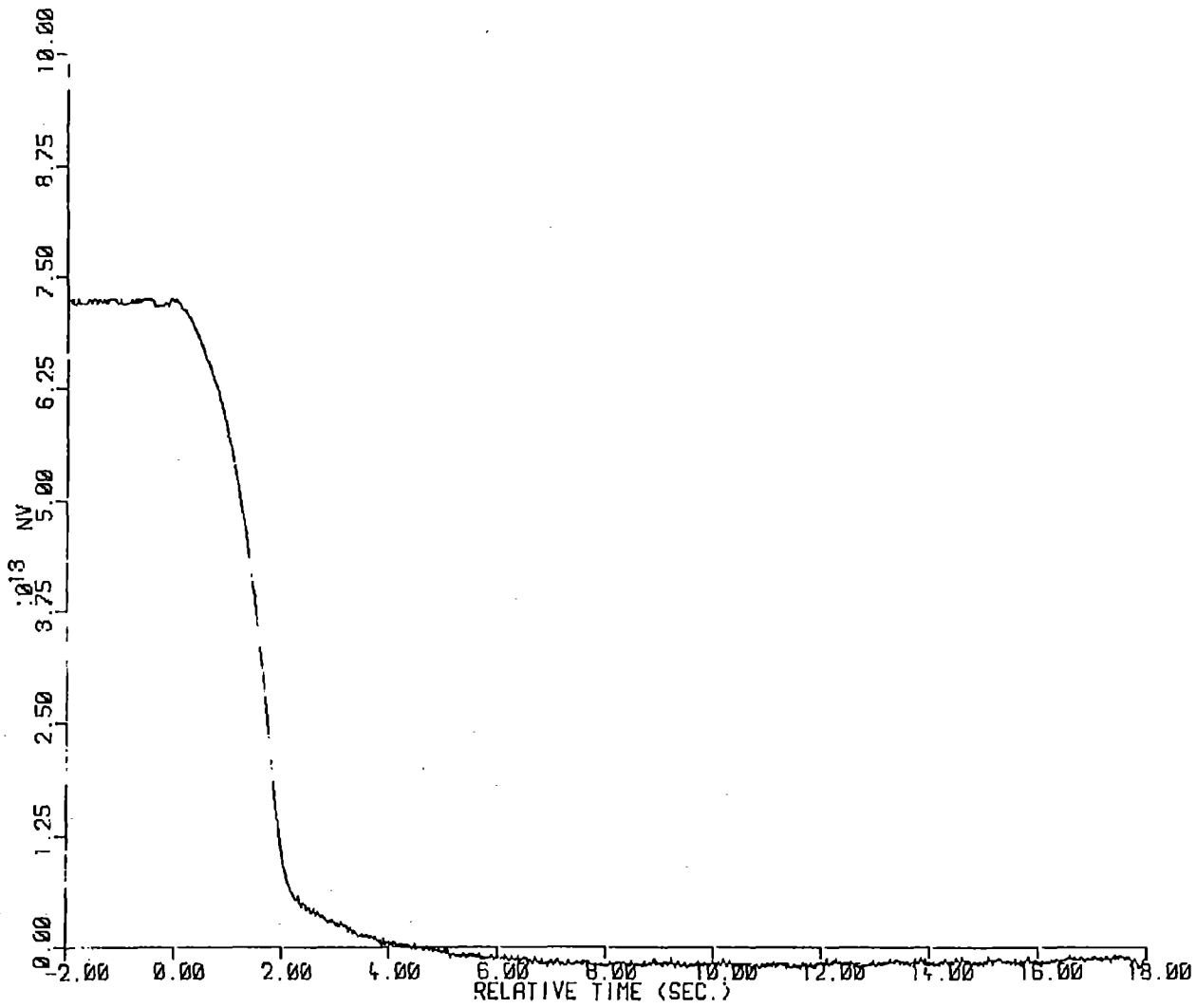

Figure 4-20. Compensated In-Core Flux - Loss of Flow - SPND G14 Level 2

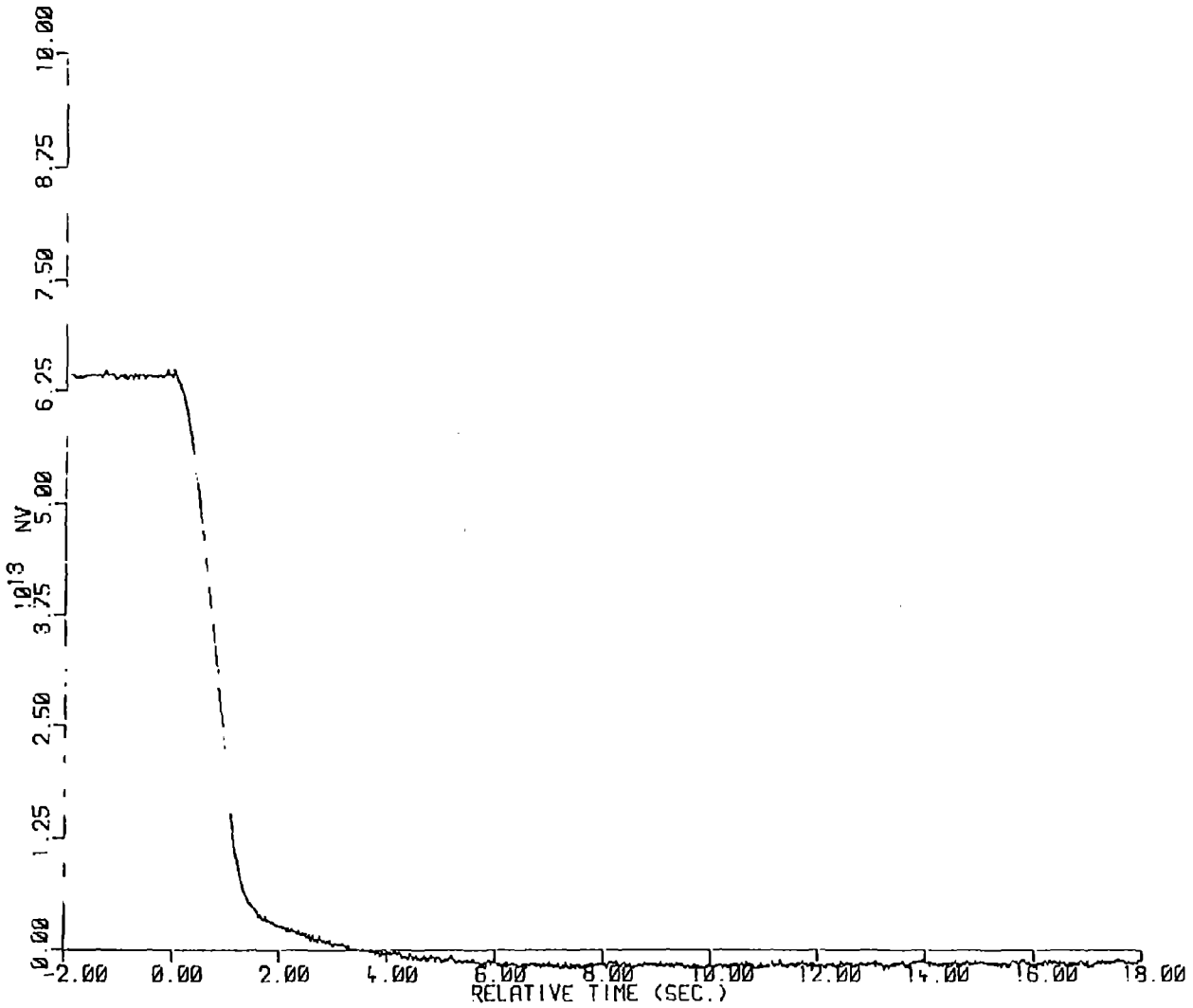

Figure 4-21. Compensated In-Core Flux - Loss of Flow - SPND G14 Level 4

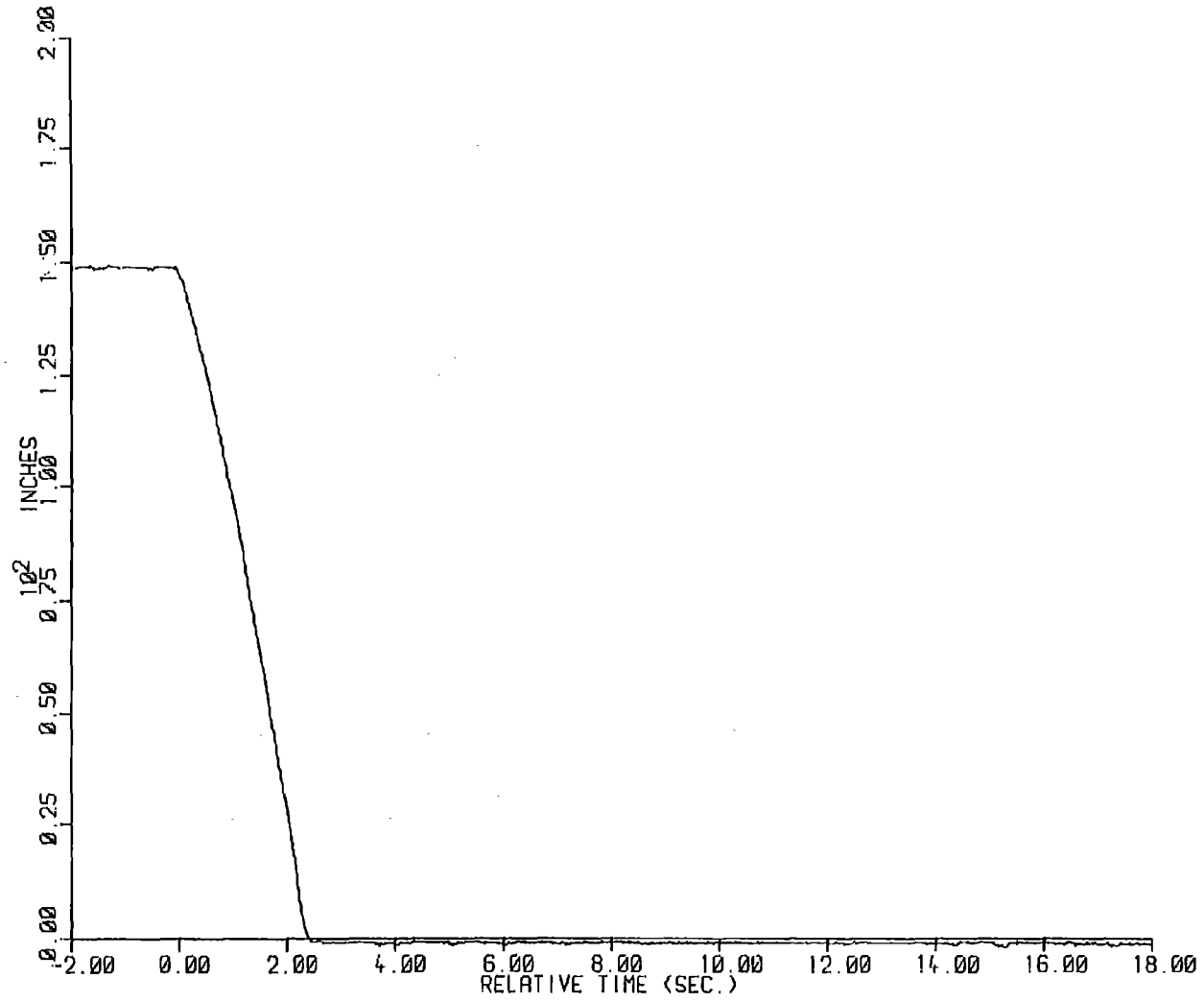

Figure 4-22. CEA Position - Loss of Flow - CEA 17

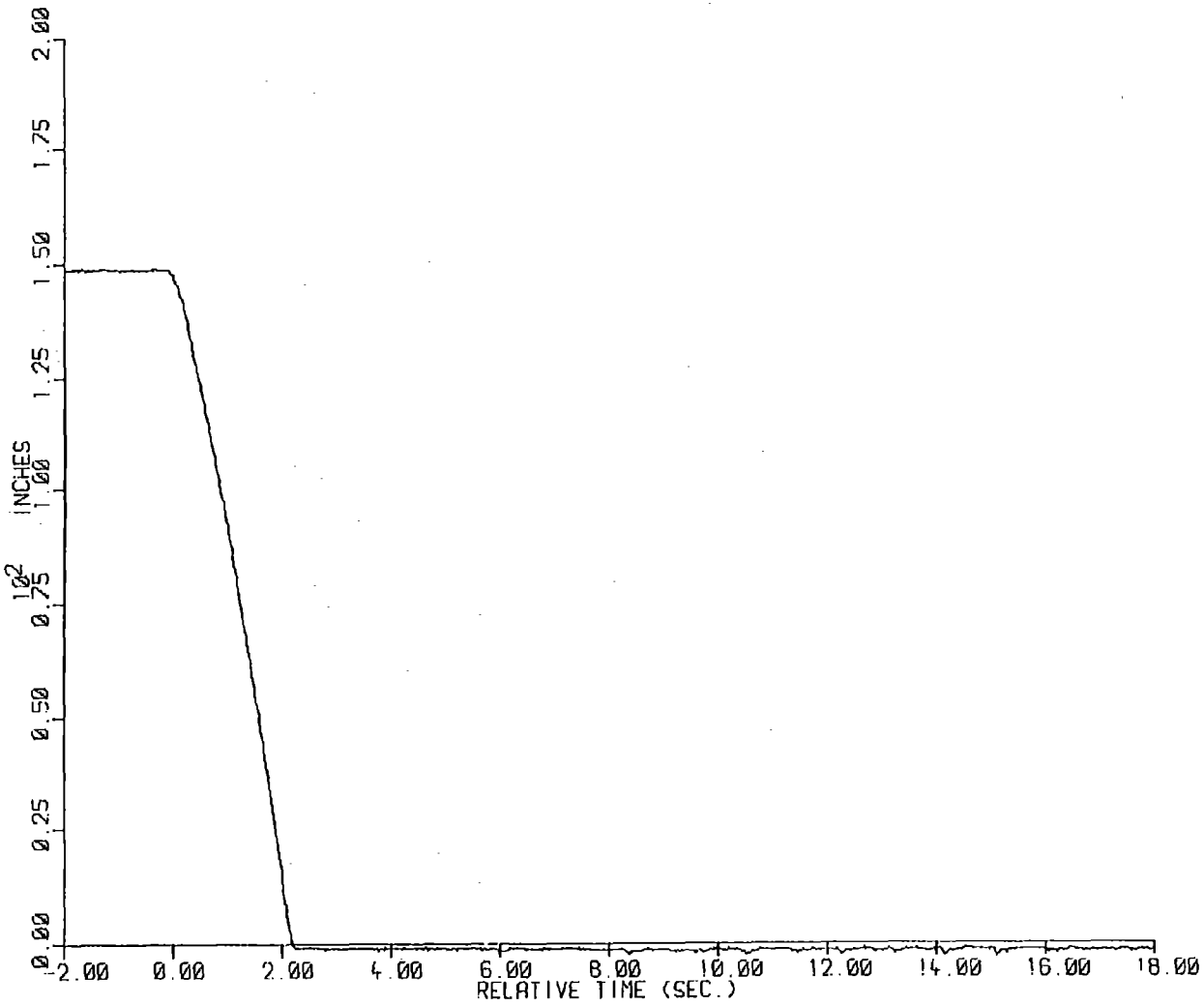

Figure 4-23. CEA Position - Loss of Flow - CEA 27

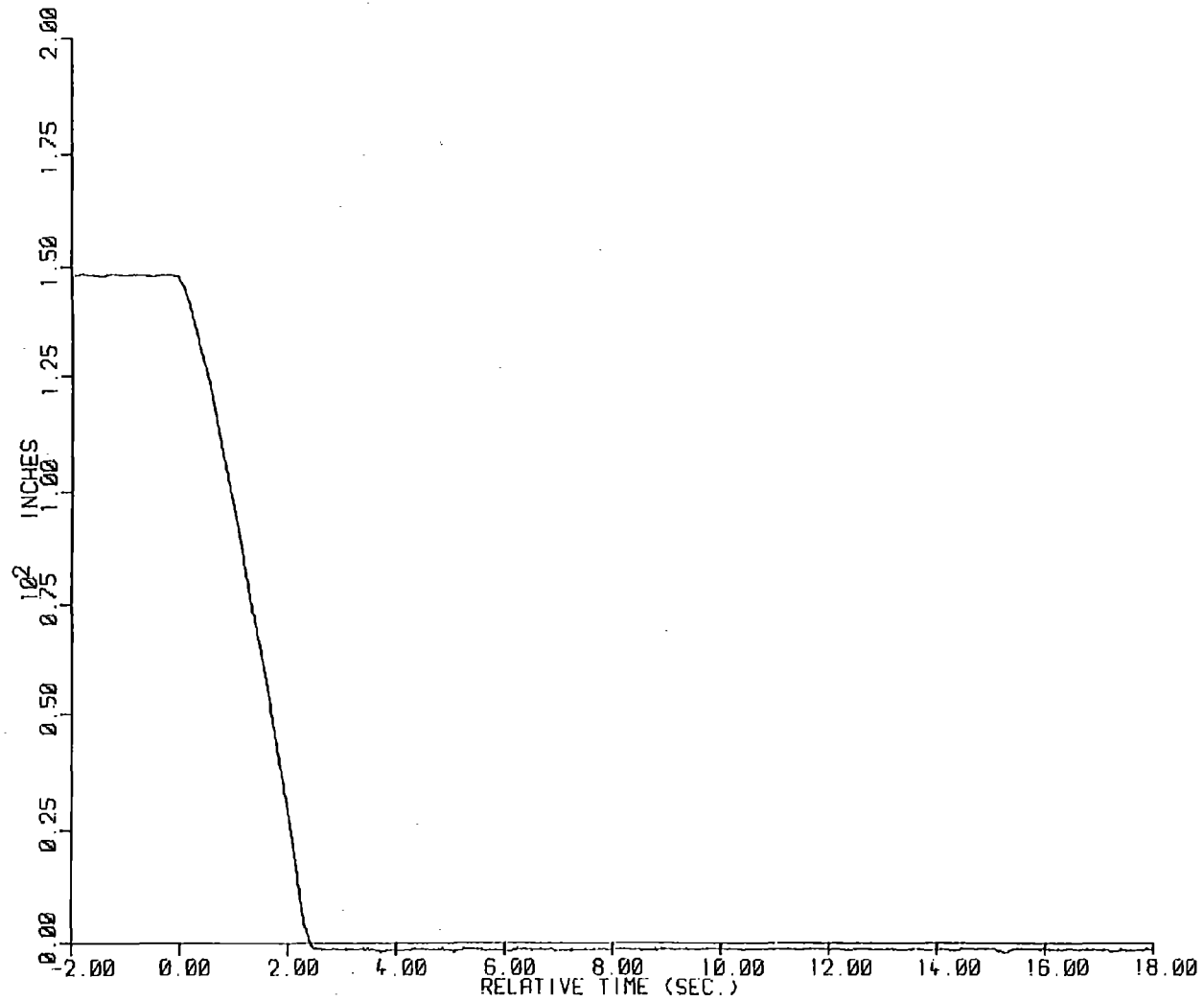

Figure 4-24. CEA Position - Loss of Flow - CEA 41

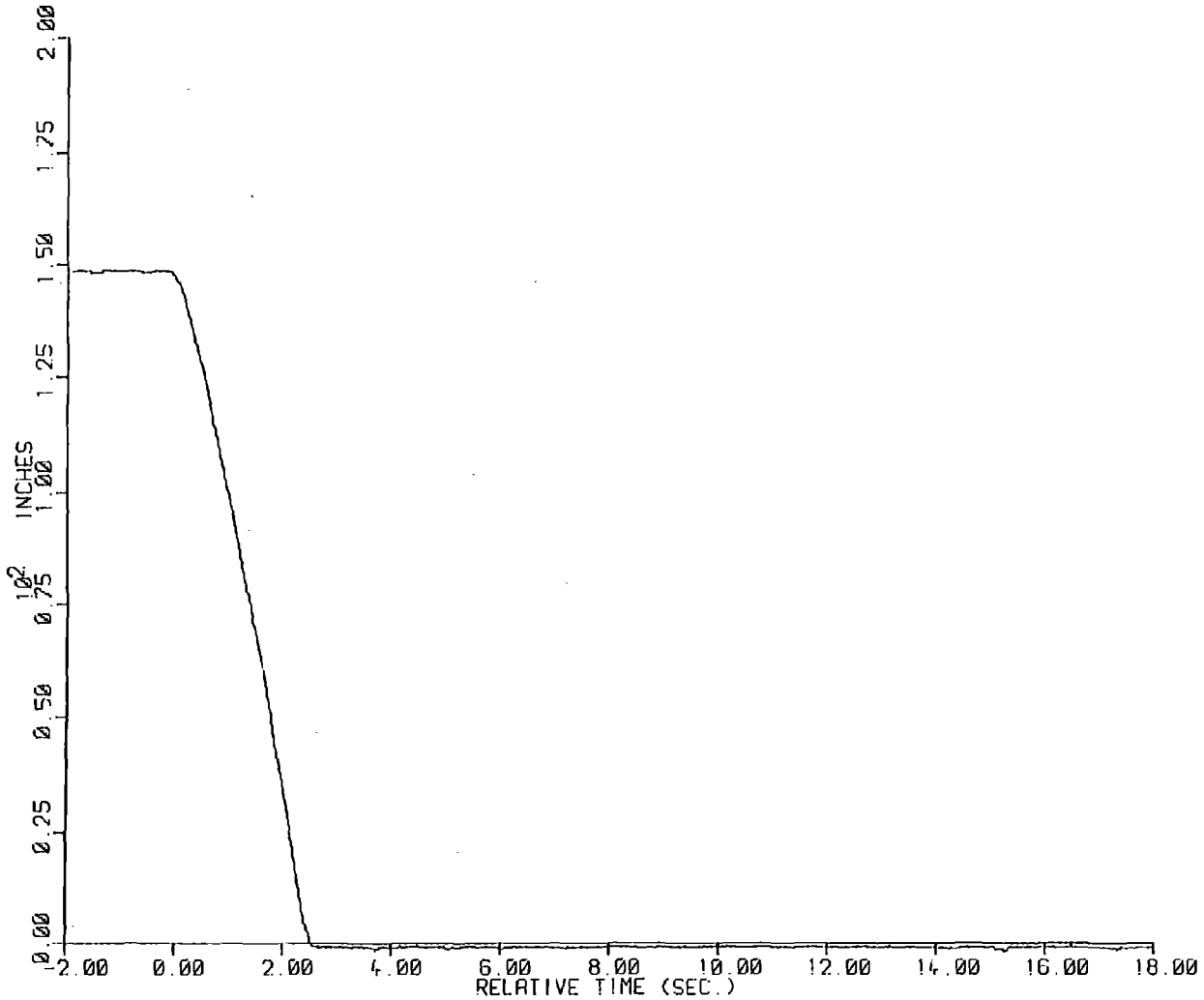

Figure 4-25. CEA Position - Loss of Flow - CEA 65

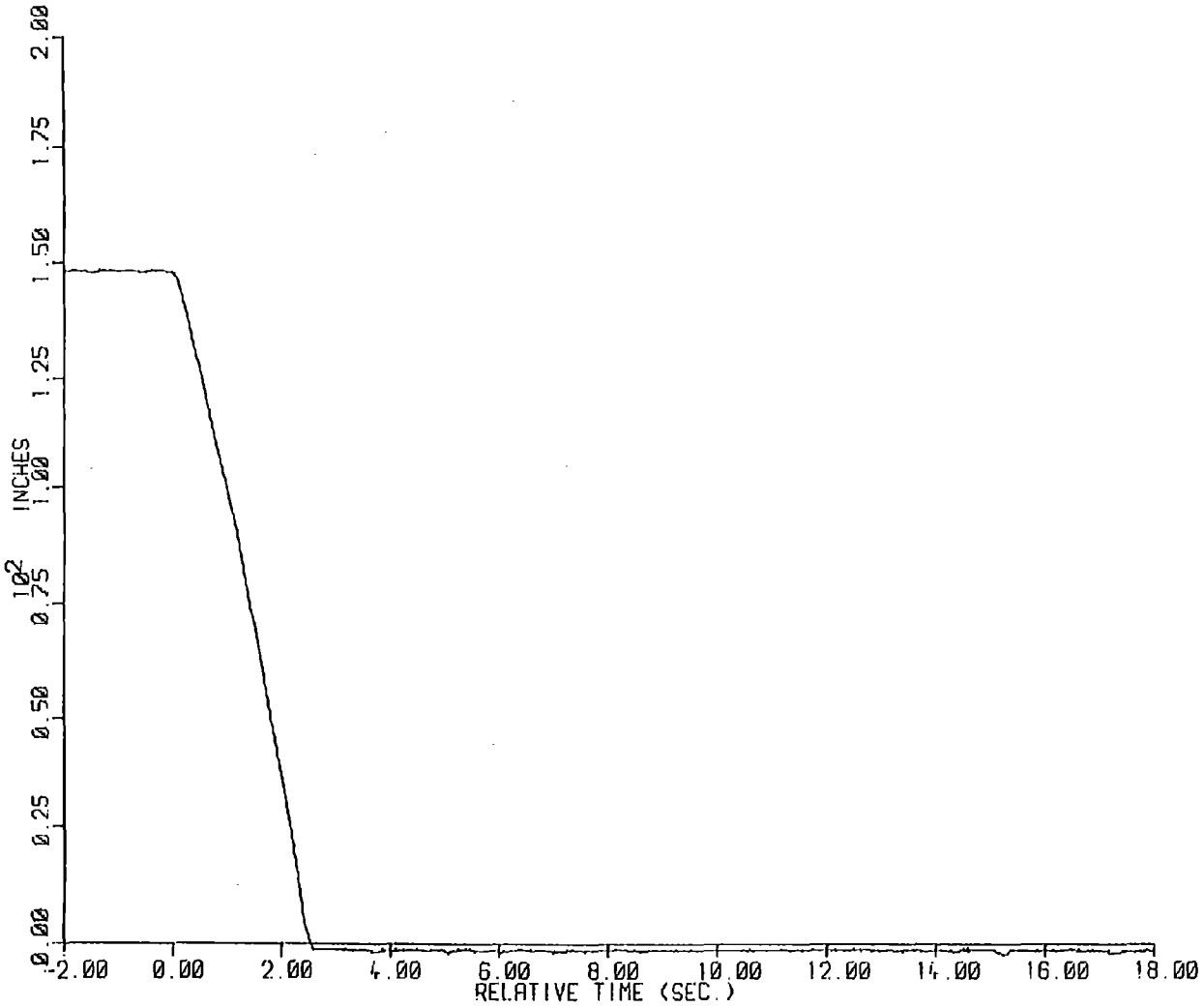

Figure 4-26. CEA Position - Loss of Flow - CEA 75

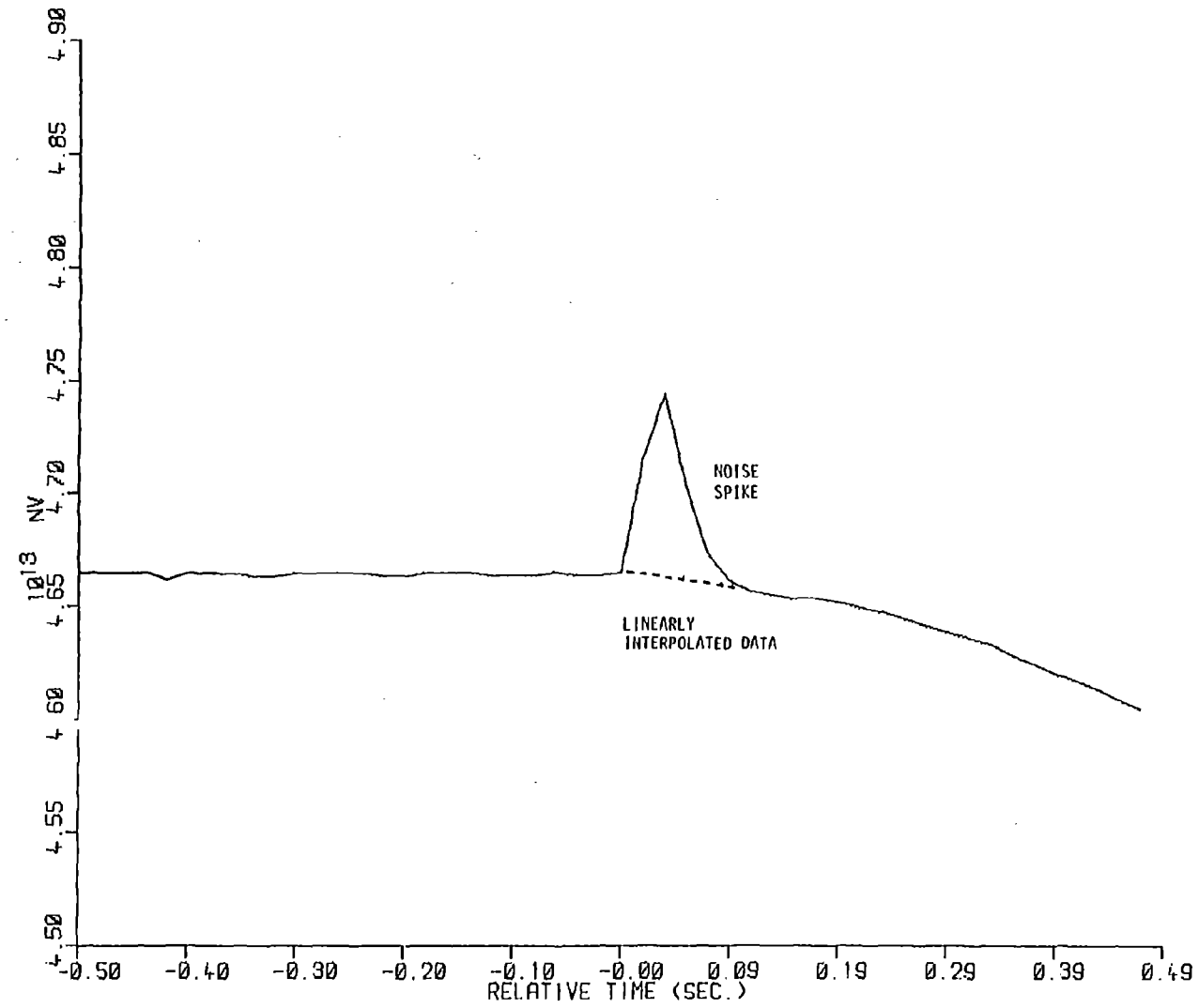

Figure 4-27. Sample of Wild-Point Editing Scheme

Process Parameter Transients

Figures 4-2 through 4-21 show the background-corrected, compensated in-core flux during the loss of flow at various radial and axial core locations. The radial coordinates and axial positions of the in-core detectors are shown in Figures 2-1 and 2-2. The compensation methodology used to compute the real-time neutron flux transient is discussed in the Appendix.

Figures 4-22 through 4-26 show the positons of various CEAs in the core during the loss of flow using the same time base as shown for the in-core flux.

The time scales for the in-core flux and CEA positon traces are synchronized using the common timing signal. Time zero corresponds to the time of turbine trip, which occurs 0.4 seconds after the reactor coolant pumps were tripped.

Wild-Point Editing

A spurious electrical noise spike was observed in the detector signals and CEA position recorder signals during the loss of flow at the time of turbine trip. These spikes would be magnified by the dynamic compensation algorithm to produce distorted neutron flux traces if not removed. In order to overcome this difficult, a wild-point editing scheme was employed, replacing the unwanted noise spike by linearly interpolated data between the last good data point before the spike and the first good data point after the spike. An illustration of the wild-point editing scheme is shown in Figure 4-27. Note that the editing scheme does not affect the signal trace except to eliminate the noise spike.

FULL-LENGTH CEA DROP

Description of Test

The initial core conditions for the full-length CEA drop are given in Table 4-5. The reactor core was stable with all rods out (ARO) equilibrium xenon conditions, 700 PPM boron, and an Axial Shape Index of approximately 0.0 SIU. The core average burnup at the time of the CEA drop was approximately 2300 MWD/T. The CEA drop was initiated by opening the CEA 5-60 disconnect circuit breaker. Immediately following the CEA drop, the turbine load limit was adjusted to match the resulting decrease in average core power (approximately 7 percent of full power). An asymptotic core power level was achieved approximately 3.5 seconds after the initiation of the CEA drop. After 600 seconds, the reactor was stable at a slightly reduced core average power level (approximately 43 percent of full power).

The core power distributions before and after the full-length CEA drop are shown in Figures 4-28 and 4-29, respectively.

Recorded Signal Locations

The locations of the rhodium in-core and background detector signals recorded during the full-length CEA drop are given in Tables 4-6 and 4-7, respectively. The dropped CEA (5-60) is located at core position H-2. The signals from two detectors (1 SPND and 1 background detector) did not have the time behavior expected for the full-length CEA drop. This non-characteristic time behavior was also observed during the part-length CEA drop for the same two detectors, which remain connected for both tests. These data were therefore judged to be from incorrect hook-ups and are not included in the report. Data which were judged to be noisy are also not included.* These data are indicated in the legends of Tables 4-6 and 4-7.

Process Parameter Transients

Figures 4-30 through 4-48 show the background-corrected, compensated in-core flux during the full-length CEA drop at various radial and axial core locations. The radial coordinates and axial positions of the in-core detectors are shown in Figures 2-1 and 2-2. The compensation methodology used to compute the real-time neutron flux transient is discussed in the Appendix.

*Visual inspection of the compensated in-core detector signals was used to determine those signals which could provide meaningful data for code qualification.

Table 4-5

INITIAL CORE CONDITIONS FOR FULL-LENGTH CEA DROP

Core Power, MWT	1391 (49.4%)
Axial Shape Index (SIU)	~ 0.0
Boron Concentration, PPM	700
Core Mass Flow Rate, 10^6 lbm/hr	134.0
Pressurizer Pressure, psia	2246
Core Inlet Coolant Temperature, °F	546
Core Outlet Coolant Temperature, °F	577
CEA Position	ARO

LEGEND:

Box Number - Instrument Number
Integrated Assembly Power, MWTH
Assembly Axial Shape Index, SIU
Assembly Relative Power Fraction

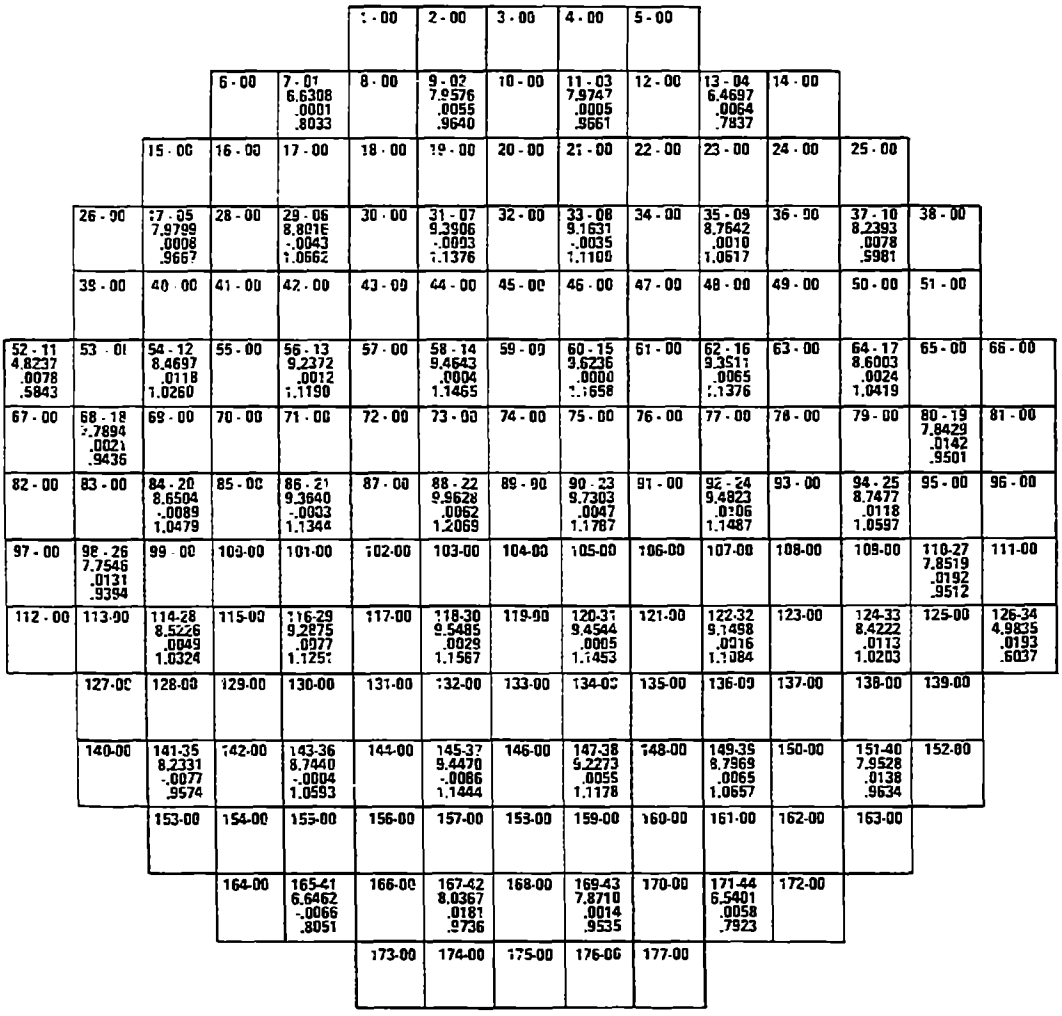

Figure 4-28. Core Power Distribution Before Full-Length CEA Drop - 1/11/80, 0:29:59

LEGEND:

Box Number - Instrument Number
Integrated Assembly Power, MWTH
Assembly Axial Shape Index, SIU
Assembly Relative Power Fraction

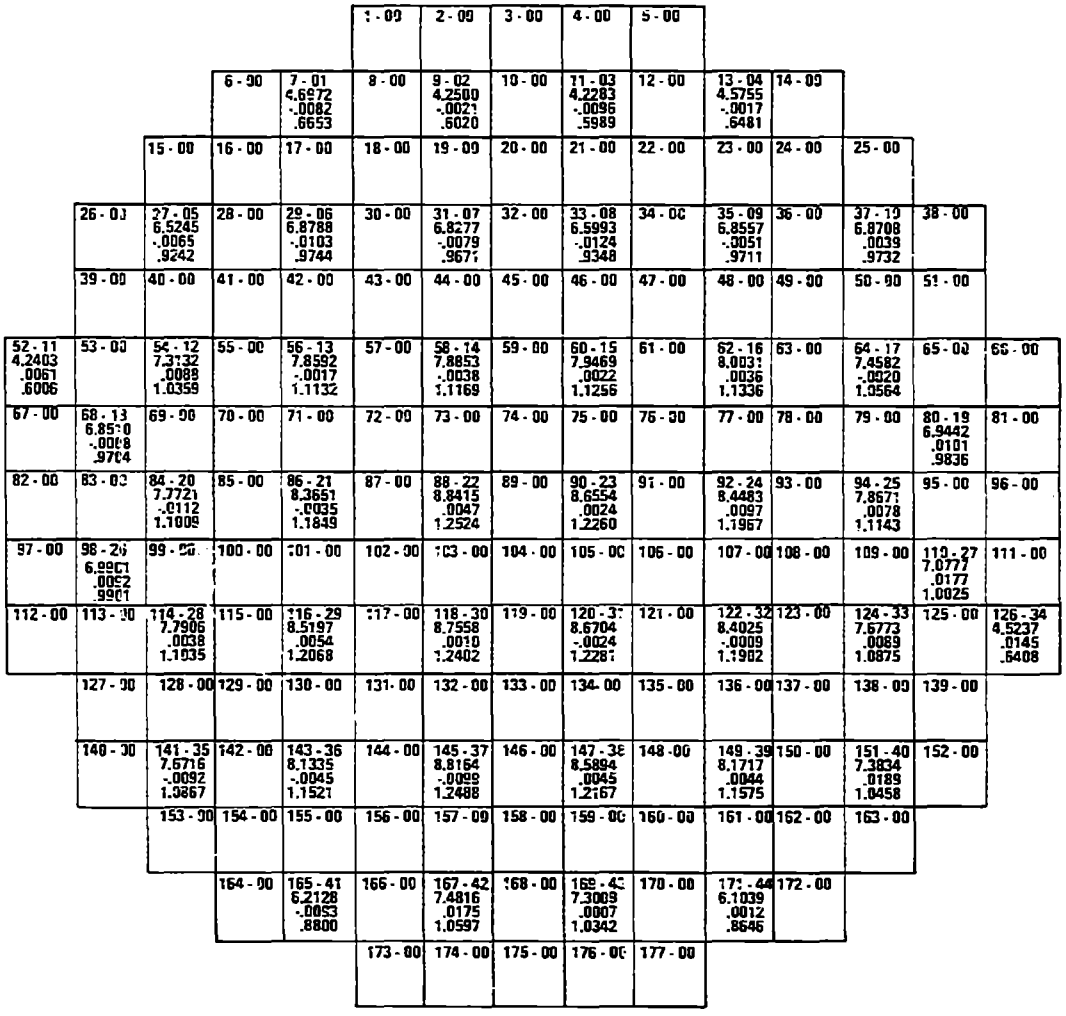

Figure 4-29. Core Power Distribution After Full-Length CEA Drop - 1/11/80, 0:44:11

Table 4-6

RECORDED RHODIUM IN-CORE DETECTOR LOCATIONS FOR FULL-LENGTH CEA DROP

Rh In-Core Detector Location	Level 1	2	3	4	5
E-2		X		X	
G-2	X	X	X	X	X
G-4		X		N	
G-6		X		X	
G-8	N	X	X	X	X
N-10		X	X		
C-12	N		W		X
G-14		X		X	

X = recorded in-core detector with good signal

N = recorded in-core detector with noisy signal

W = probable wrong hook-up

Table 4-7

RECORDED BACKGROUND DETECTOR LOCATIONS FOR
FULL-LENGTH CEA DROP

Background Detector Location	Level	
	Long	Short
E-2	X	X
E-4	X	X
G-6	X	X
P-7	X	X
G-8	X	X
N-10	X	X
C-12	W	X

X = recorded background detector with good signal

W = wrong hook-up

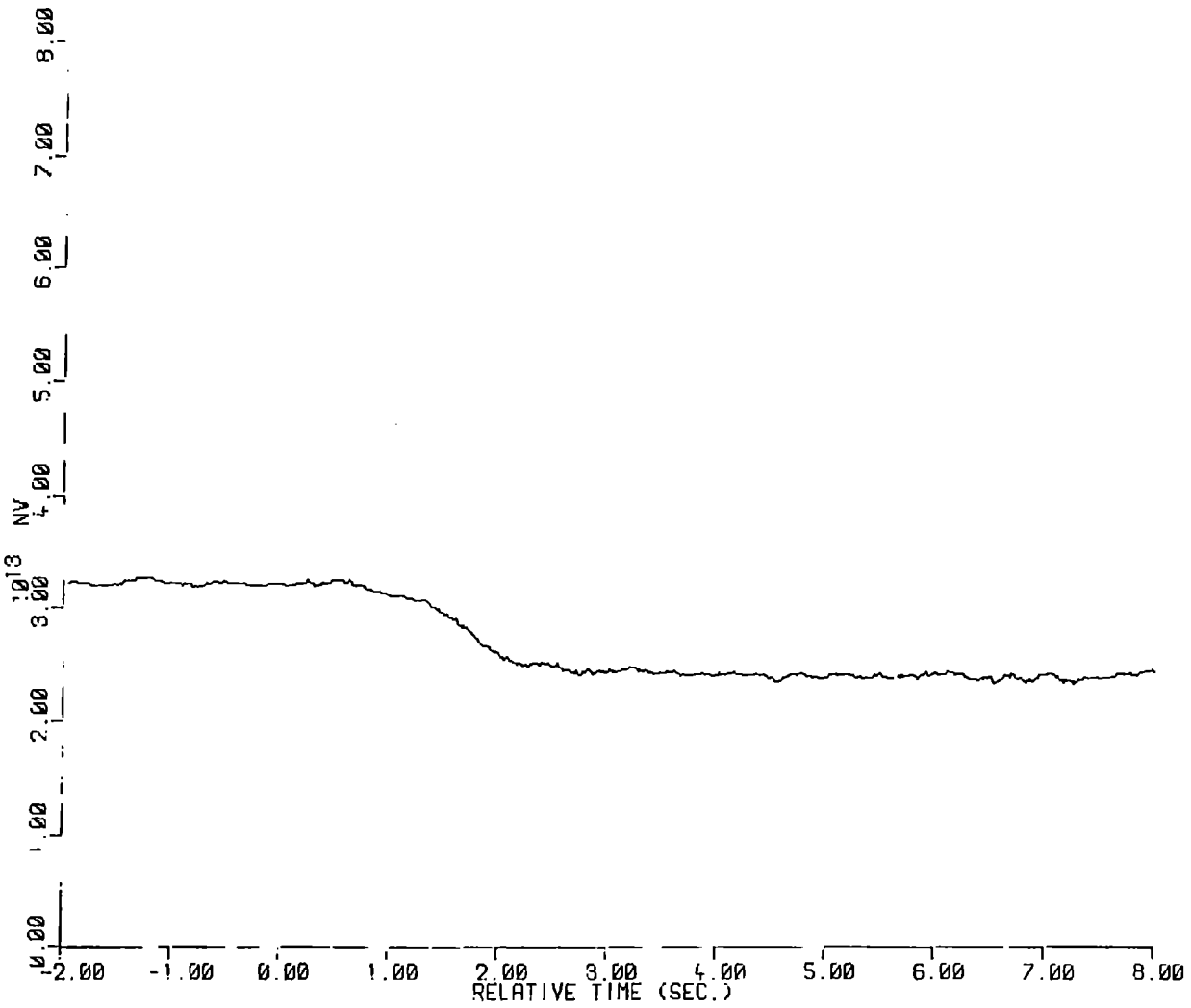

Figure 4-30. Compensated In-Core Flux - Full-Length CEA Drop - SPND E2 Level 2

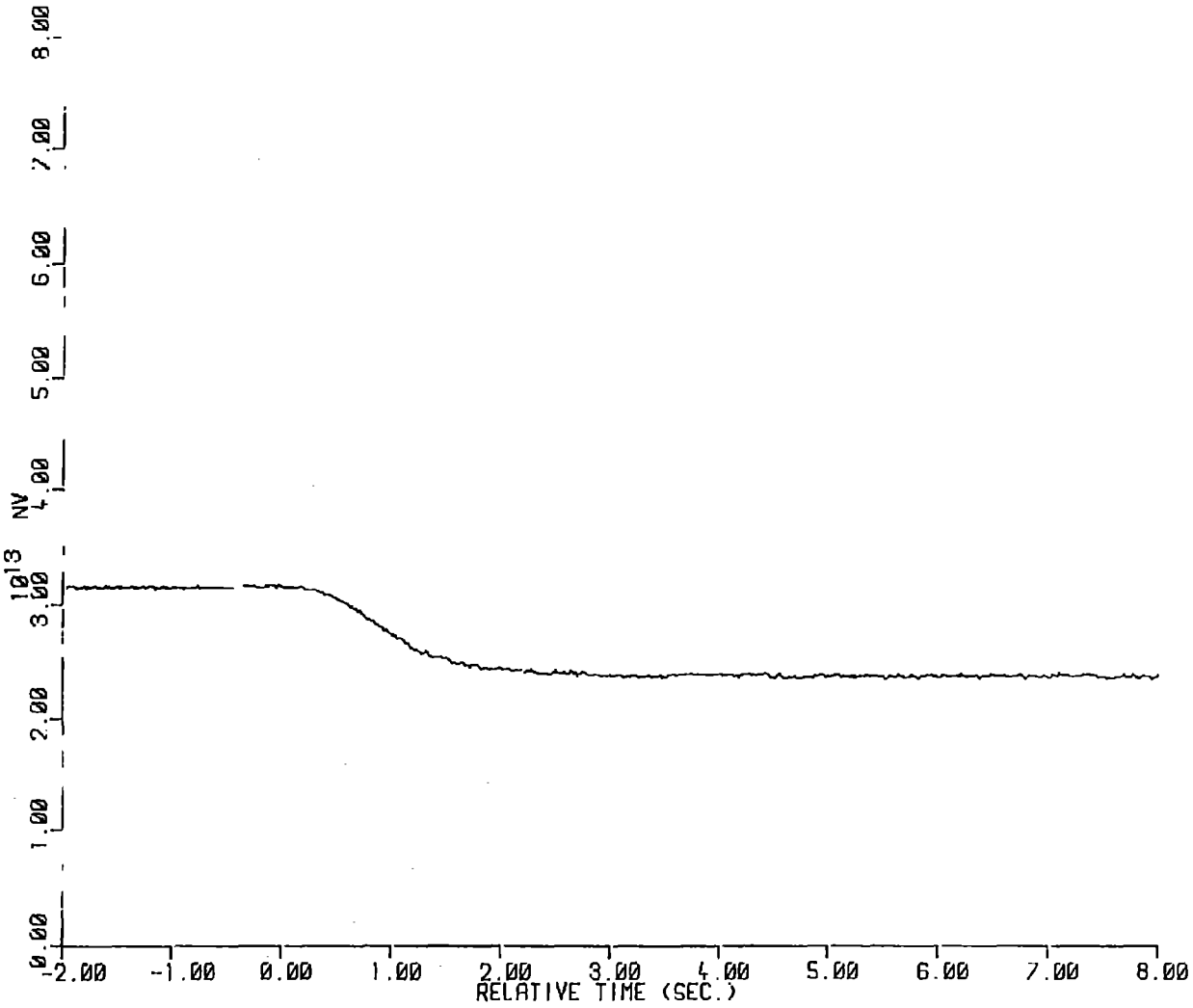

Figure 4-31. Compensated In-Core Flux - Full Length CEA Drop - SPND E2 Level 4

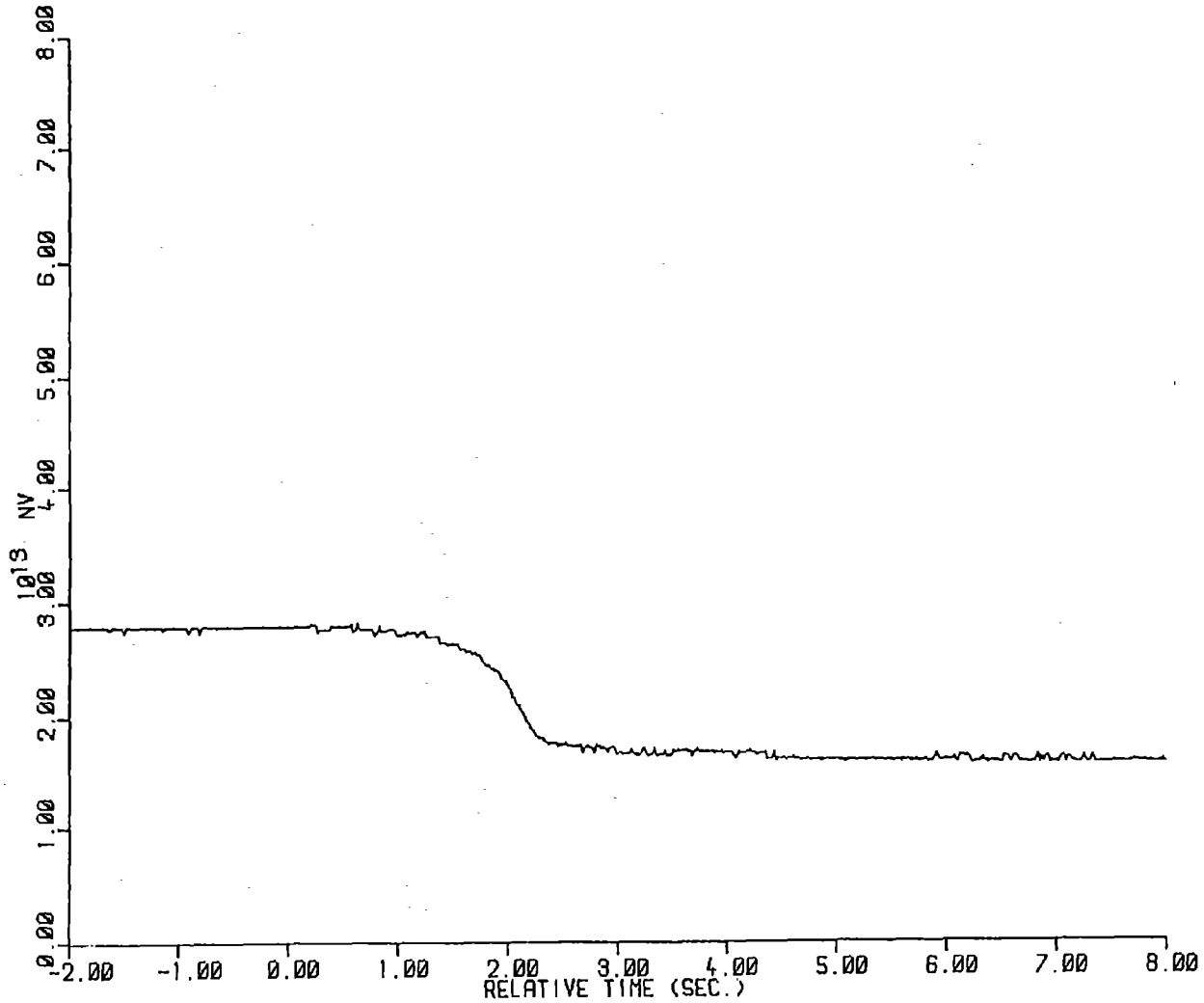

Figure 4-32. Compensated In-Core Flux - Full-Length CEA Drop - SPND G2 Level 1

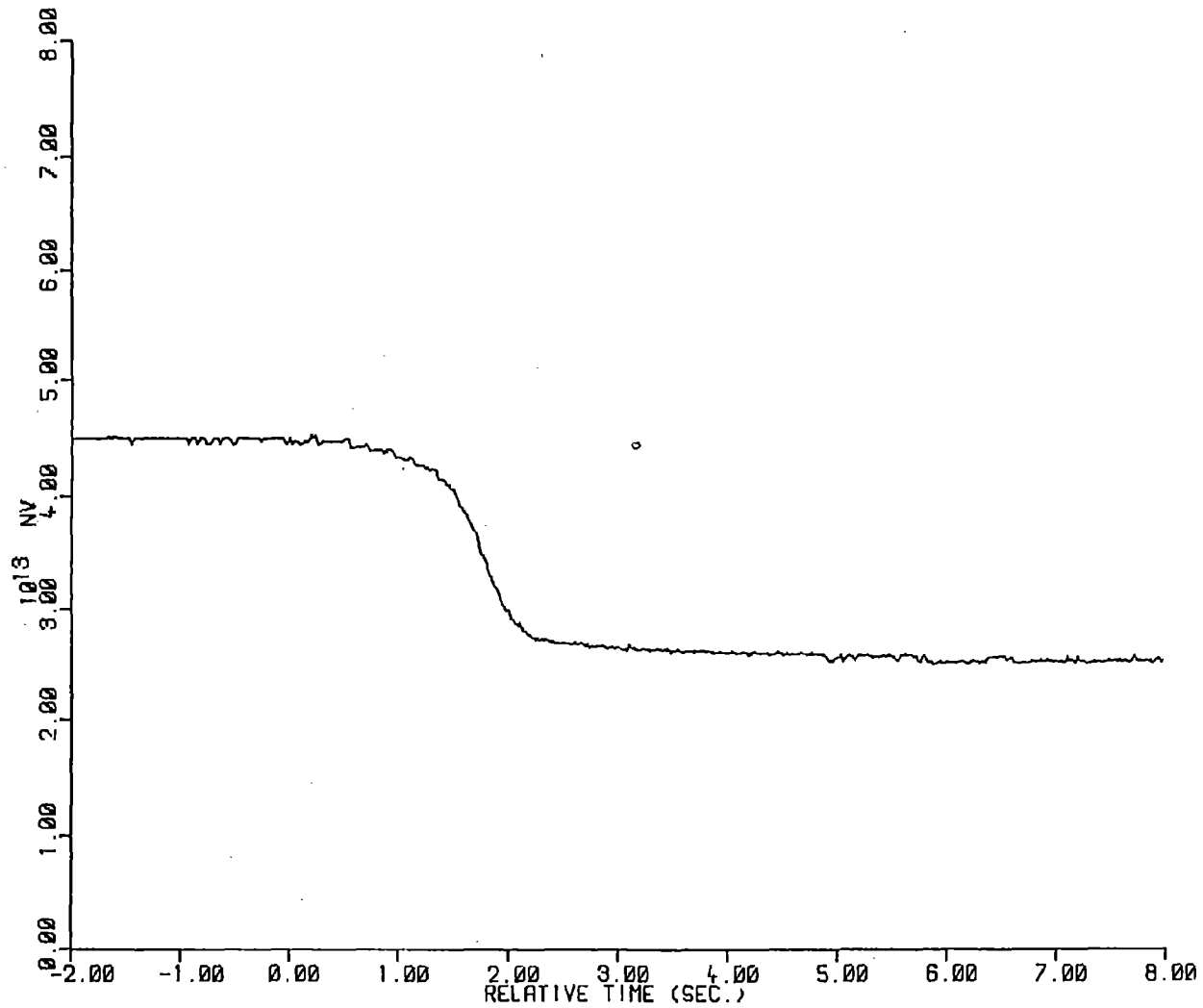

Figure 4-33. Compensated In-Core Flux - Full-Length CEA Drop - SPND G2 Level 2

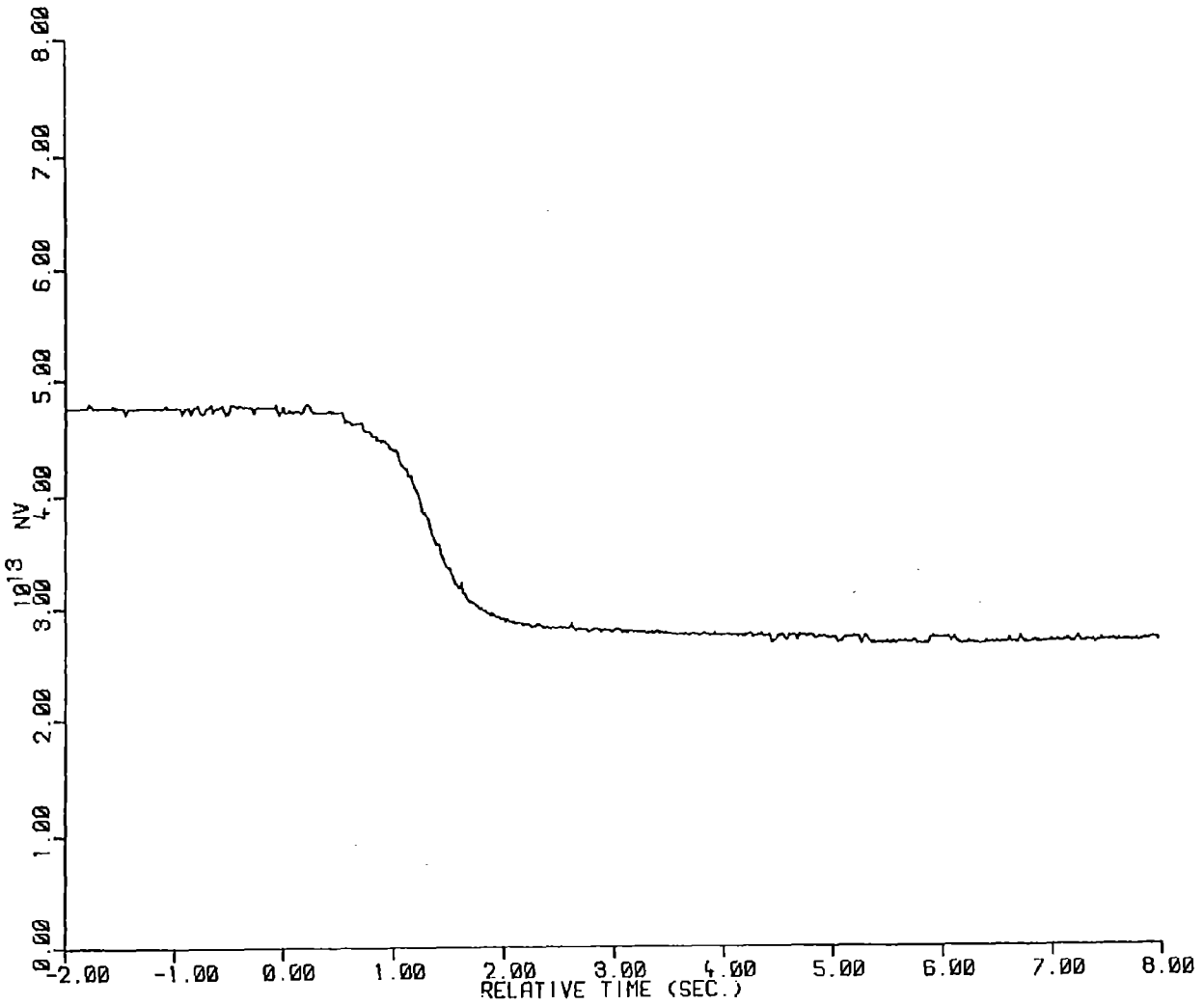

Figure 4-34. Compensated In-Core Flux - Full Length CEA Drop - SPND G2 Level 3

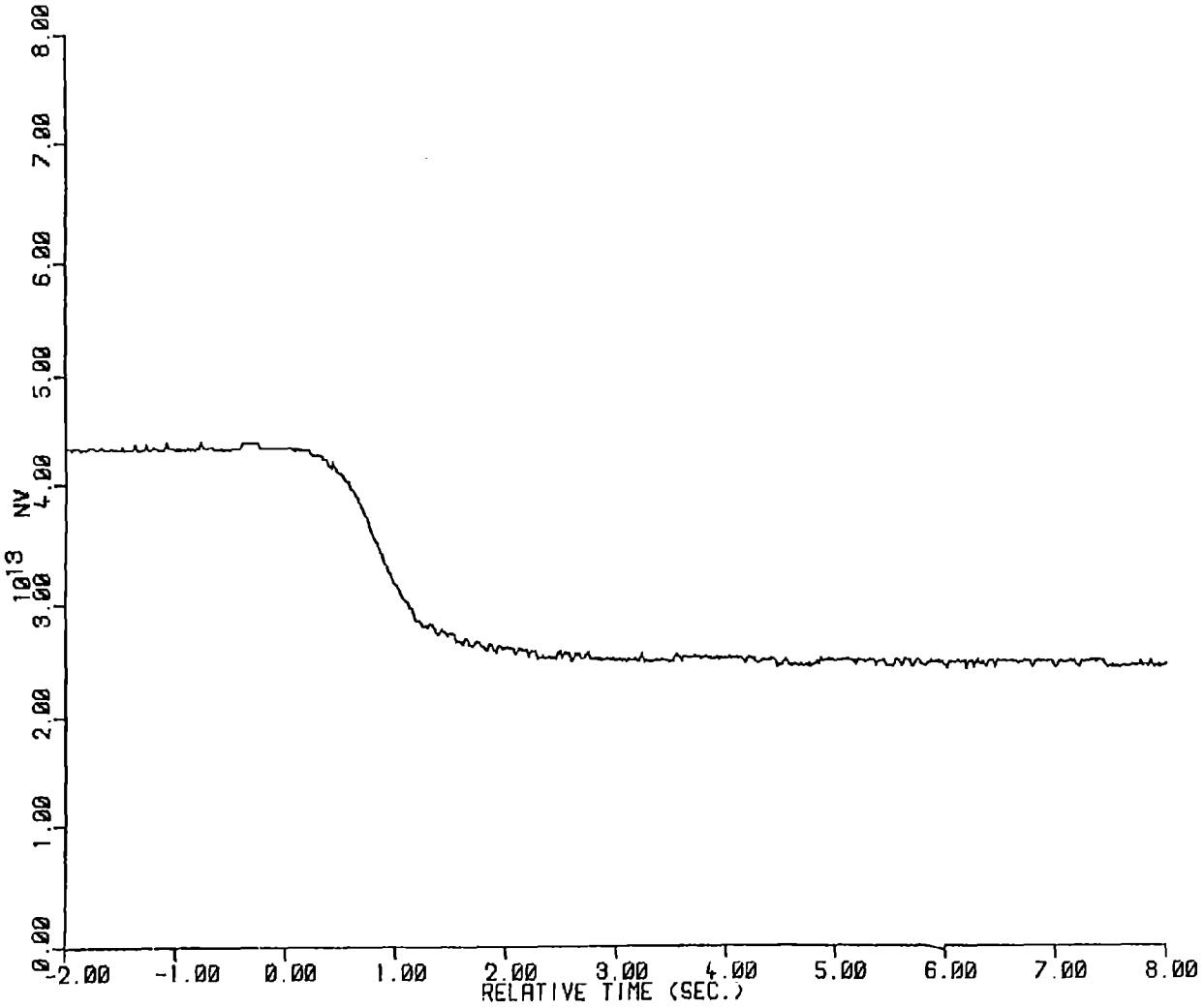

Figure 4-35. Compensated In-Core Flux - Full-Length CEA Drop - SPND G2 Level 4

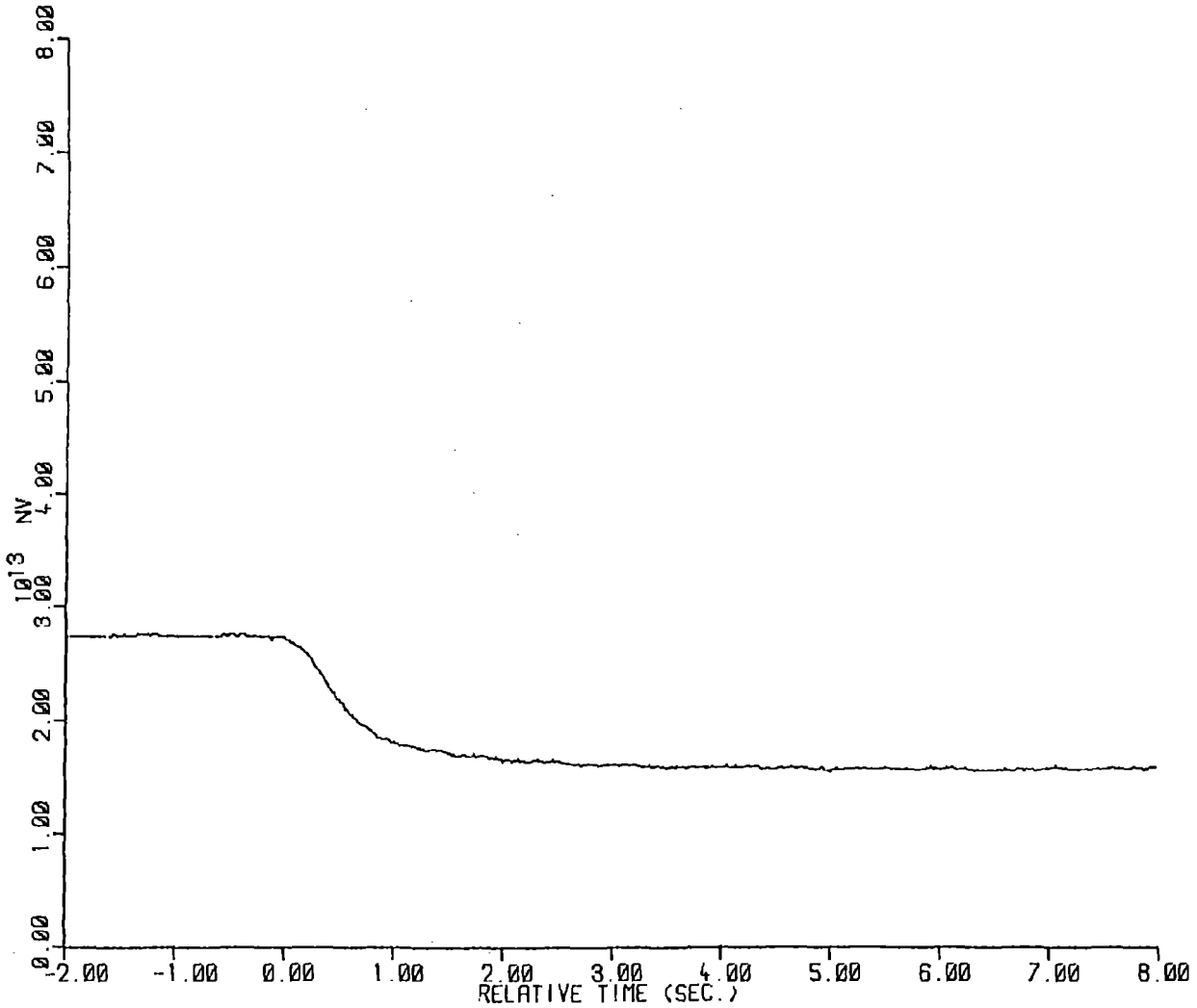

Figure 4-36. Compensated In-Core Flux - Full Length CEA Drop - SPND G2 Level 5

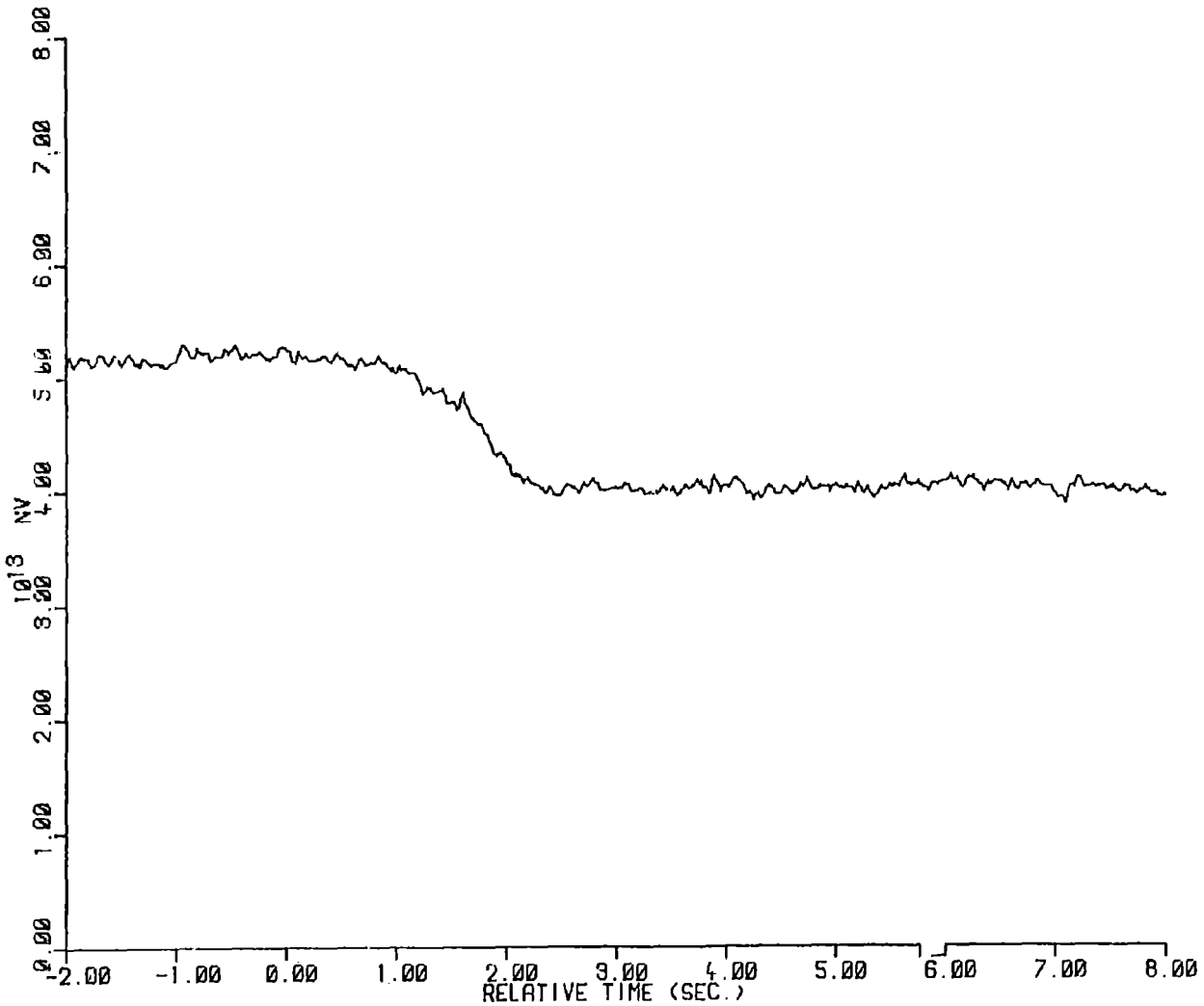

Figure 4-37. Compensated In-Core Flux - Full-Length CEA Drop - SPND G4 Level 2

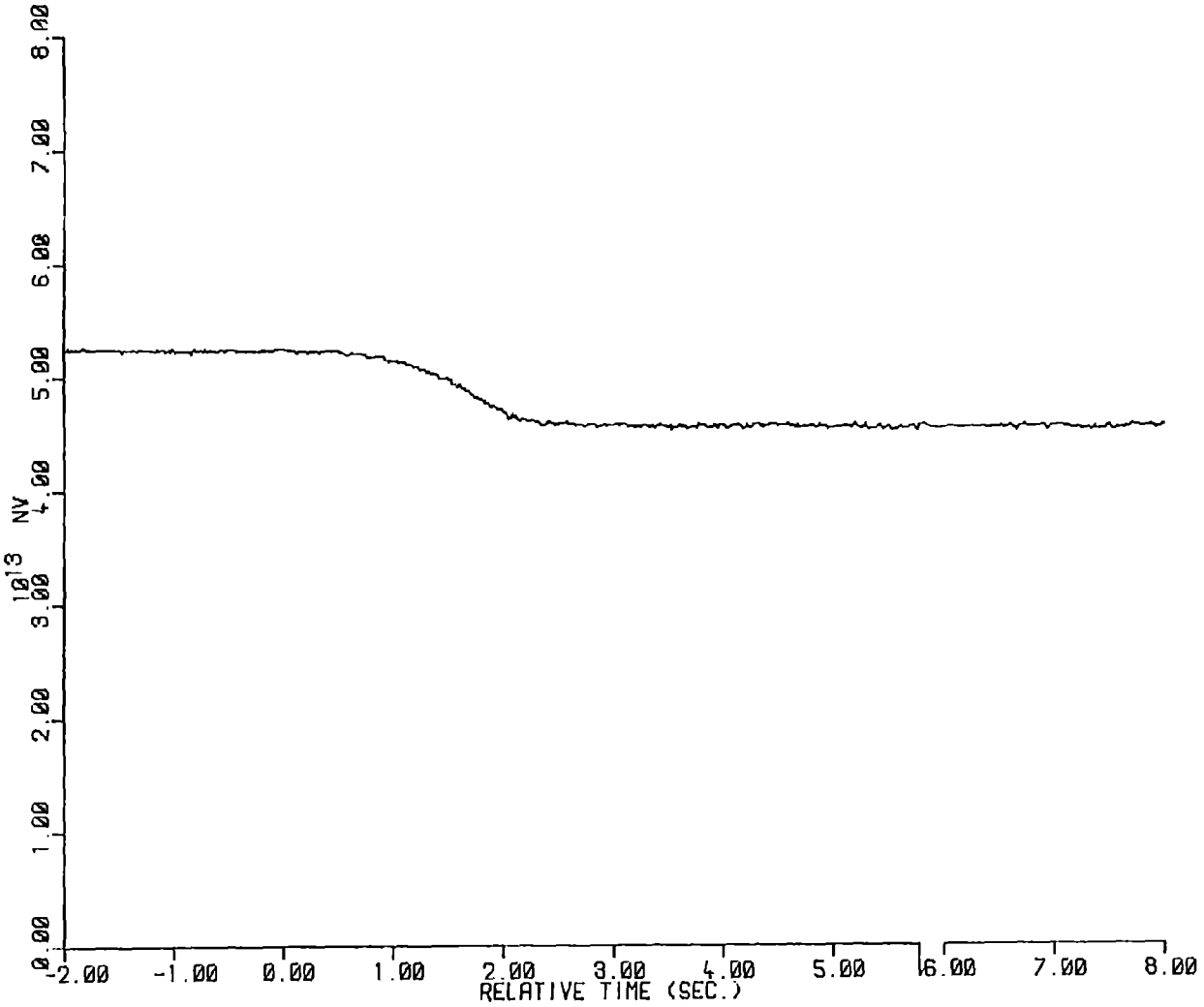

Figure 4-38. Compensated In-Core Flux - Full-Length CEA Drop - SPND G6 Level 2

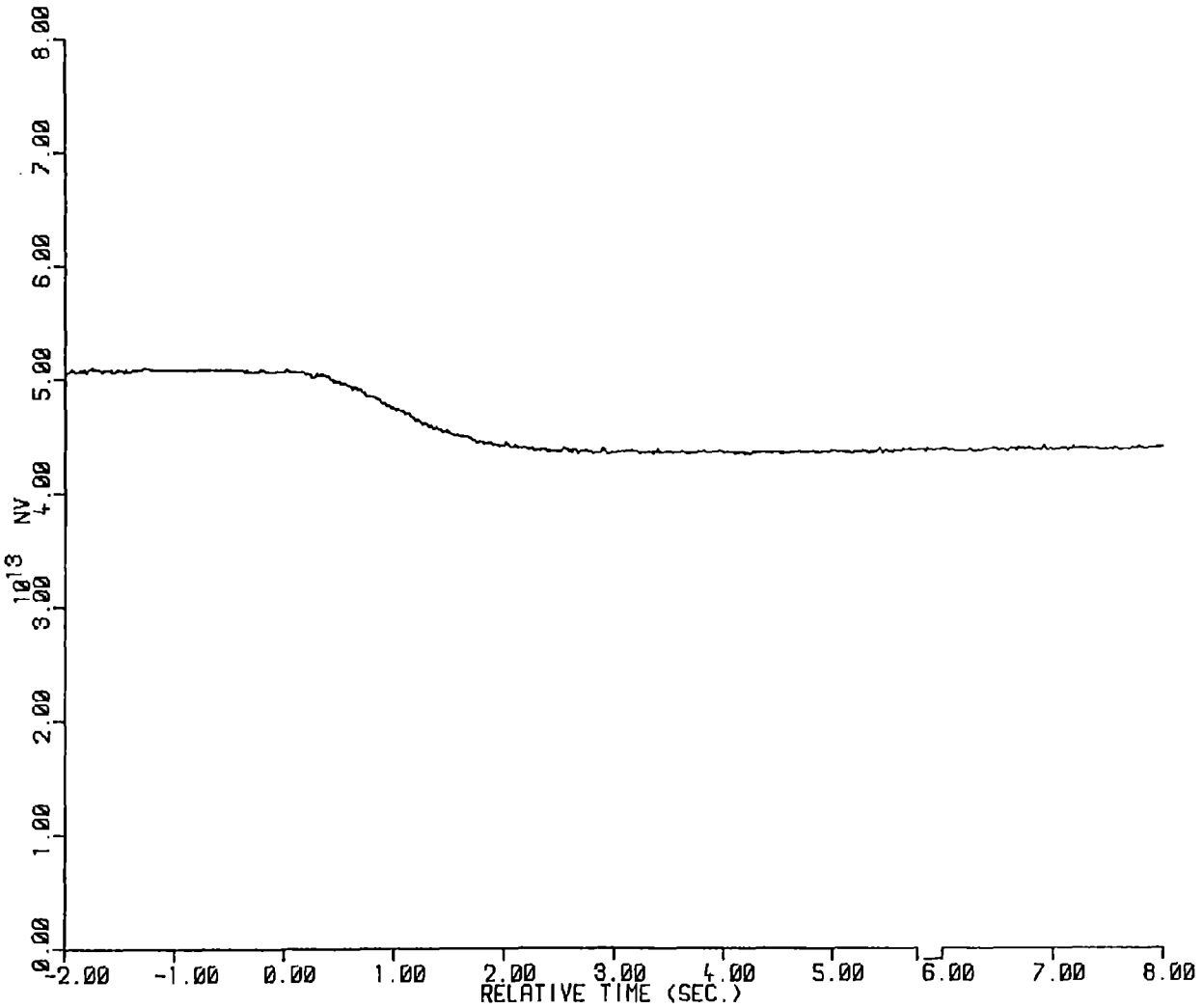

Figure 4-39. Compensated In-Core Flux - Full-Length CEA Drop - SPND G6 Level 4

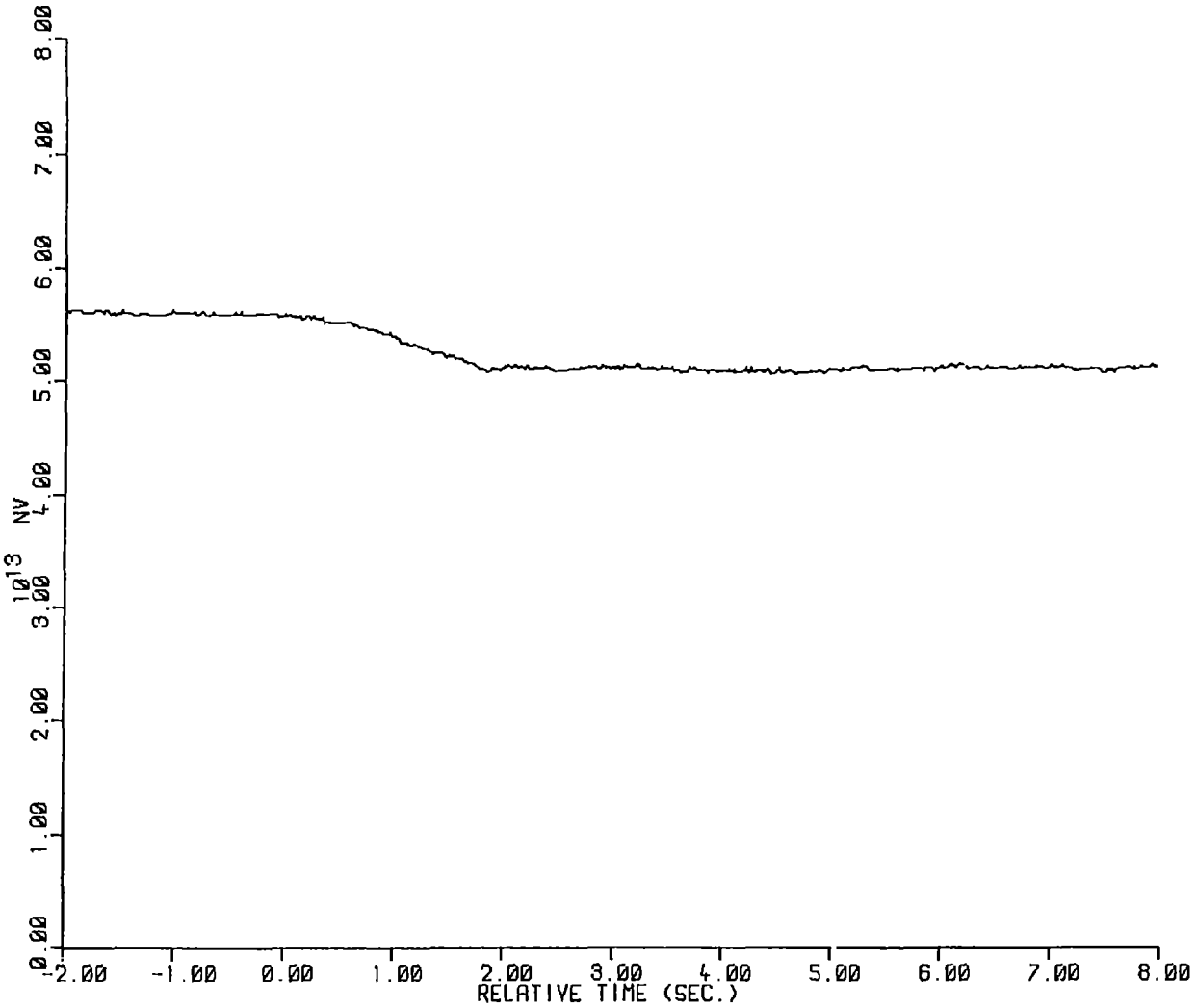

Figure 4-40. Compensated In-Core Flux - Full-Length CEA Drop - SPND G3 Level 2

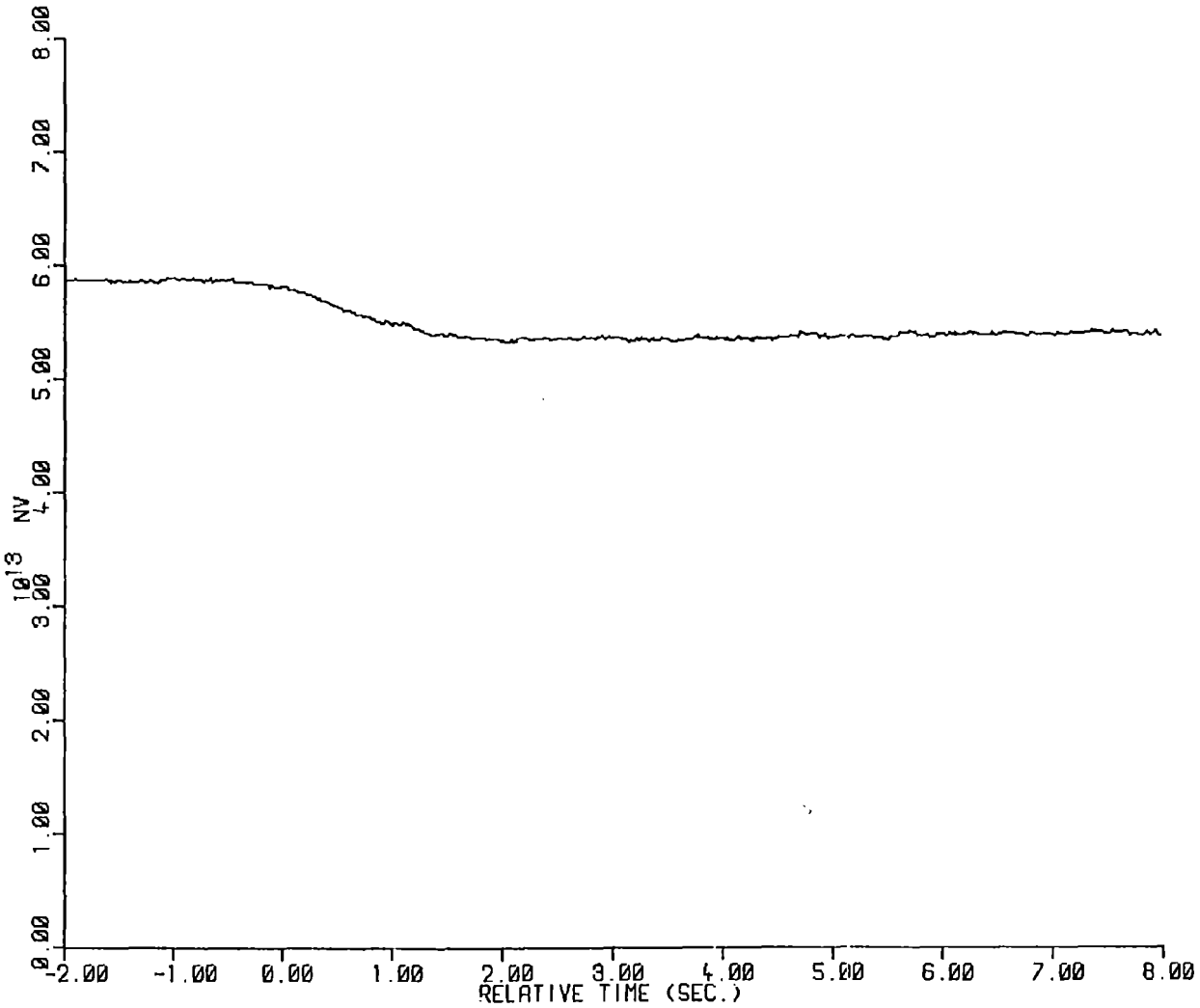

Figure 4-41. Compensated In-Core Flux - Full-Length CEA Drop - SPND G8 Level 3

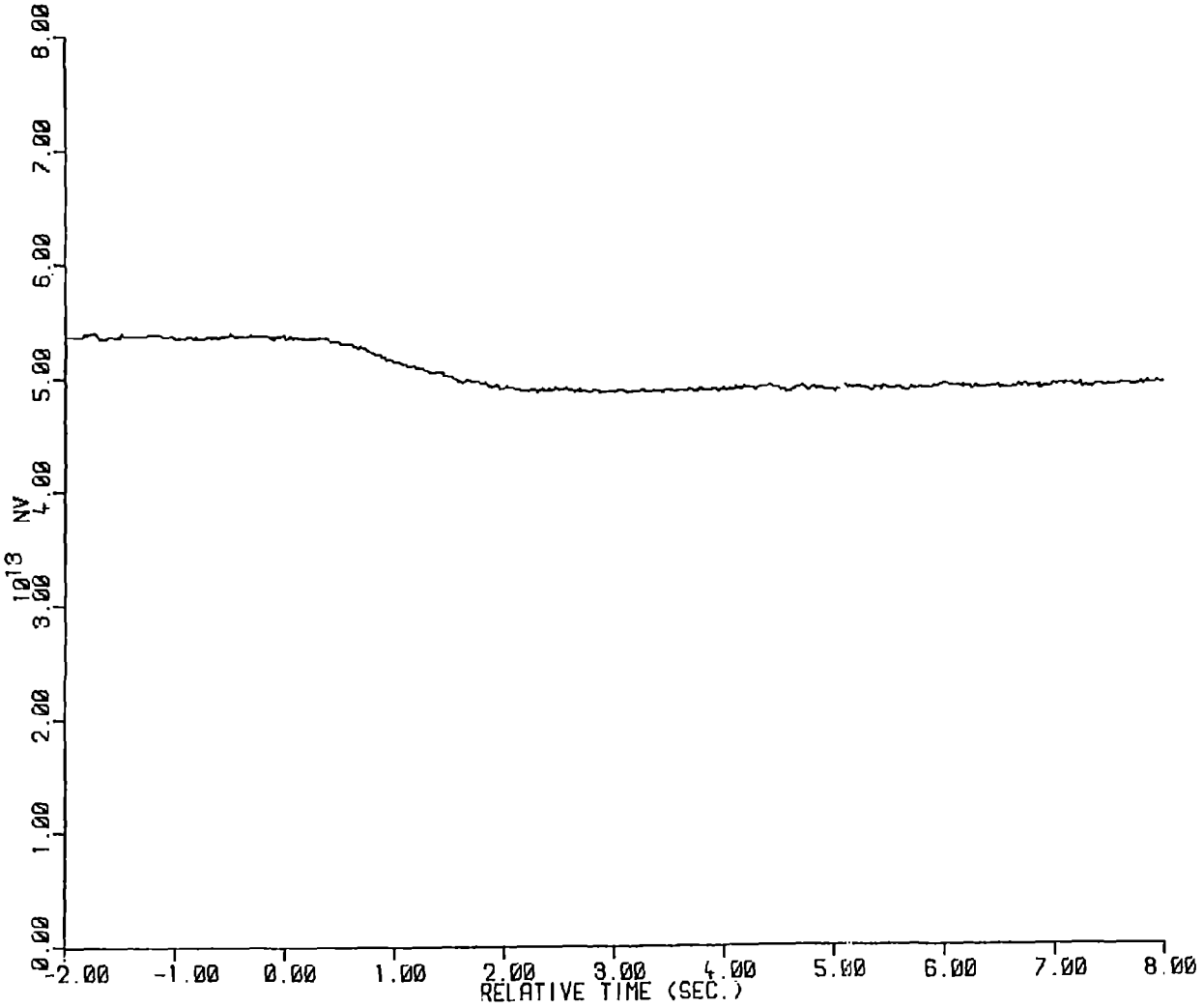

Figure 4-42. Compensated In-Core Flux - Full-Length CEA Drop - SPND 38 Level 4

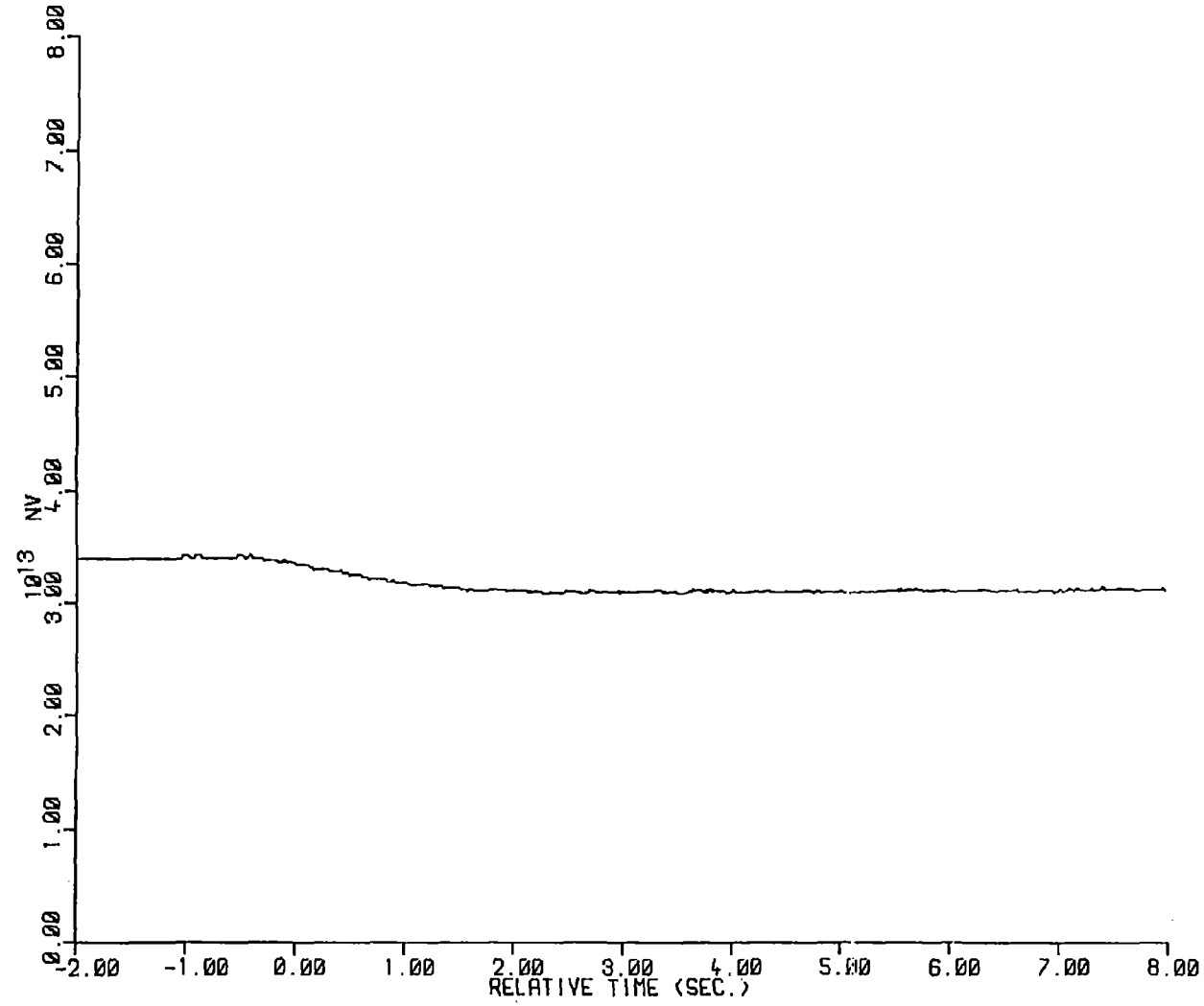

Figure 4-43. Compensated In-Core Flux - Full Length CEA Drop - SPND G8 Level 5

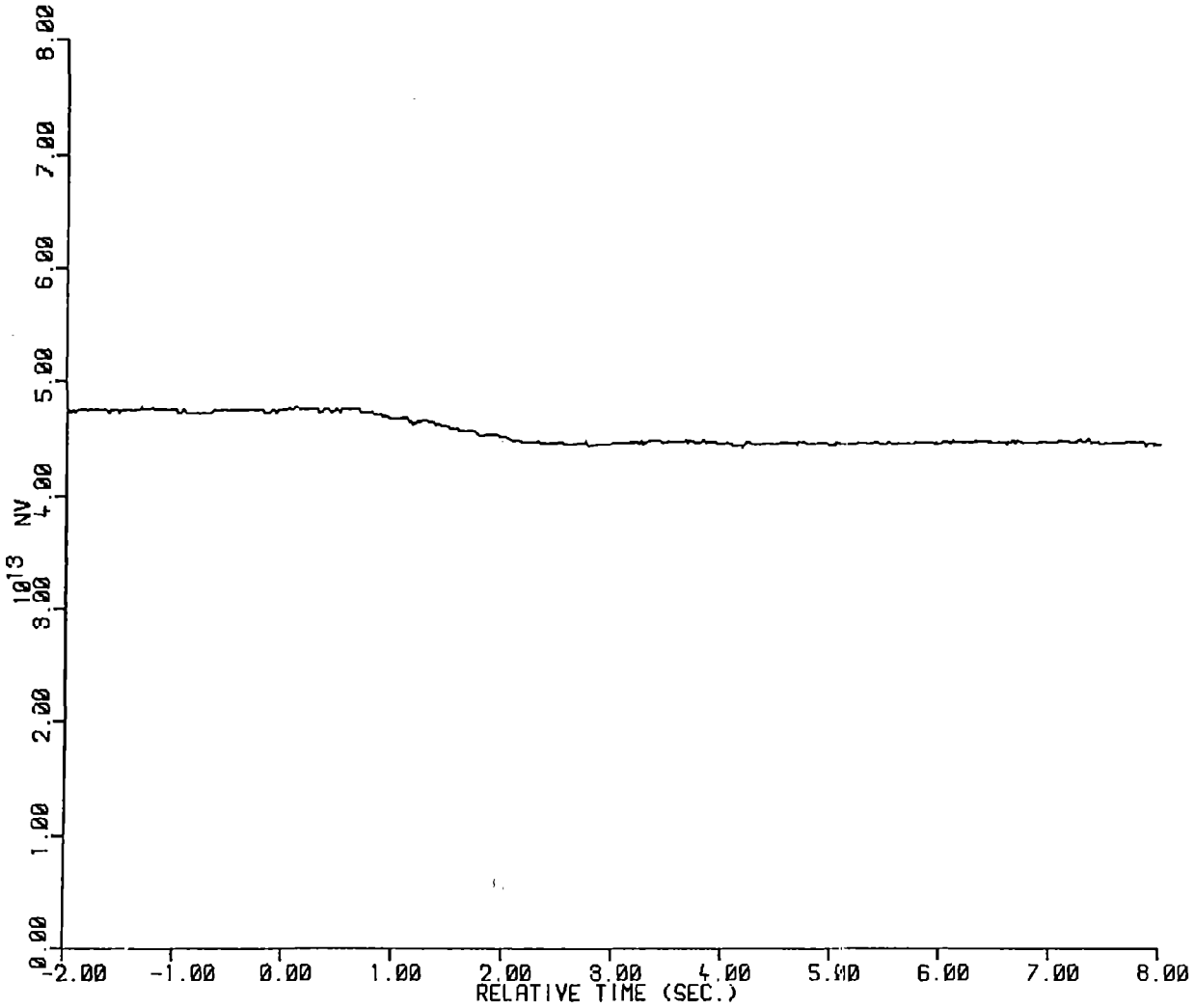

Figure 4-44. Compensated In-Core Flux - Full-Length CEA Drop - SPND H10 Level 2

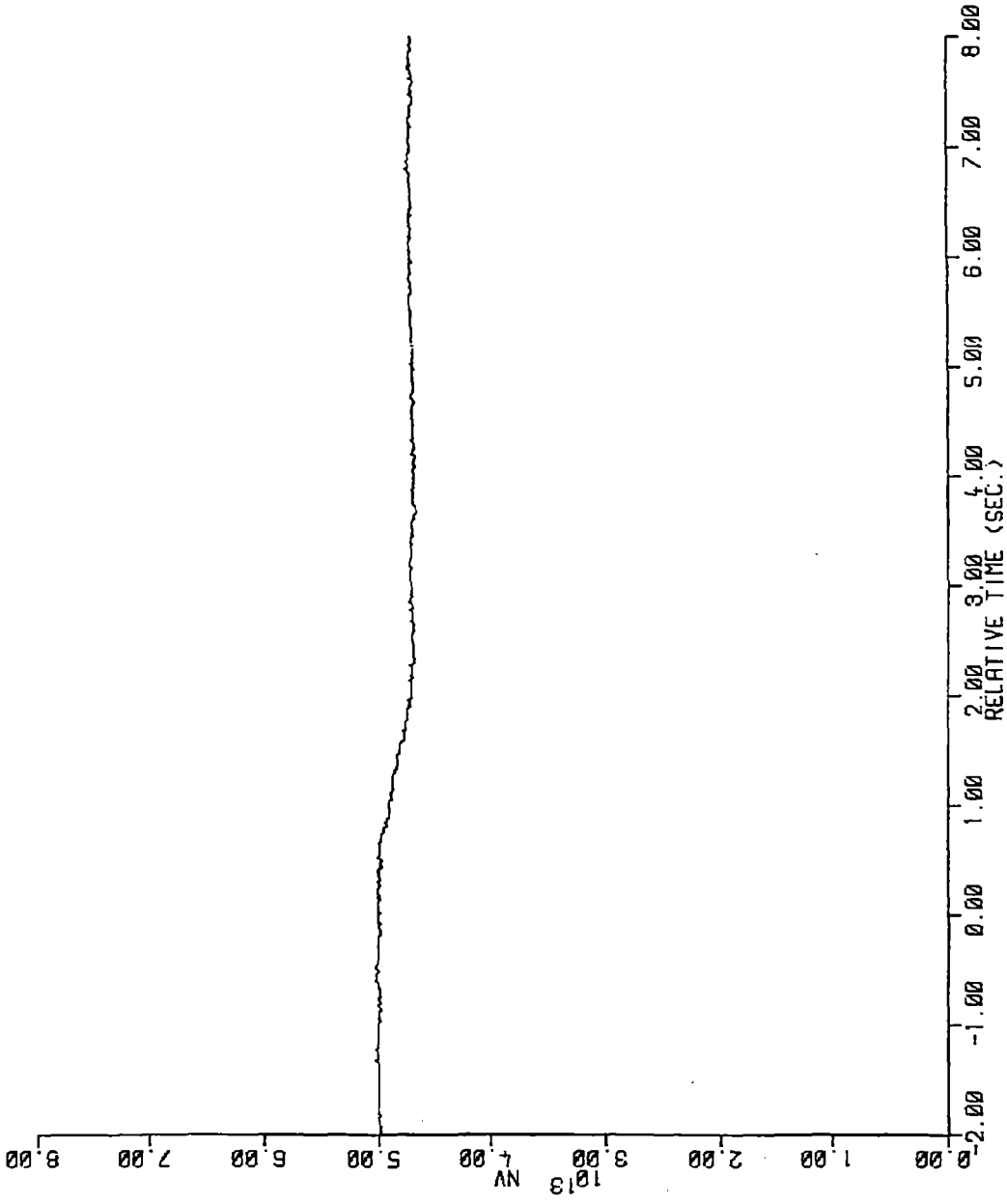

Figure 4-45. Compensated In-Core Flux - Full-Length CEA Drop - SPND N10 Level 3

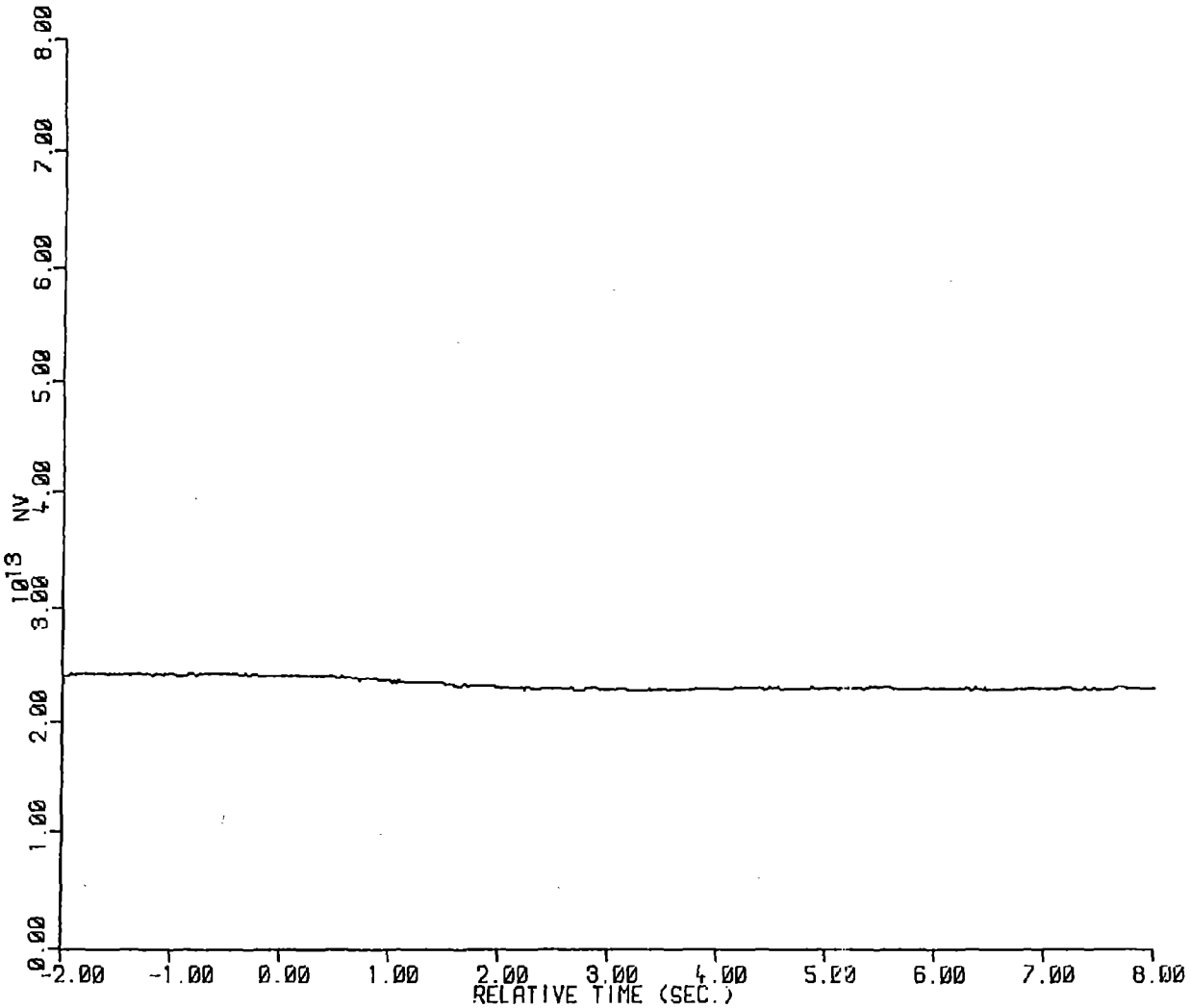

Figure 4-46. Compensated In-Core Flux - Full-Length CEA Drop - SPND C12 Level 5

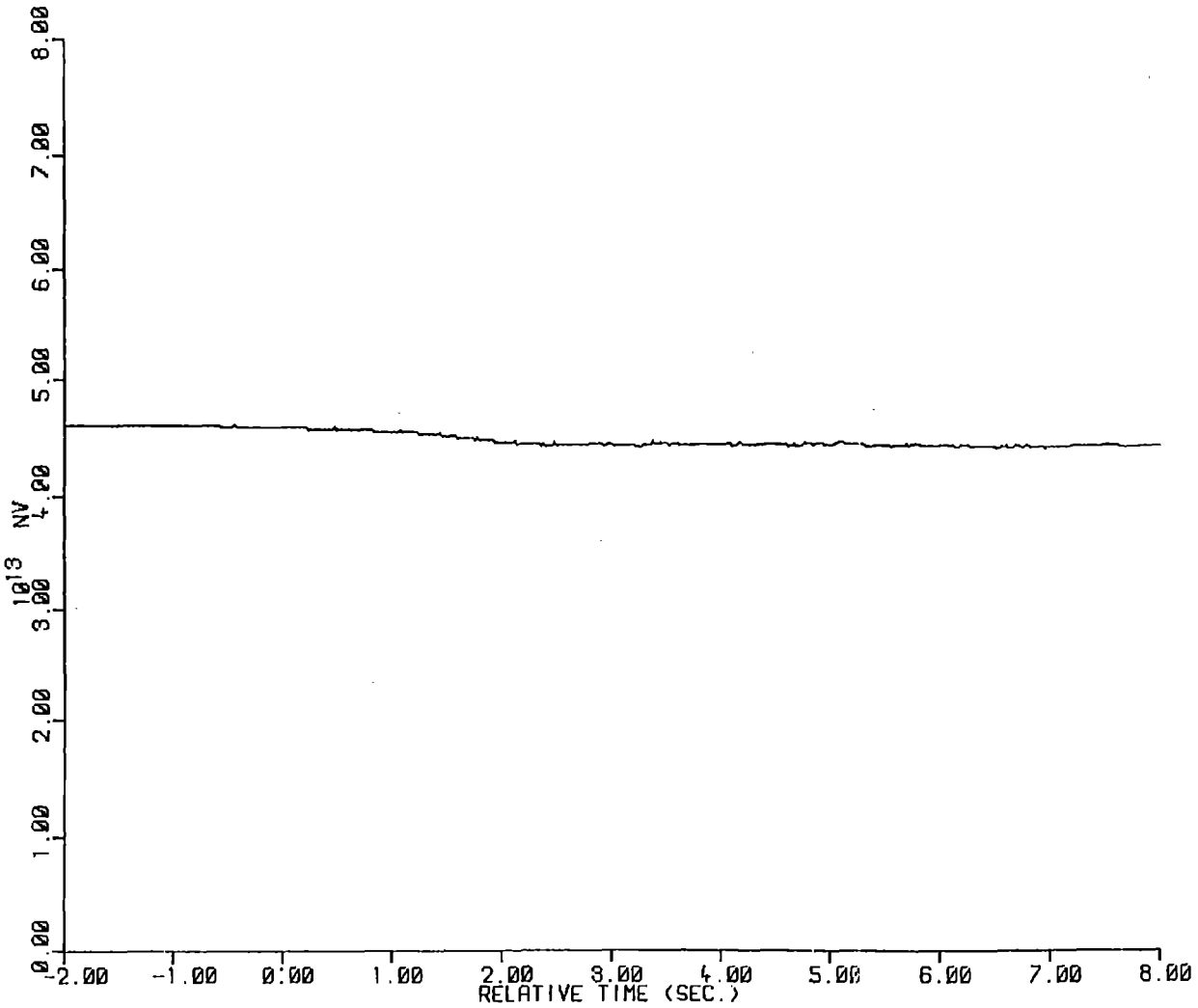

Figure 4-47. Compensated In-Core Flux - Full-Length CEA Drop - SPND G14 Level 2

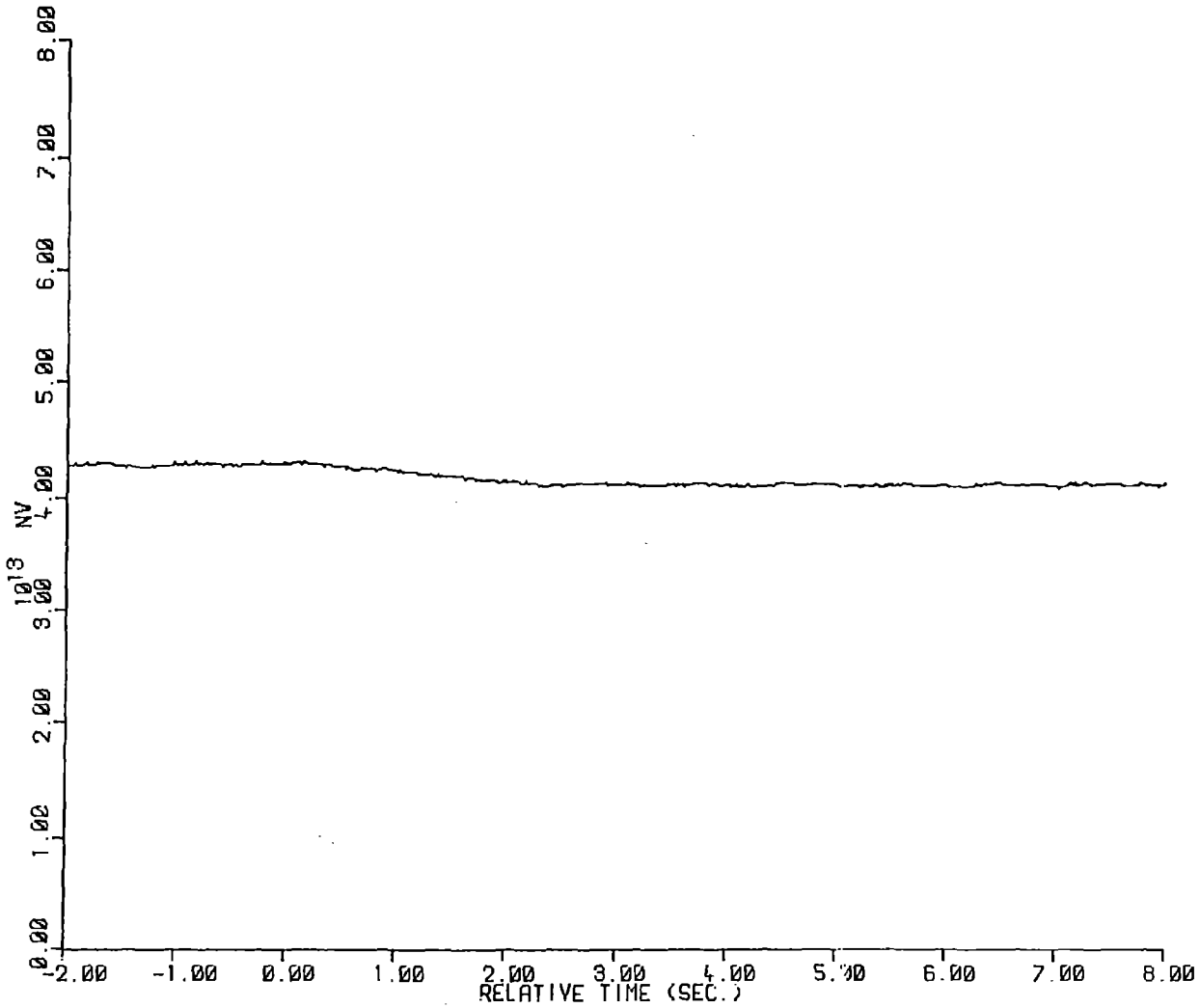

Figure 4-48. Compensated In-Core Flux - Full-Length CEA Drop - SPND G14 Level 4

The position of the dropped CEA as a function of time is shown in Figure 4-49.

The common timing signal failed for the full-length CEA drop. Therefore, the in-core flux and CEA position time scales for this test could not be synchronized by the same method as for the loss of flow and part-length CEA drop. Time zero for the in-core flux traces corresponds to the time at which the flux at level 5 in the assembly next to the dropped CEA (assembly G-2) begins to decrease. Time zero for the CEA position trace corresponds to the time at which the full-length CEA drop begins. Results from the loss of flow indicate that these two events occur very close together in time and were used as the basis for this means of time base correlation. The in-core flux and CEA position time scales are, therefore, synchronized well (probably within 0.1 seconds).

PART-LENGTH CEA DROP

Description of Test

The initial core conditions for the part-length CEA drop are given in Table 4-8. This test was performed approximately 12 hours after the full-length CEA drop with ARO near-equilibrium xenon, 702 PPM boron and an Axial Shape Index of approximately 0.0 SIU. The CEA drop was initiated by opening the CEA P-24 disconnect circuit breaker. Immediately following the CEA drop, the turbine load limit was adjusted to match the resulting decrease in average core power (approximately 3 percent of full power). An asymptotic core power level was achieved approximately 2.4 seconds after the initiation of the CEA drop. After 250 seconds, the reactor was stable at a slightly reduced core-average power level (approximately 46 percent of full power).

The core power distributions before and after the part-length CEA drop are shown in Figures 4-50 and 4-51, respectively.

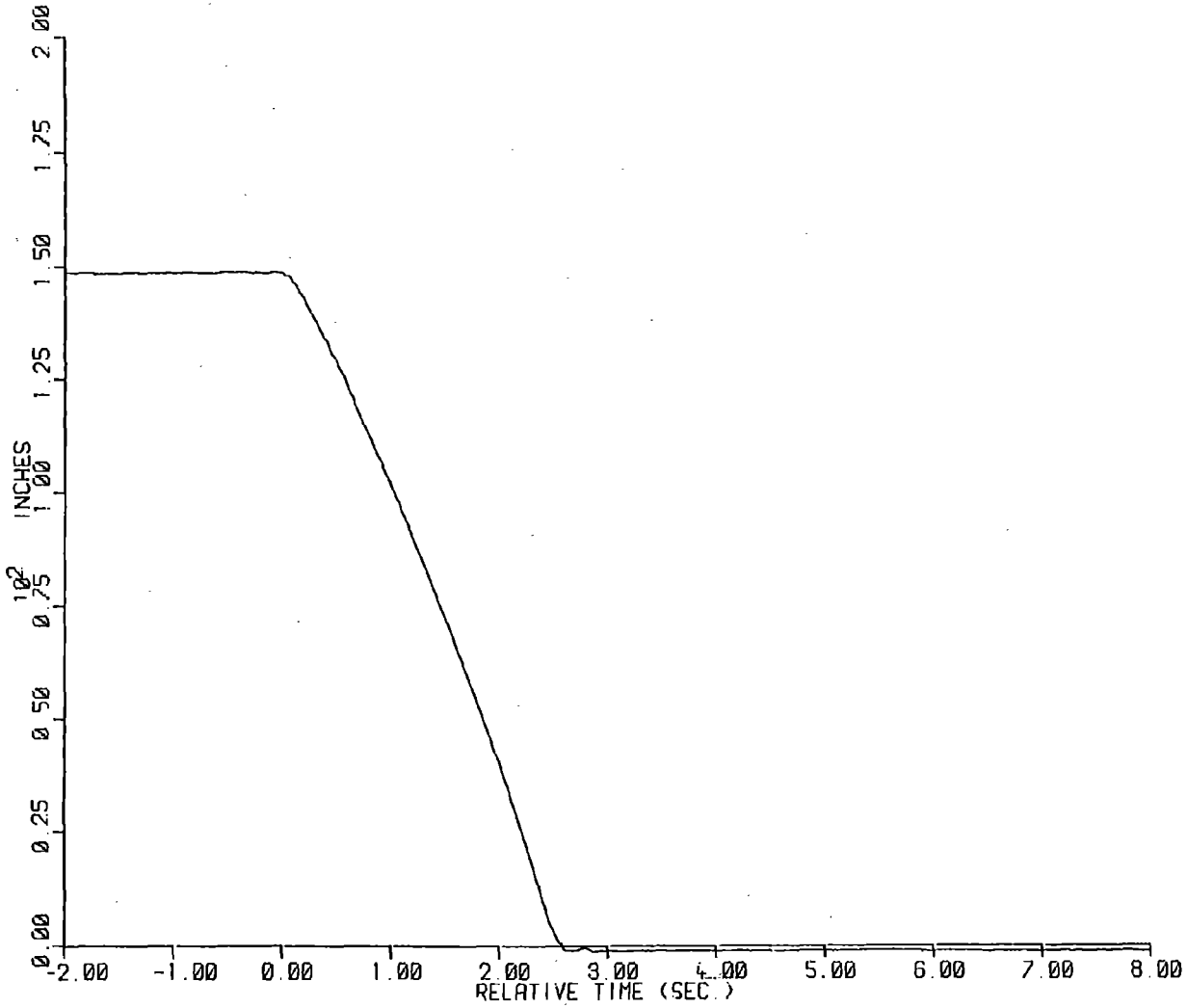

Figure 4-49. CEA Position - Full-Length CEA Drop - CEA 5-60

Table 4-8

INITIAL CORE CONDITIONS FOR PART-LENGTH CEA DROP

Core Power, MWt	1384 (49.2%)
Axial Shape Index (SIU)	~ 0.0
Boron Concentration, PPM	702
Core Mass Flow Rate, 10^6 lbm/hr	134.0
Presssurizer Pressure, psia	2247
Core Inlet Coolant Temperature, °F	546
Core Outlet Coolant Temperature, °F	577
CEA Position	ARO

LEGEND:

Box Number - Instrument Number
Integrated Assembly Power, MWTH
Assembly Axial Shape Index, SIU
Assembly Relative Power Fraction

				1 - 00	2 - 00	3 - 00	4 - 00	5 - 00						
		6 - 00	7 - 01 6.7650 -.0007 .8230	8 - 00	9 - 02 8.1801 .0029 .9951	10 - 00	11 - 03 8.1568 -.0006 .9923	12 - 00	13 - 04 6.6364 .0051 .8073	14 - 00				
	15 - 00	16 - 00	17 - 00	18 - 00	19 - 00	20 - 00	21 - 00	22 - 00	23 - 00	24 - 00	25 - 00			
26 - 00	27 - 05 8.0597 -.0010 .9805	28 - 00	29 - 06 8.9264 -.0050 1.0859	30 - 00	31 - 07 9.5554 -.0016 1.1624	32 - 00	33 - 08 9.3234 -.0070 1.1342	34 - 00	35 - 09 8.8883 .0002 1.0813	36 - 00	37 - 10 8.3220 .0066 1.0124	38 - 00		
39 - 00	40 - 00	41 - 00	42 - 00	43 - 00	44 - 00	45 - 00	46 - 00	47 - 00	48 - 00	49 - 00	50 - 00	51 - 00		
52 - 11 4.8398 .0025 .5888	53 - 00	54 - 12 8.4898 .0102 1.0328	55 - 00	56 - 13 9.2886 .0002 1.1300	57 - 00	58 - 14 9.4148 -.0012 1.1453	59 - 00	60 - 15 9.6625 -.0002 1.1754	61 - 00	62 - 16 9.4415 .0043 1.1486	63 - 00	64 - 17 8.5890 .0015 1.0448	65 - 00	66 - 00
67 - 00	68 - 18 7.7551 -.0007 .9434	69 - 00	70 - 00	71 - 00	72 - 00	73 - 00	74 - 00	75 - 00	76 - 00	77 - 00	78 - 00	79 - 00	80 - 19 7.8304 .0125 .9526	81 - 00
82 - 00	83 - 00	84 - 20 8.5100 -.0095 1.0352	85 - 00	86 - 21 9.3030 -.0025 1.1317	87 - 00	88 - 22 9.5896 .0044 1.2055	89 - 00	90 - 23 9.5743 .0037 1.1647	91 - 00	92 - 24 9.4326 .0057 1.1475	93 - 00	94 - 25 8.7038 .0094 1.0588	95 - 00	96 - 00
97 - 00	98 - 26 7.7004 .0112 .9368	99 - 00	100 - 00	101 - 00	102 - 00	103 - 00	104 - 00	105 - 00	106 - 00	107 - 00	108 - 00	109 - 00	110 - 27 7.7667 .0169 .9448	111 - 00
112 - 00	113 - 00	114 - 28 8.3935 .0040 1.0211	115 - 00	116 - 29 9.1646 .0062 1.1149	117 - 00	118 - 30 9.4046 .0016 1.1441	119 - 00	120 - 31 9.3173 -.0018 1.1334	121 - 00	122 - 32 9.0288 .0002 1.0984	123 - 00	124 - 33 8.3181 .0090 1.0119	125 - 00	126 - 34 4.9566 .0149 .6030
	127 - 00	128 - 00	129 - 00	130 - 00	131 - 00	132 - 00	133 - 00	134 - 00	135 - 00	136 - 00	137 - 00	138 - 00	139 - 00	
	140 - 00	141 - 35 8.1104 -.0061 .9866	142 - 00	143 - 36 8.5767 -.0030 1.0434	144 - 00	145 - 37 9.2687 -.0109 1.1275	146 - 00	147 - 38 9.0354 .0050 1.0992	148 - 00	149 - 39 8.6211 .0056 1.0488	150 - 00	151 - 40 7.8409 .0139 .9538	152 - 00	
		153 - 00	154 - 00	155 - 00	156 - 00	157 - 00	158 - 00	159 - 00	160 - 00	161 - 00	162 - 00	163 - 00		
			164 - 00	165 - 41 6.5255 -.0079 .7938	166 - 00	167 - 42 7.8103 .0172 .9501	168 - 00	169 - 43 7.6674 .0005 .9327	170 - 00	171 - 44 6.3902 .0011 .7774	172 - 00			
				173 - 00	174 - 00	175 - 00	176 - 00	177 - 00						

Figure 4-50. Core Power Distribution Before Part-Length CEA Drop - 1/11/80, 12:56:01

LEGEND:

Box Number - Instrument Number
Integrated Assembly Power, MWTH
Assembly Axial Shape Index, SIU
Assembly Relative Power Fraction

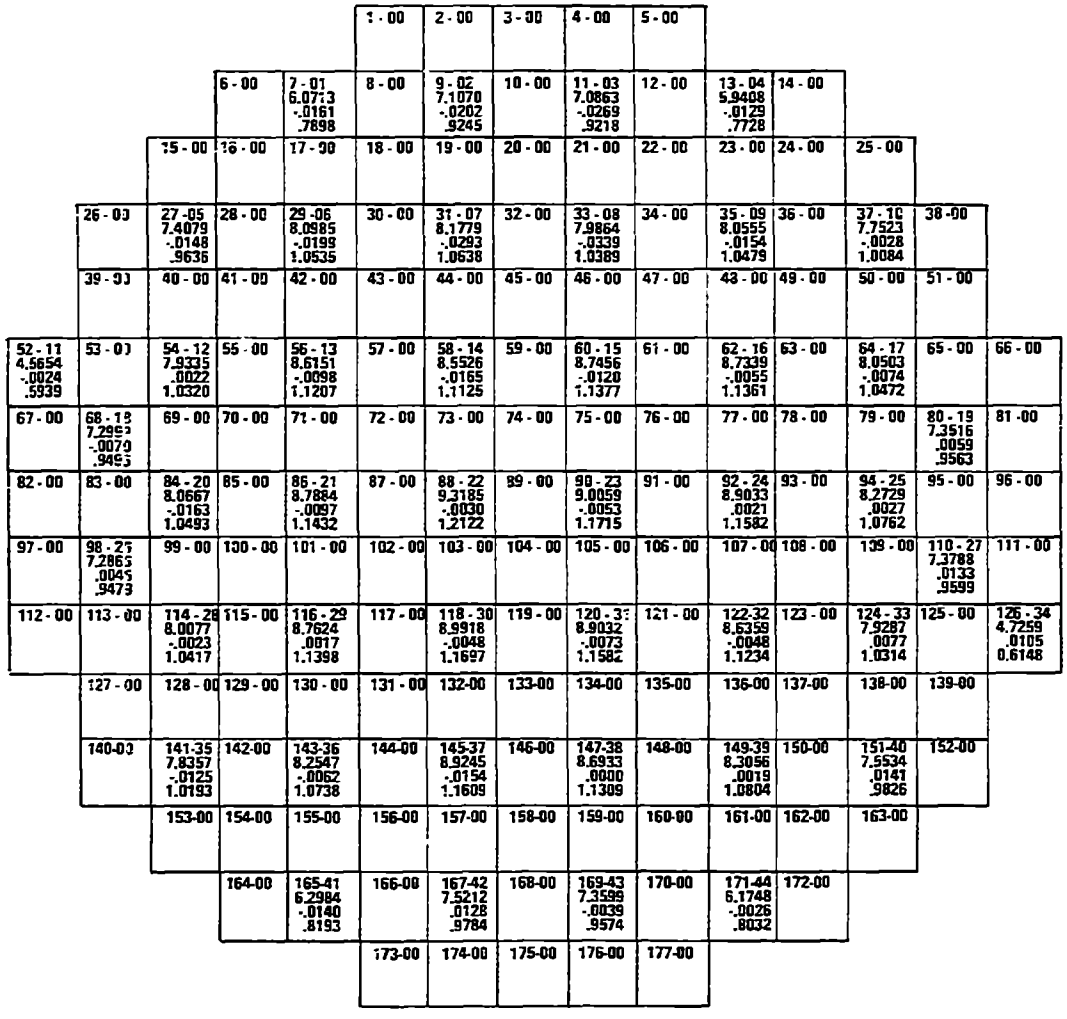

Figure 4-51. Core Power Distribution After Part-Length CEA Drop - 1/11/80, 13:32:59

Recorded Signal Locations

The locations of the rhodium in-core and background detector signals recorded during the part-length CEA drop are given in Table 4-9 and 4-10, respectively. The dropped CEA (P-24) is located at core positon H-4. Data which were judged to be noisy, from an incorrect hook-up, or taken from a bad detector are indicated in the legends of Tables 4-9 and 4-10.* These data are not included in the report. In addition, background correction could not be properly applied to two of the in-core detector signals. These detectors are indicated in Table 4-9, and the compensated in-core fluxes at these locations are not included in the report.

Process Parameter Transients

Figures 4-52 through 4-69 show the background-corrected, compensated in-core flux during the part-length CEA drop at various radial and axial core locations. The radial coordinates and axial positions of the in-core detectors are shown in Figures 2-1 and 2-2. The compensation methodology used to compute the real-time nuetron flux transient is discussed in the Appendix.

The position of the dropped CEA as a function of time is shown in Figure 4-70.

The time scales for the in-core flux and CEA position traces are synchronized using the common timing signal. Time zero corresponds to the time at which the part-length CEA drop begins.

---

*Visual inspection of the compensated in-core detector signals was used to determine those signals which could provide meaningful data for code qualification.

Table 4-9

RECORDED RHODIUM IN-CORE DETECTOR LOCATIONS FOR
PART-LENGTH CEA DROP

Rh In-Core Detector Location	Level 1	2	3	4	5
E-2		X	X	X	
G-2		X		X	
L-2			B		
G-4	X	X	Y	X	X
J-4			Y		
A-6		X		X	
G-8		X		X	
N-10		X	X	N	
C-12	N		W		X
G-14		X		X	

X = recorded in-core detector with good signal

N = recorded in-core detector with noisy signal

W = possible wrong hook-up

B = bad in-core detector

Y = background correction not applied

Table 4-10

RECORD BACKGROUND DETECTOR LOCATIONS FOR PART-LENGTH CEA DROP

Background Detector Location	Level	
	Long	Short
E-2	X	X
E-4		X
G-6	X	X
P-7	X	X
G-8	X	X
N-10	X	X
C-12	W	X

X = recorded background detector with good signal

W = wrong hook-up

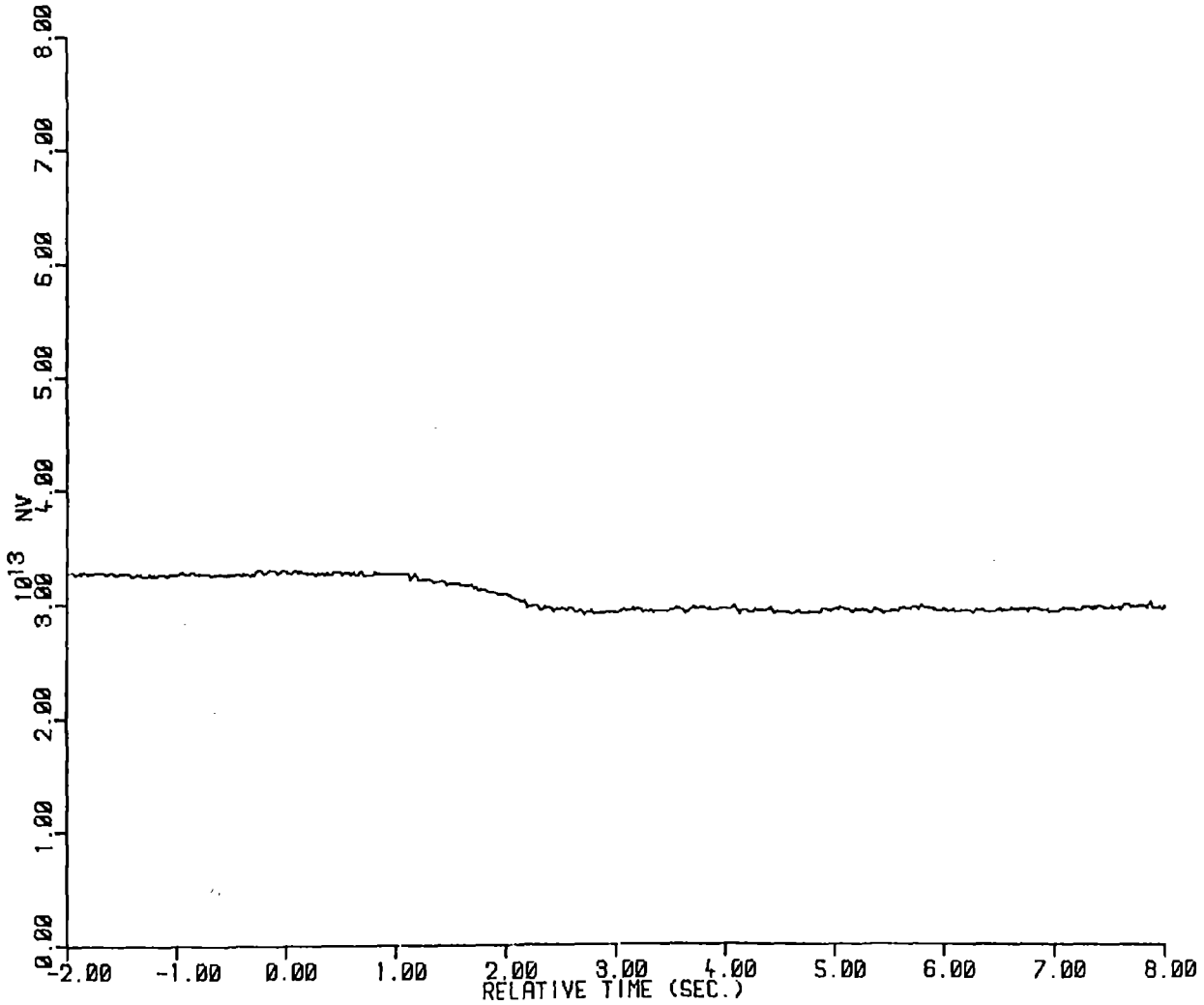

Figure 4-52. Compensated In-Core Flux - Part-Length CEA Drop - SPND E2 Level 2

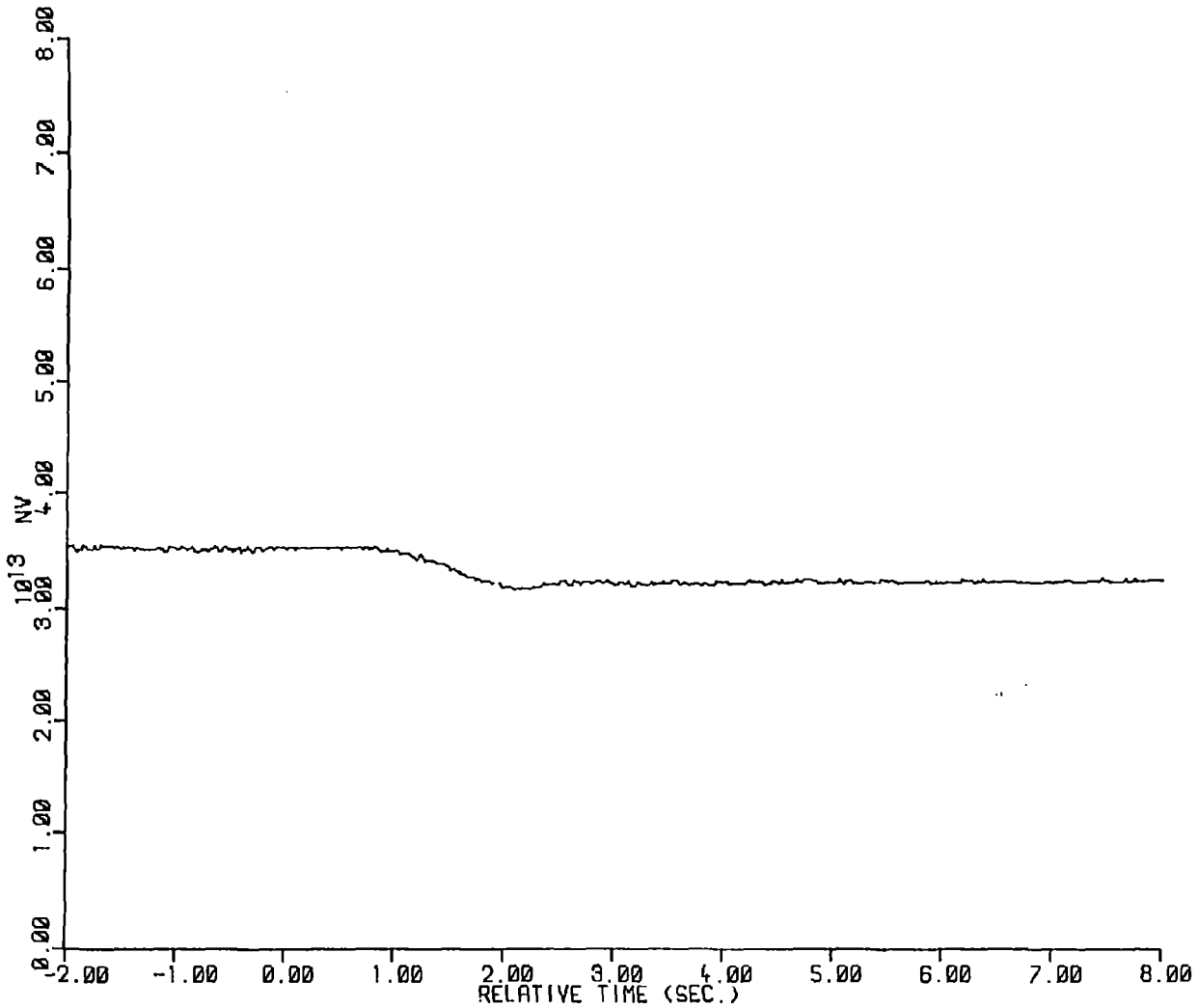

Figure 4-53. Compensated In-Core Flux - Part-Length CEA Drop - SPND E2 Level 3

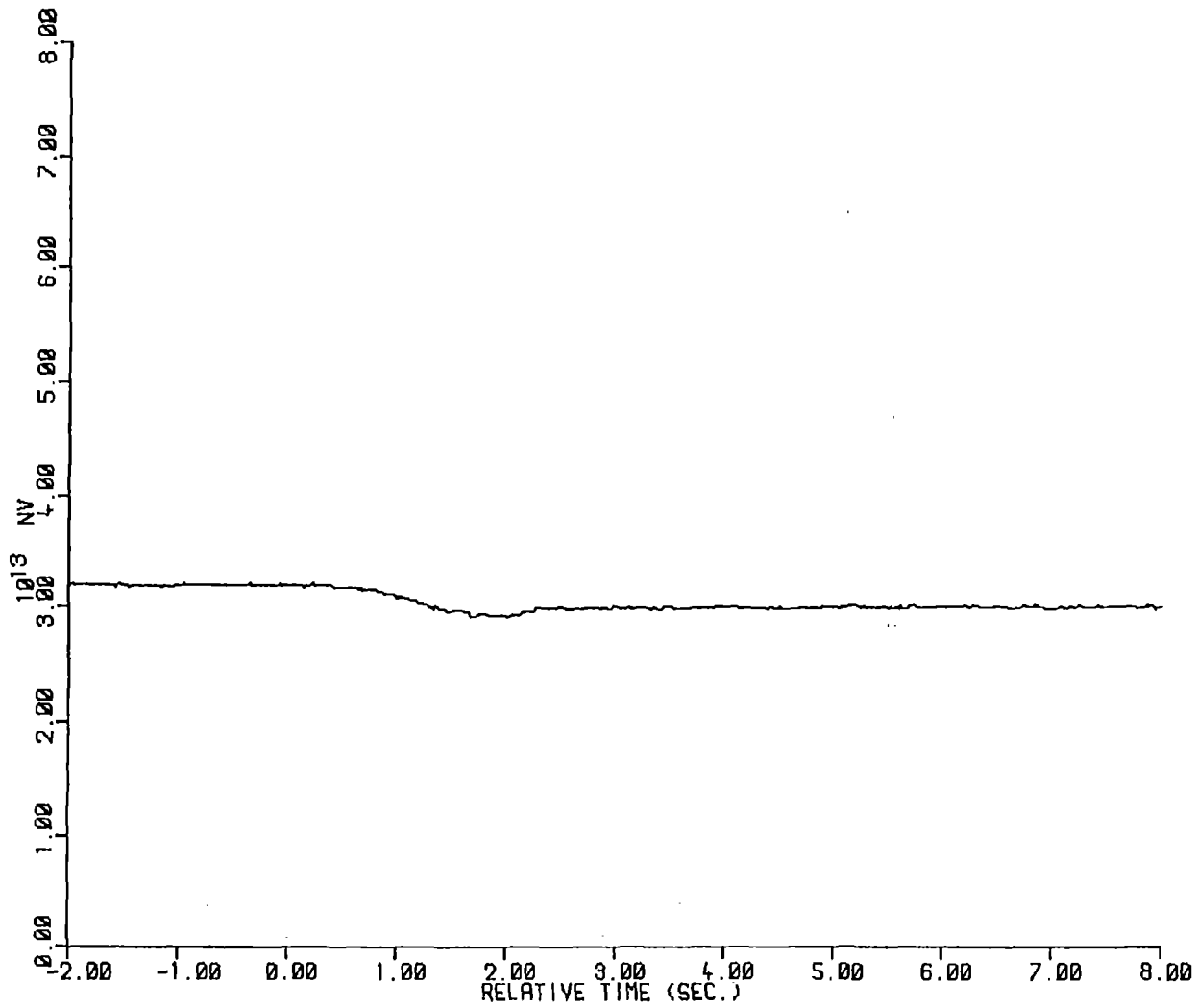

Figure 4-54. Comepnsated In-Core Flux - Part-Length CEA Drop - SPND E2 Level 4

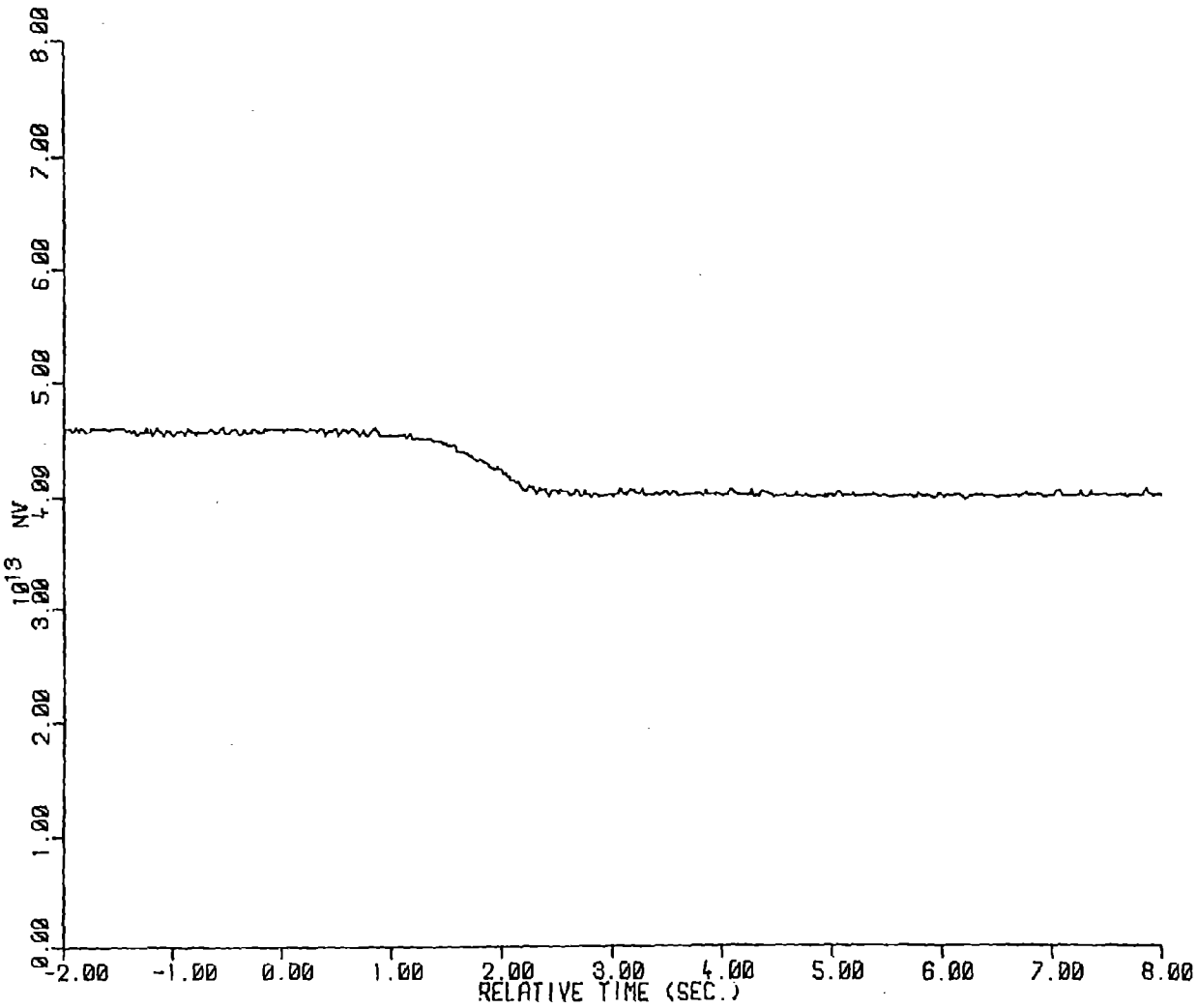

Figure 4-55. Comepnsated In-Core Flux - Part-Length CEA Drop - SPND G2 Level 2

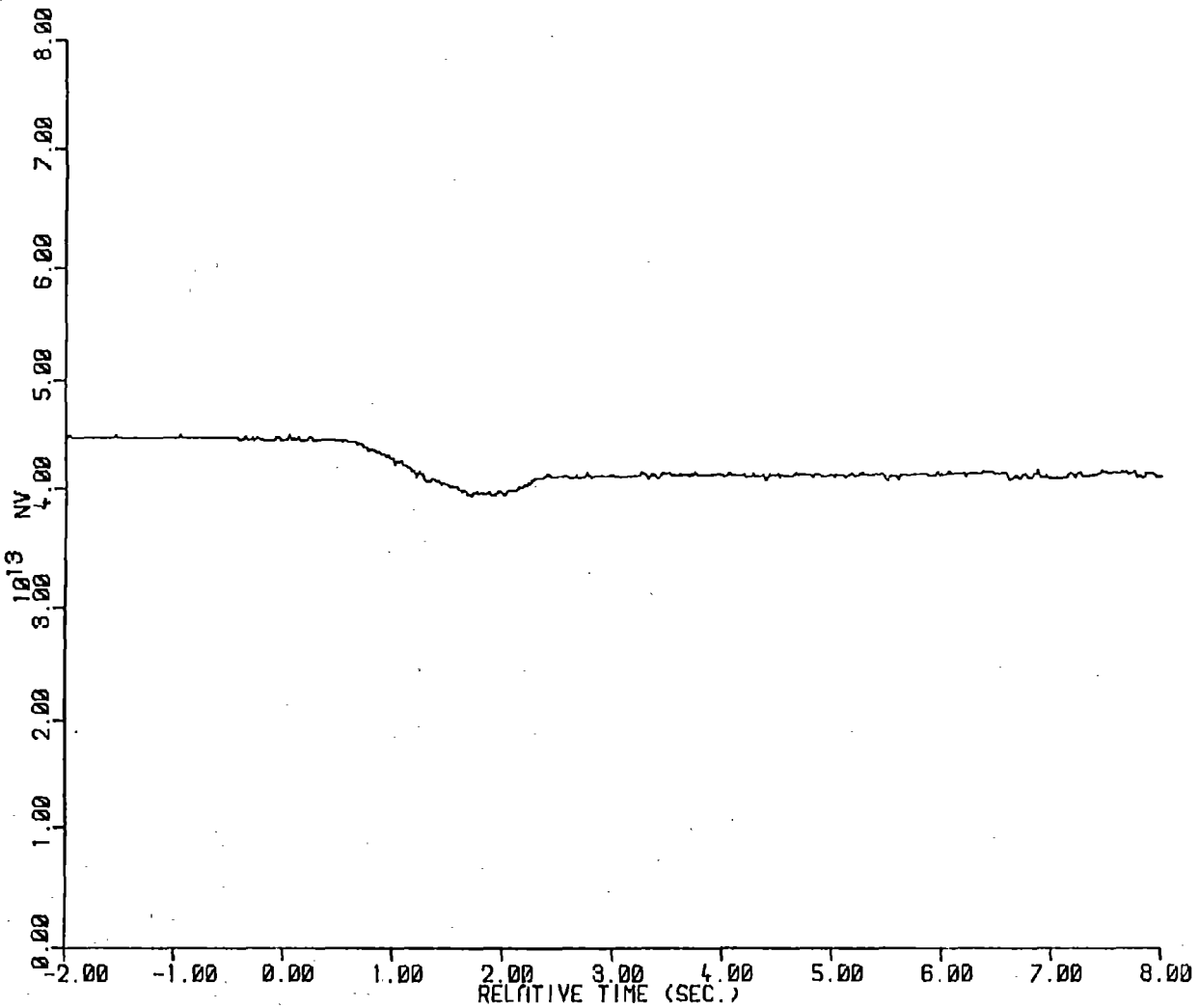

Figure 4-56. Compensated In-Core Flux - Part-Length CEA Drop - SPND G2 Level 4

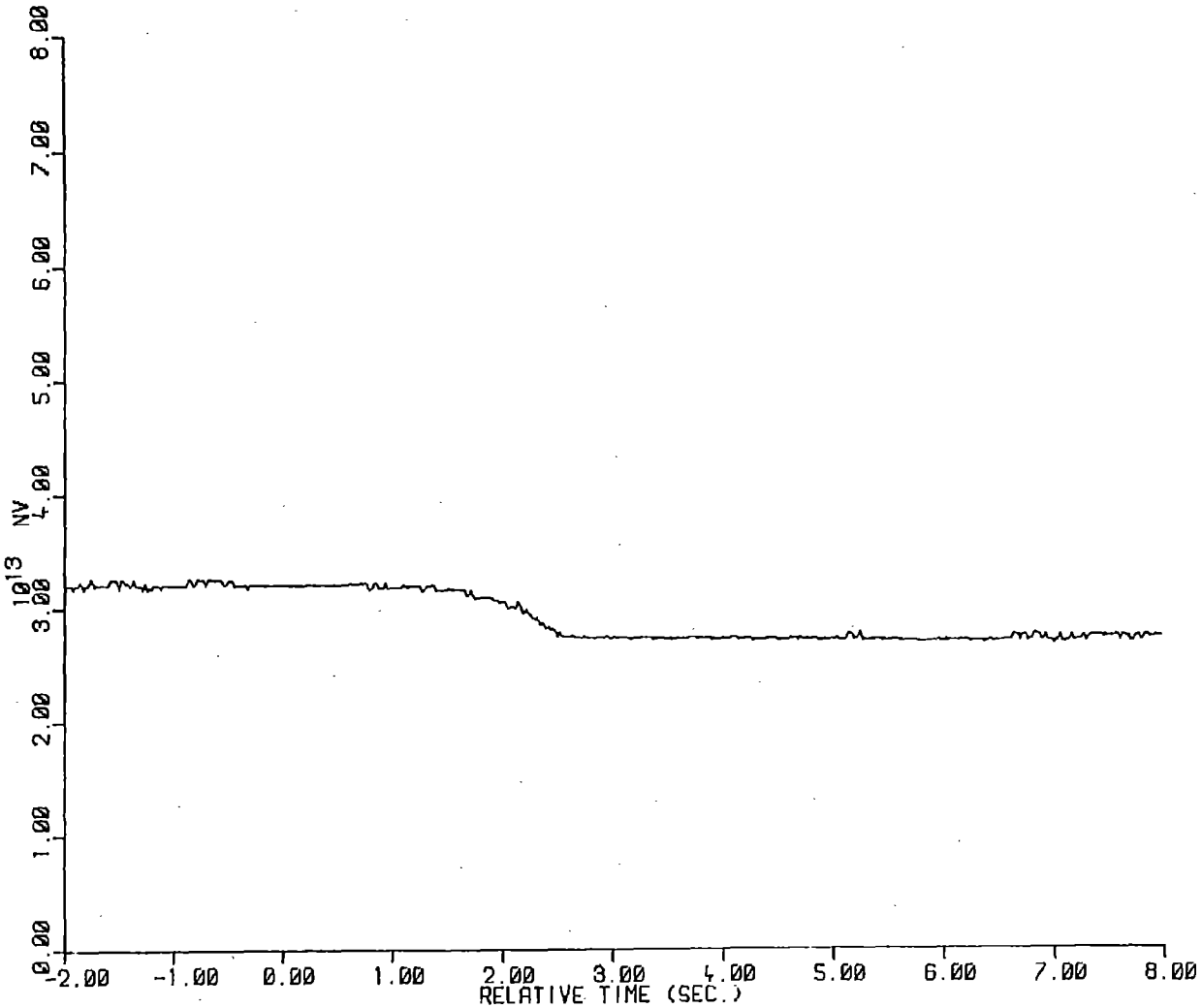

Figure 4-57. Compensated In-Core Flux - Part-Length CEA Drop - SPND G4 Level 1

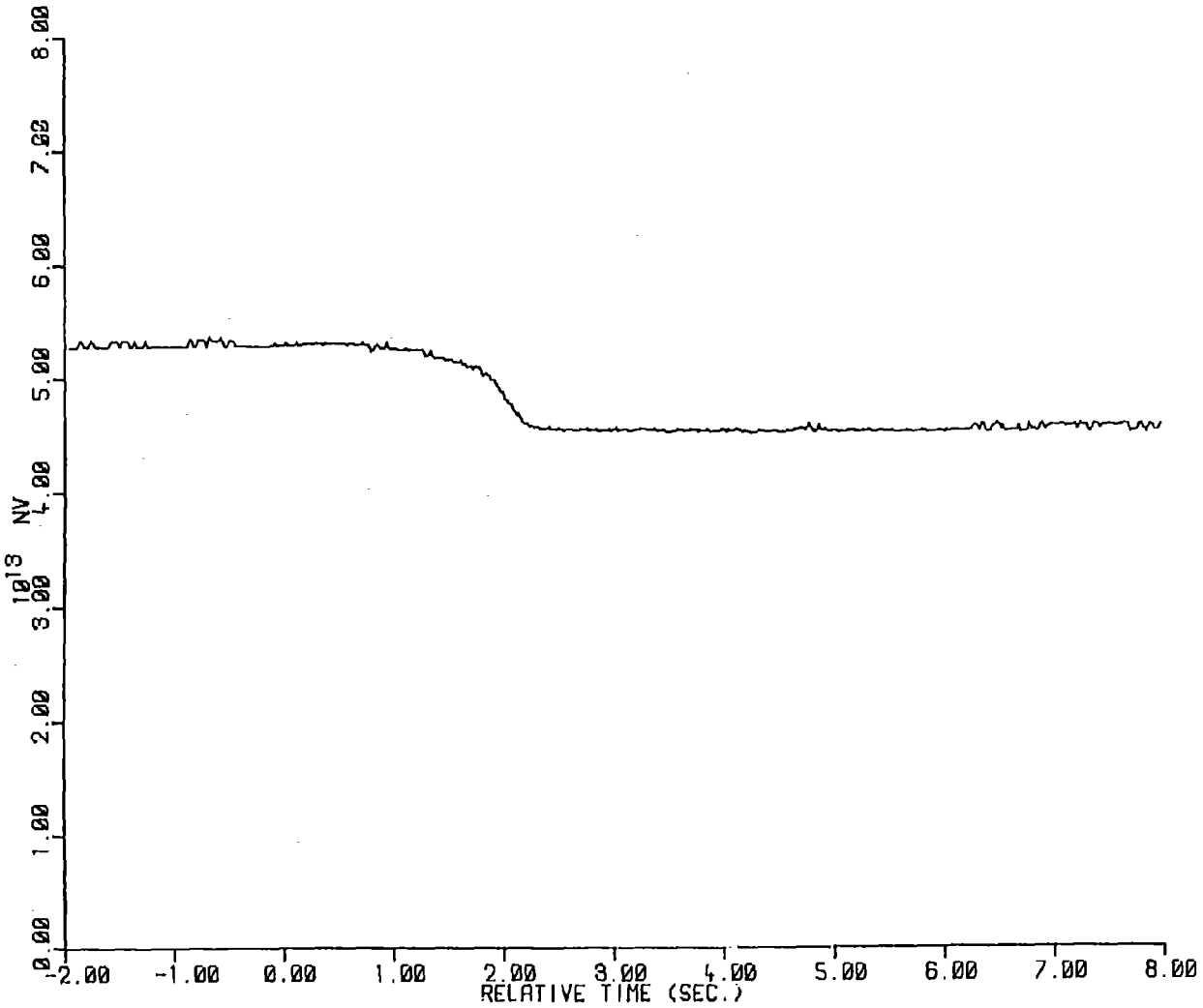

Figure 4-58. Compensated In-Core Flux - Part-Length CEA Drop - SPND G4 Level 2

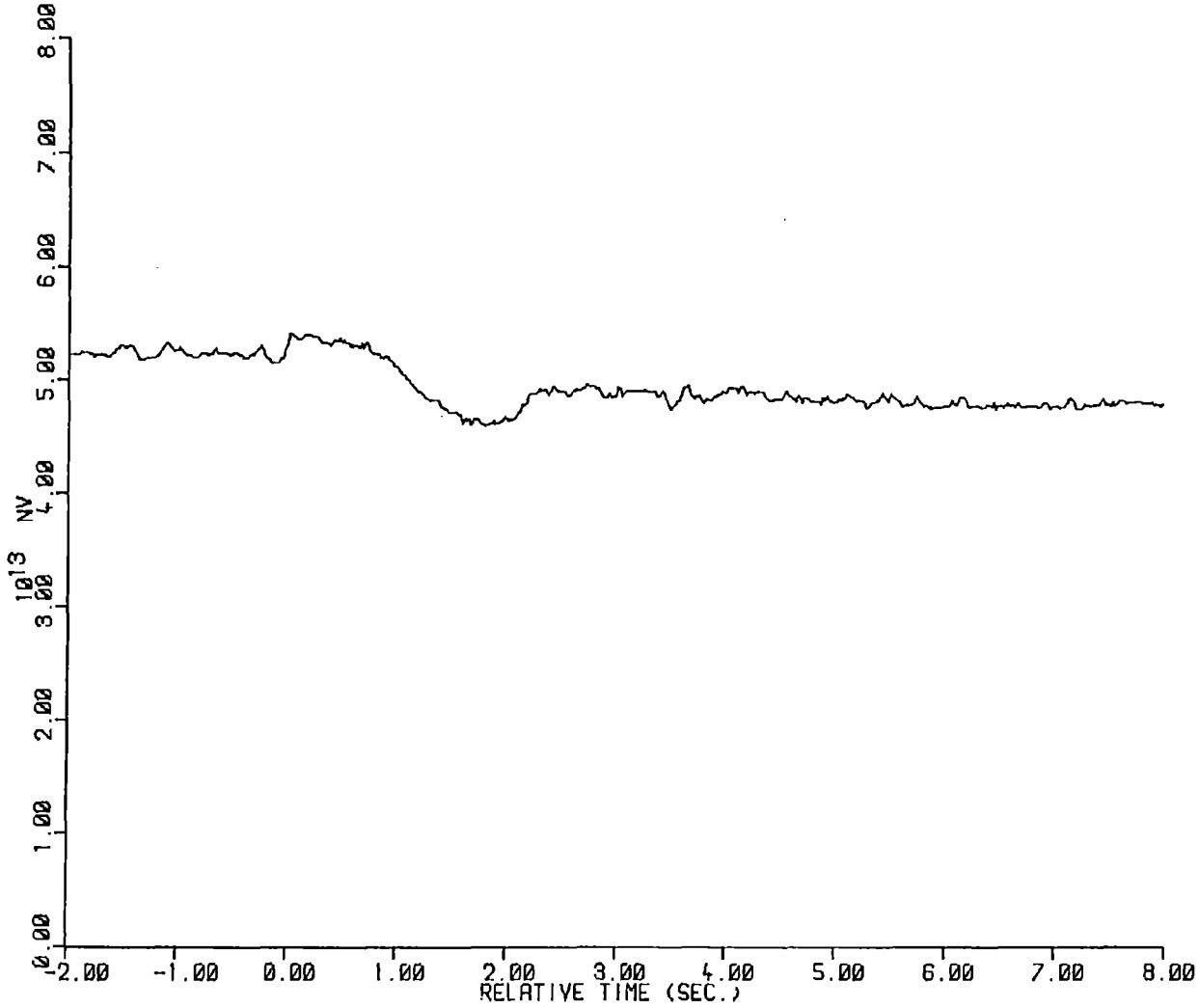

Figure 4-59. Compensated In-Core Flux - Part-Length CEA Drop - SPND G4 Level 4

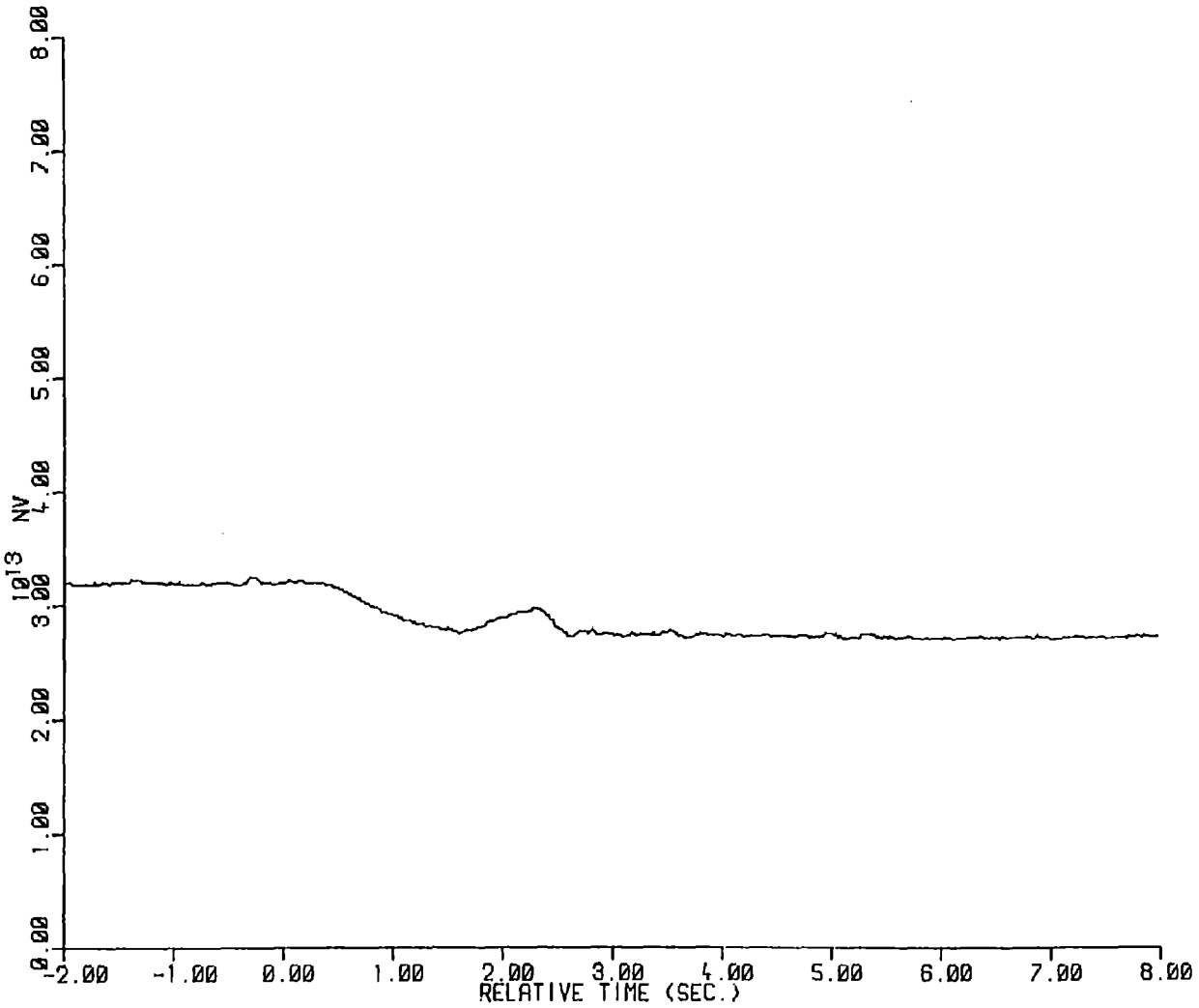

Figure 4-60. Compensated In-Core Flux - Part-Length CEA Drop - SPND G4 Level 5

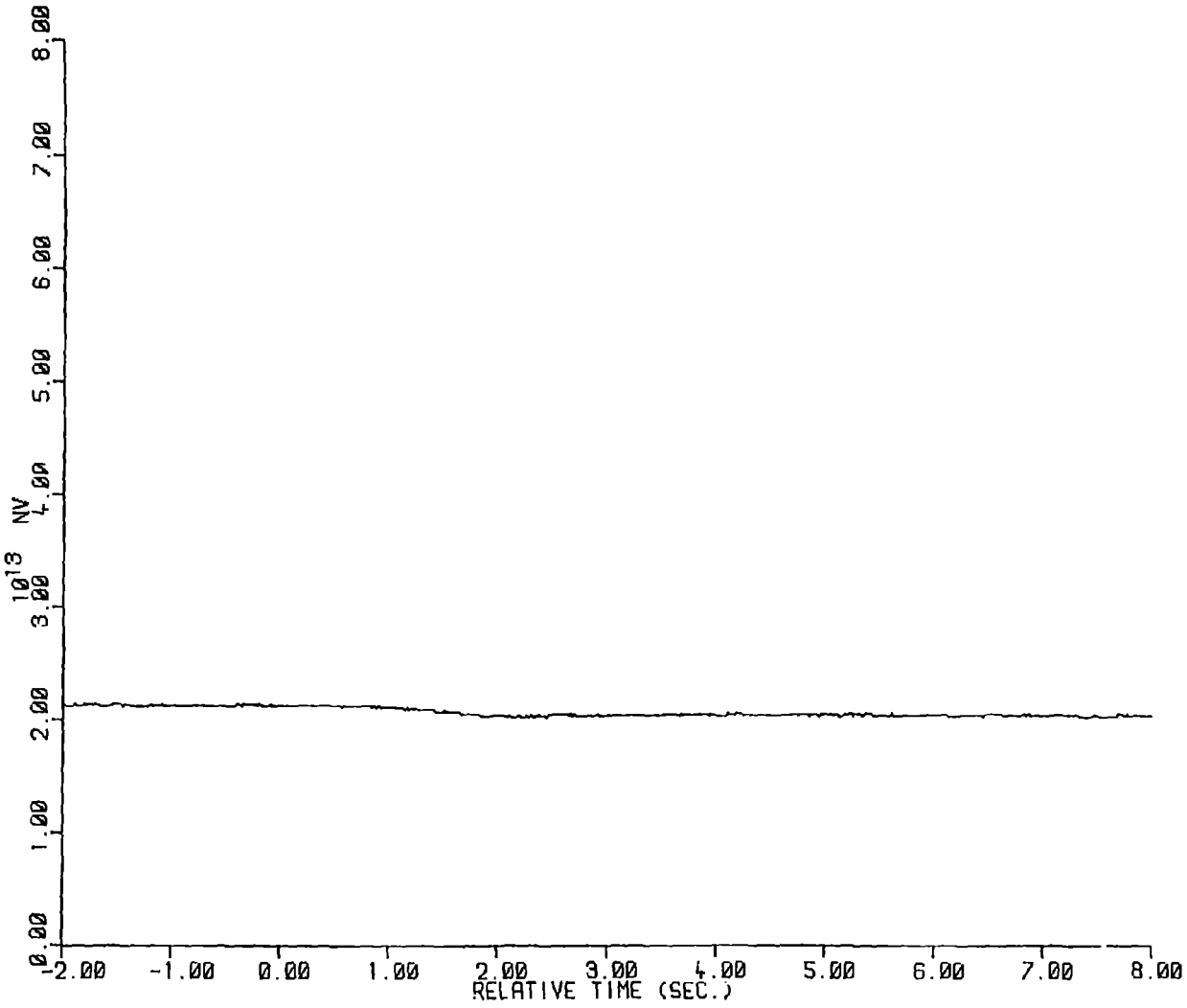

Figure 4-61. Compensated In-Core Flux - Part-Length CEA Drop - SPND A6 Level 2

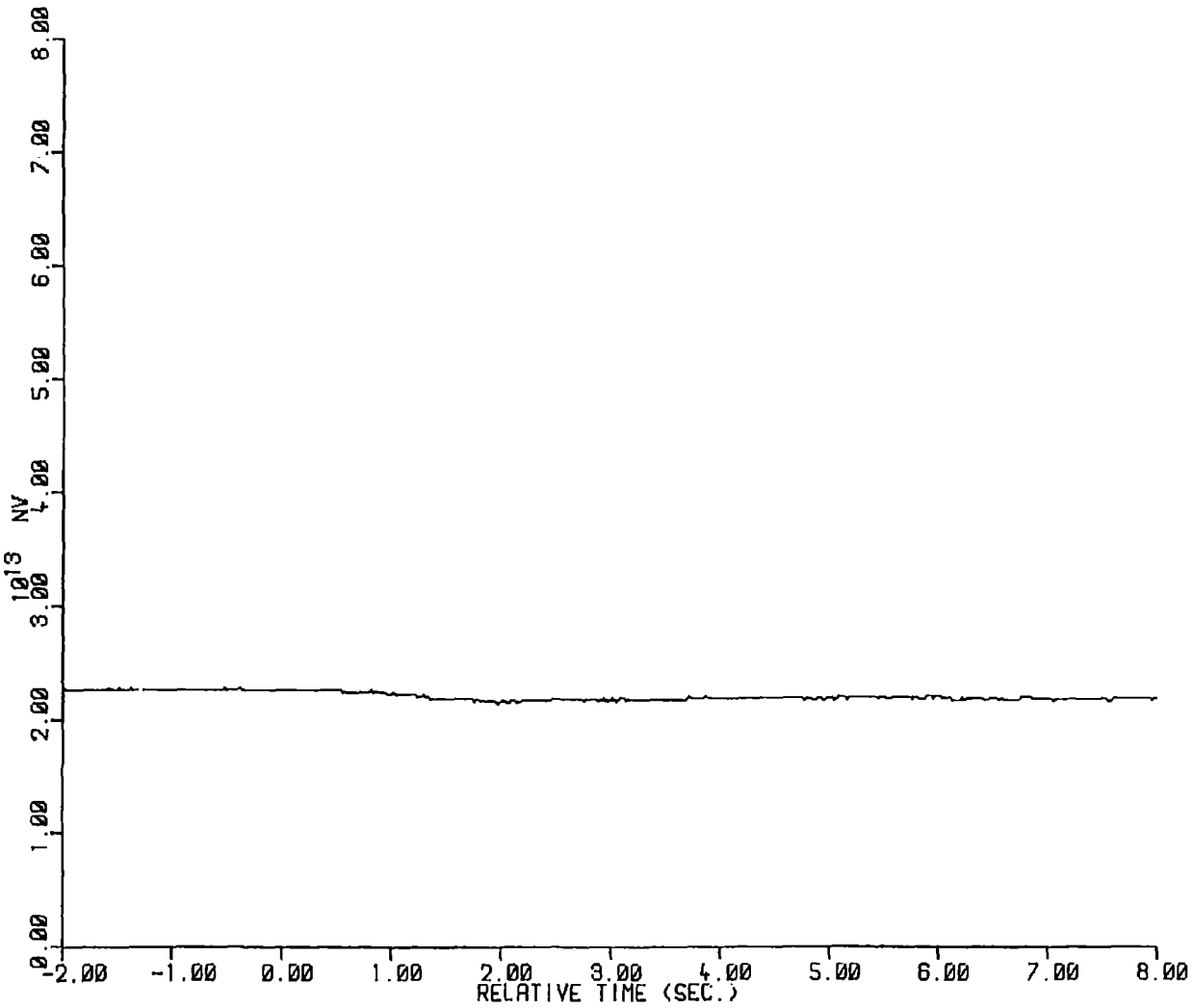

Figure 4-62. Compensated In-Core Flux - Part-Length CEA Drop - SPND A6 Level 4

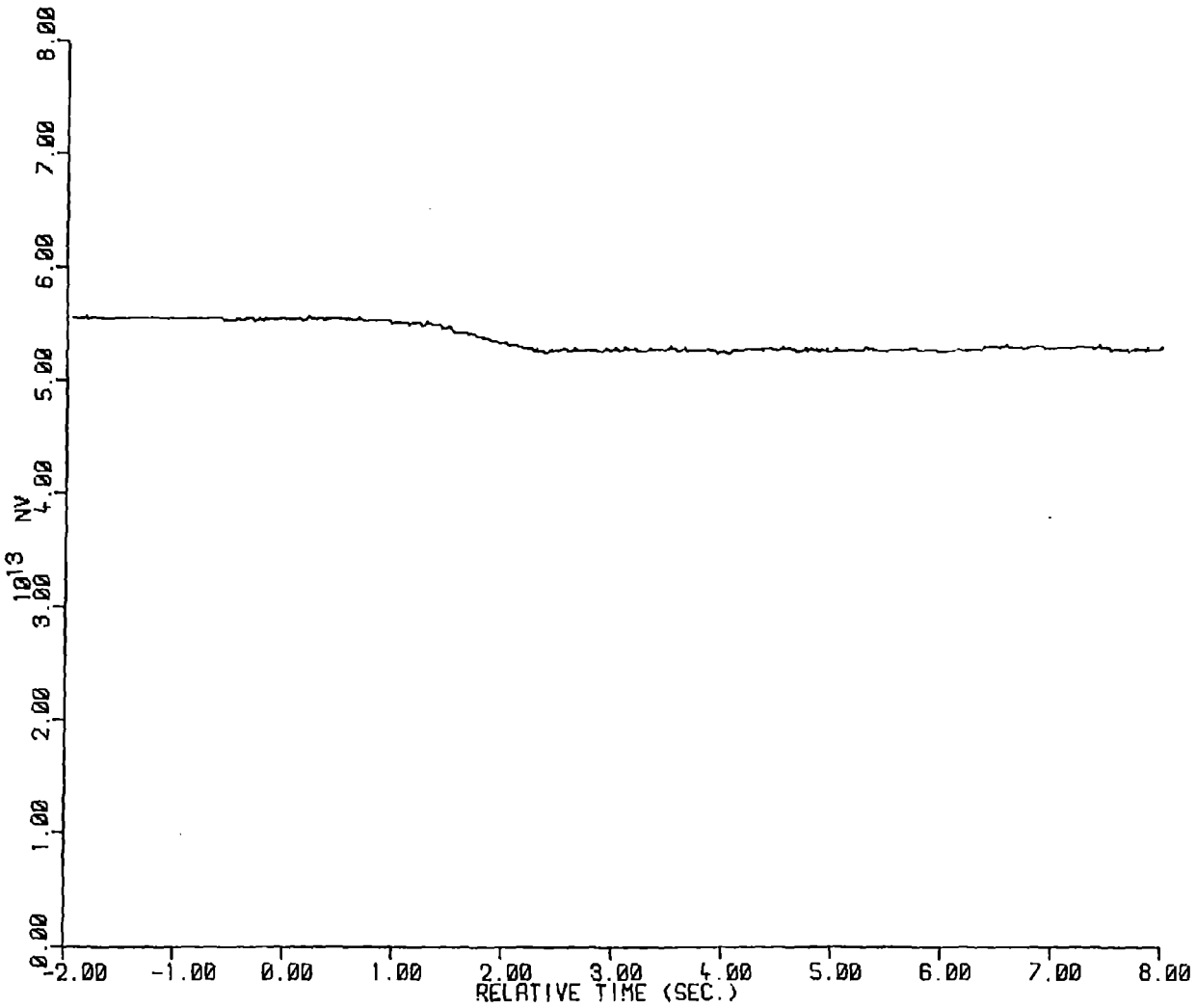

Figure 4-63. Compensated In-Core Flux - Part-Length CEA Drop - SPND G8 Level 2

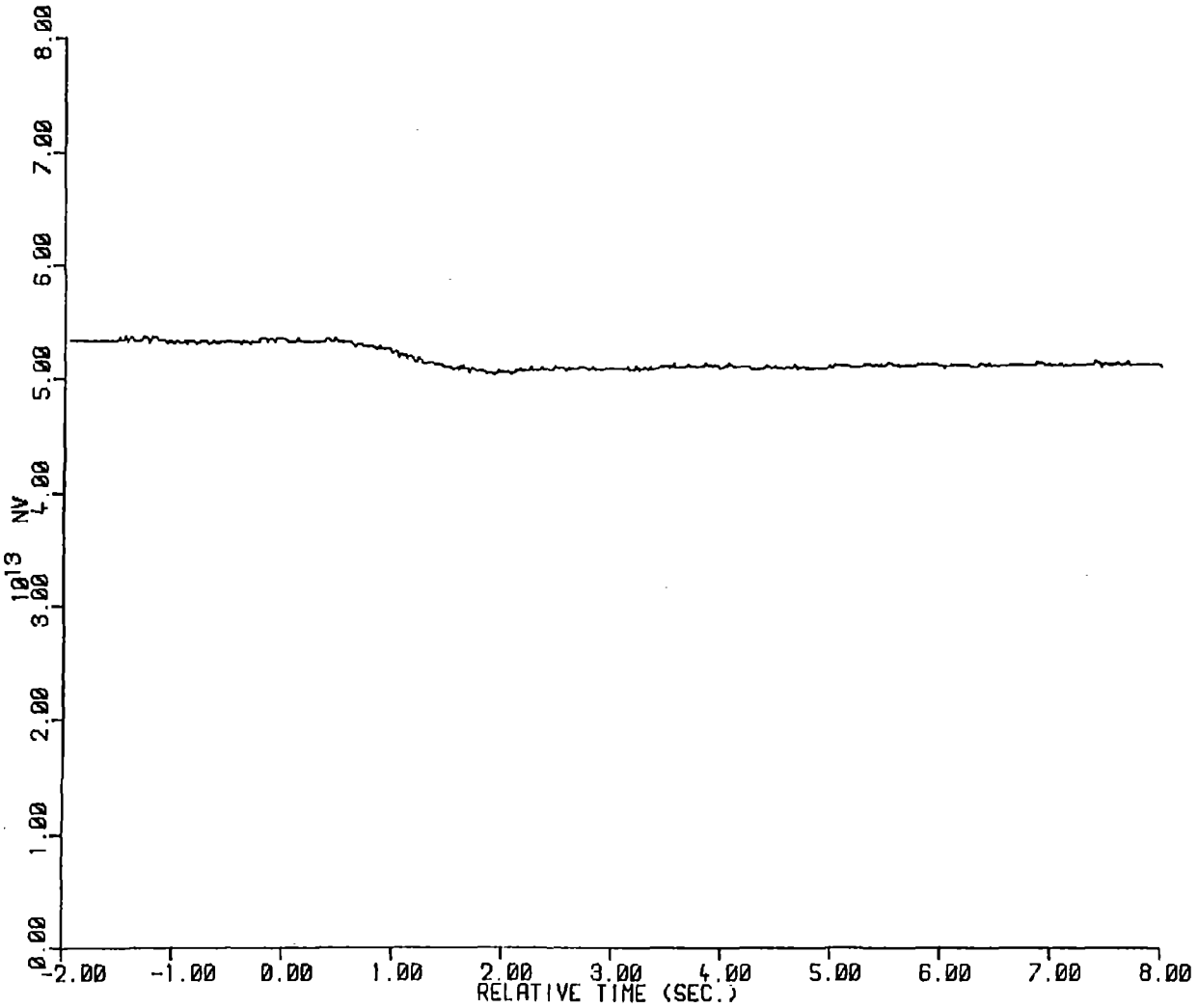

Figure 4-64. Compensated In-Core Flux - Part-Length CEA Drop - SPND G8 Level 4

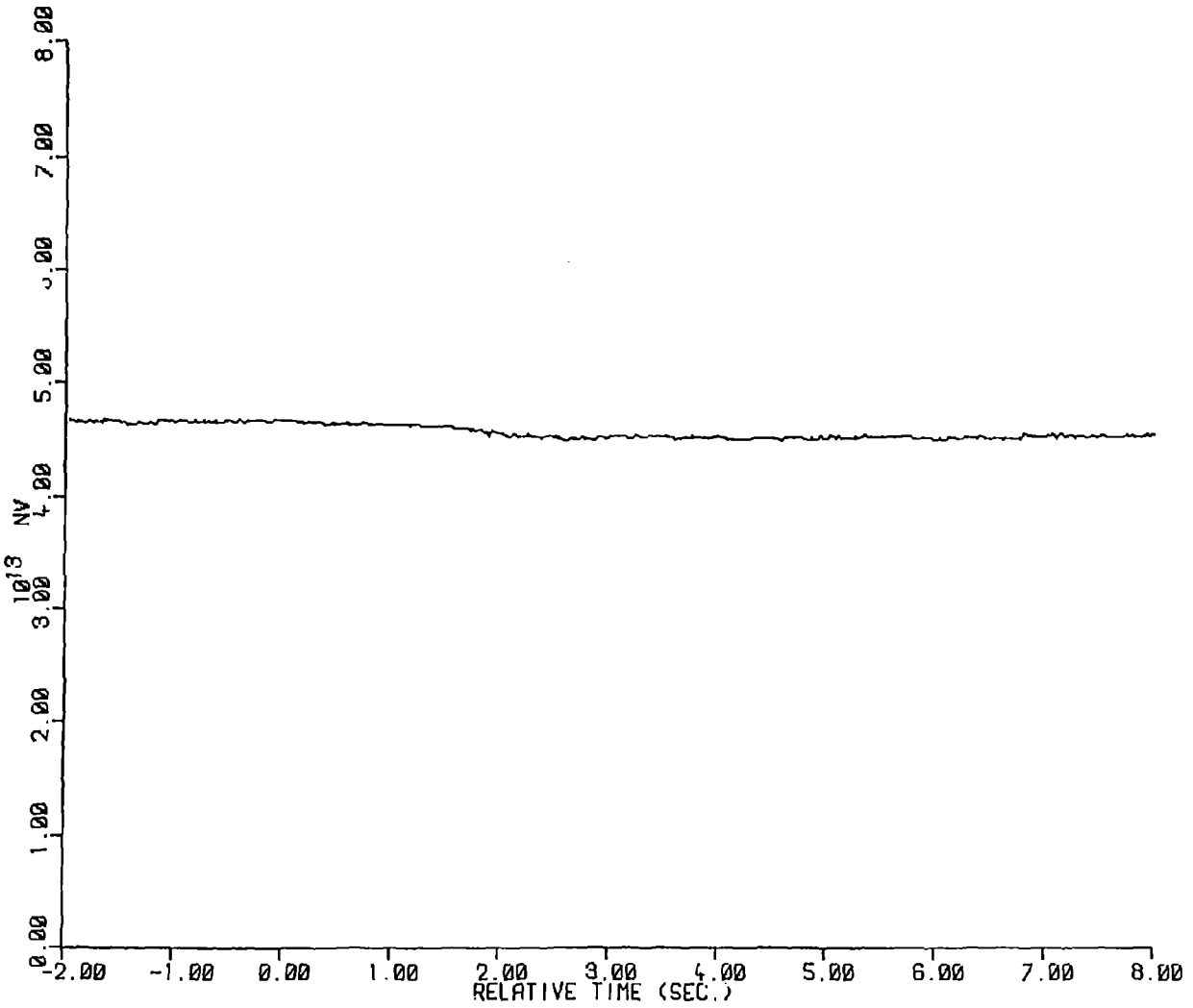

Figure 4-65. Compensated In-Core Flux - Part-Length CEA Drop - SPND N10 Level 2

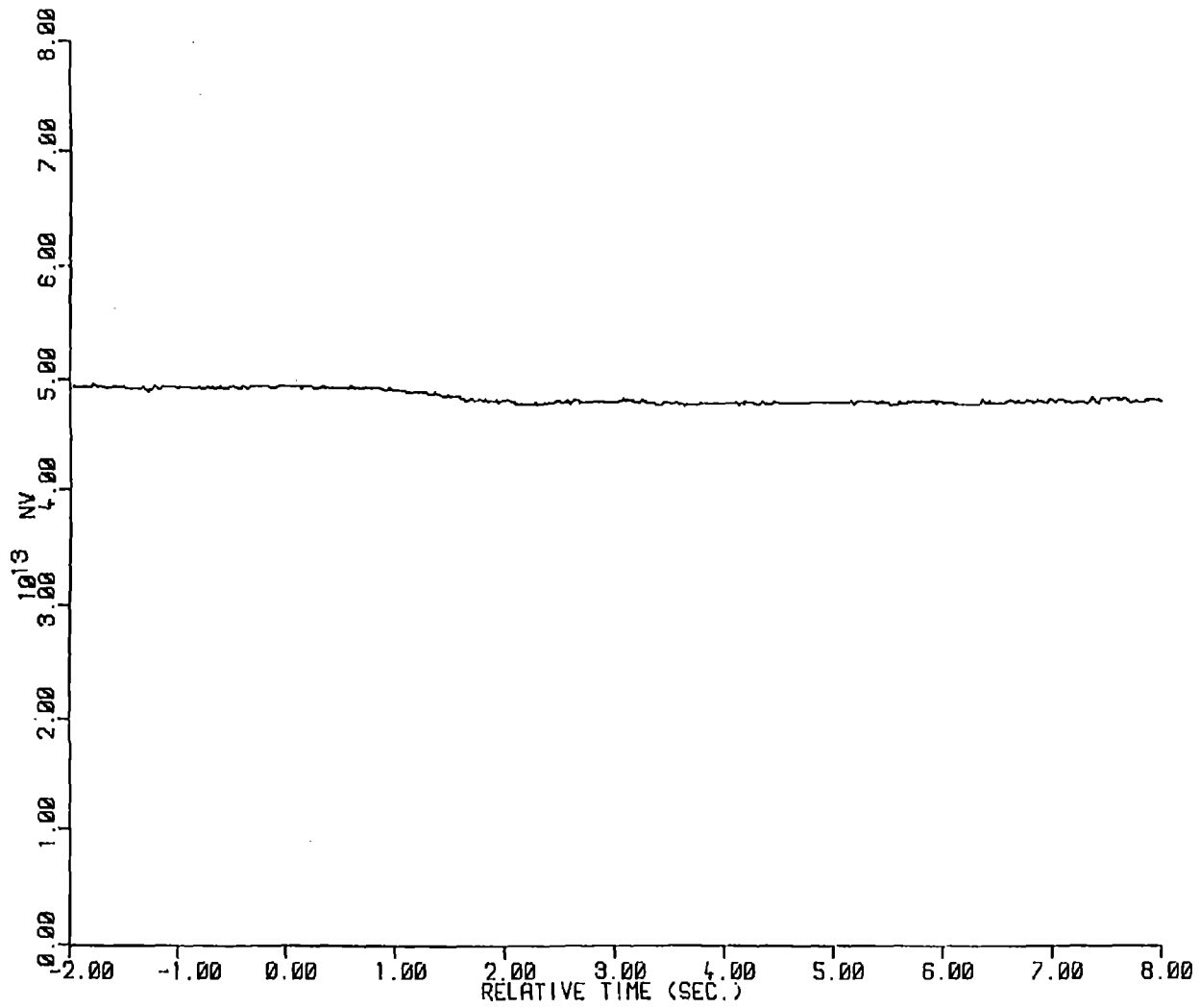

Figure 4-66. Compensated In-Core Flux - Part-Length CEA Drop - SPND N10 Level 3

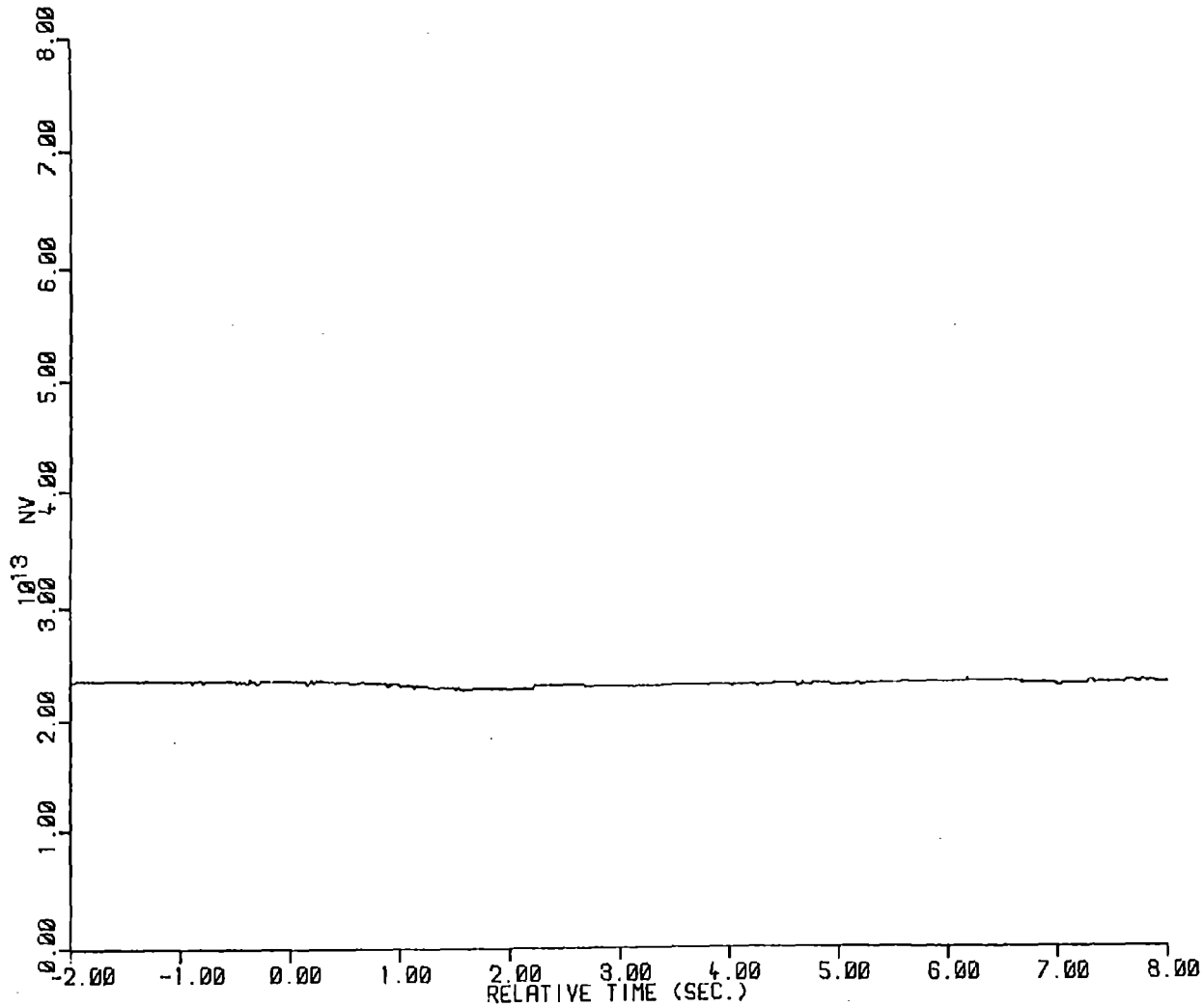

Figure 4-67. Compensated In-Core Flux - Part-Length CEA Drop - SPND C12 Level 5

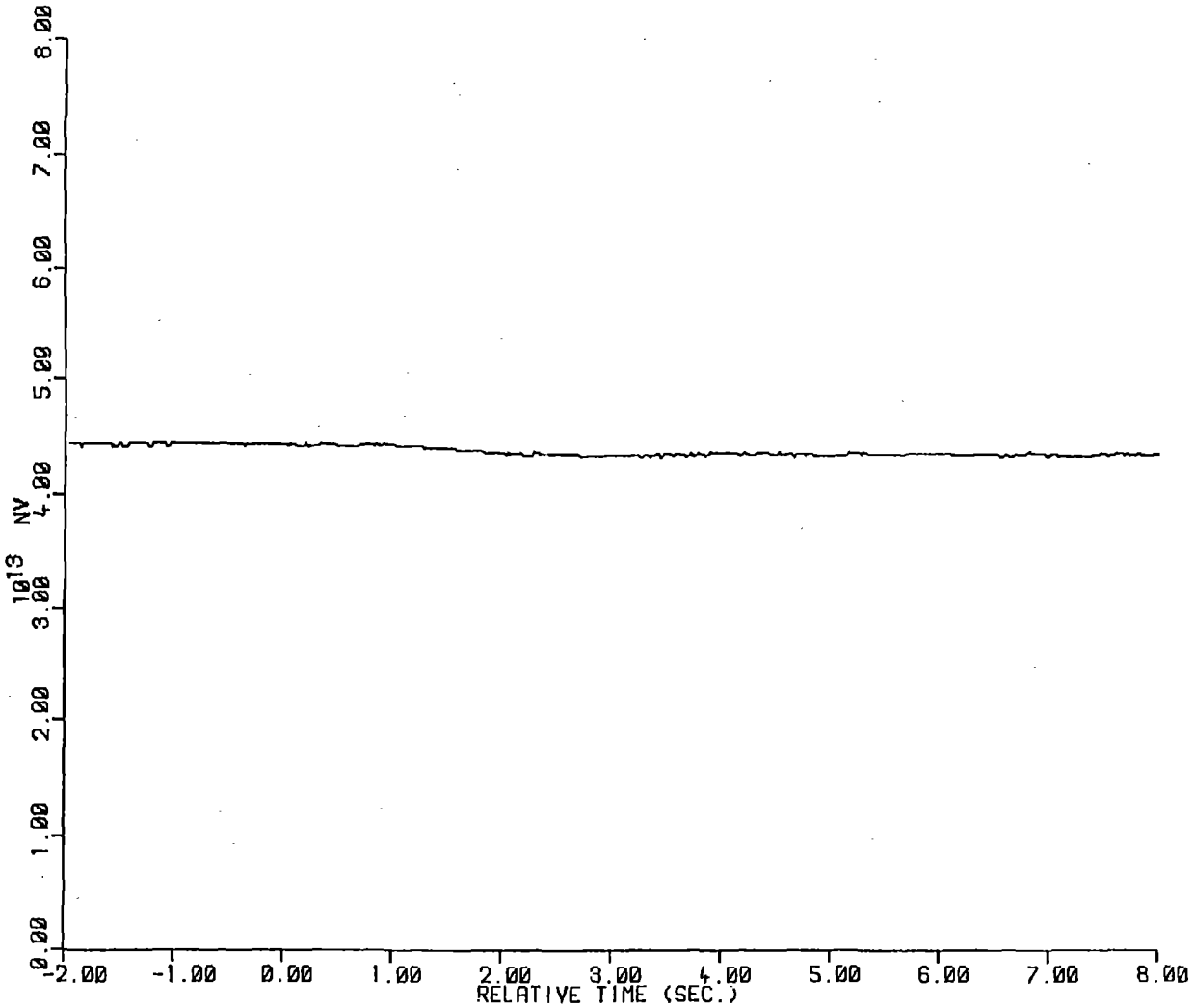

Figure 4-68. Compensated In-Core Flux - Part-Length CEA Drop - SPND G14 Level 2

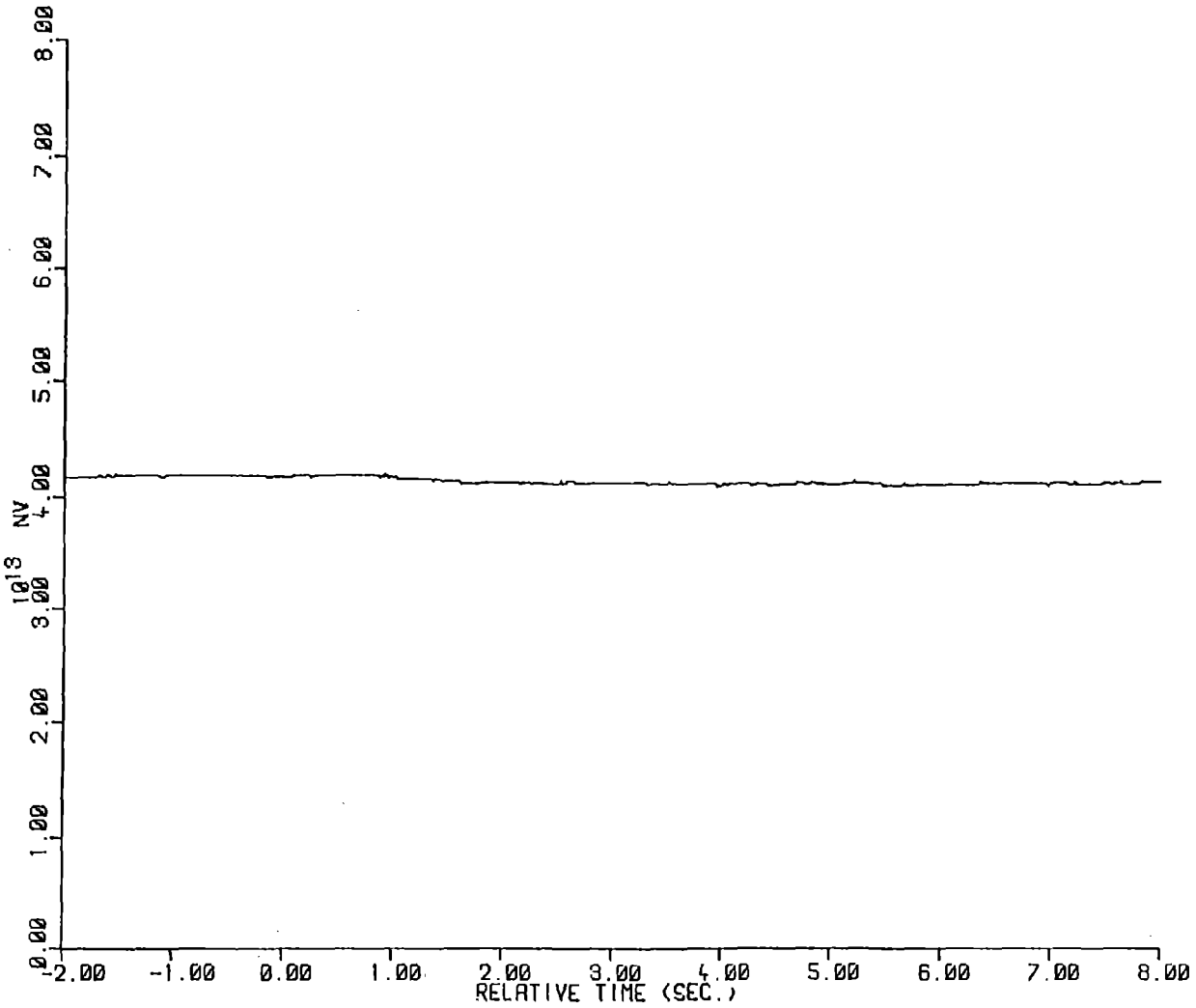

Figure 4-69. Compensated In-Core Flux - Part-Length CEA Drop - SPND G14 Level 4

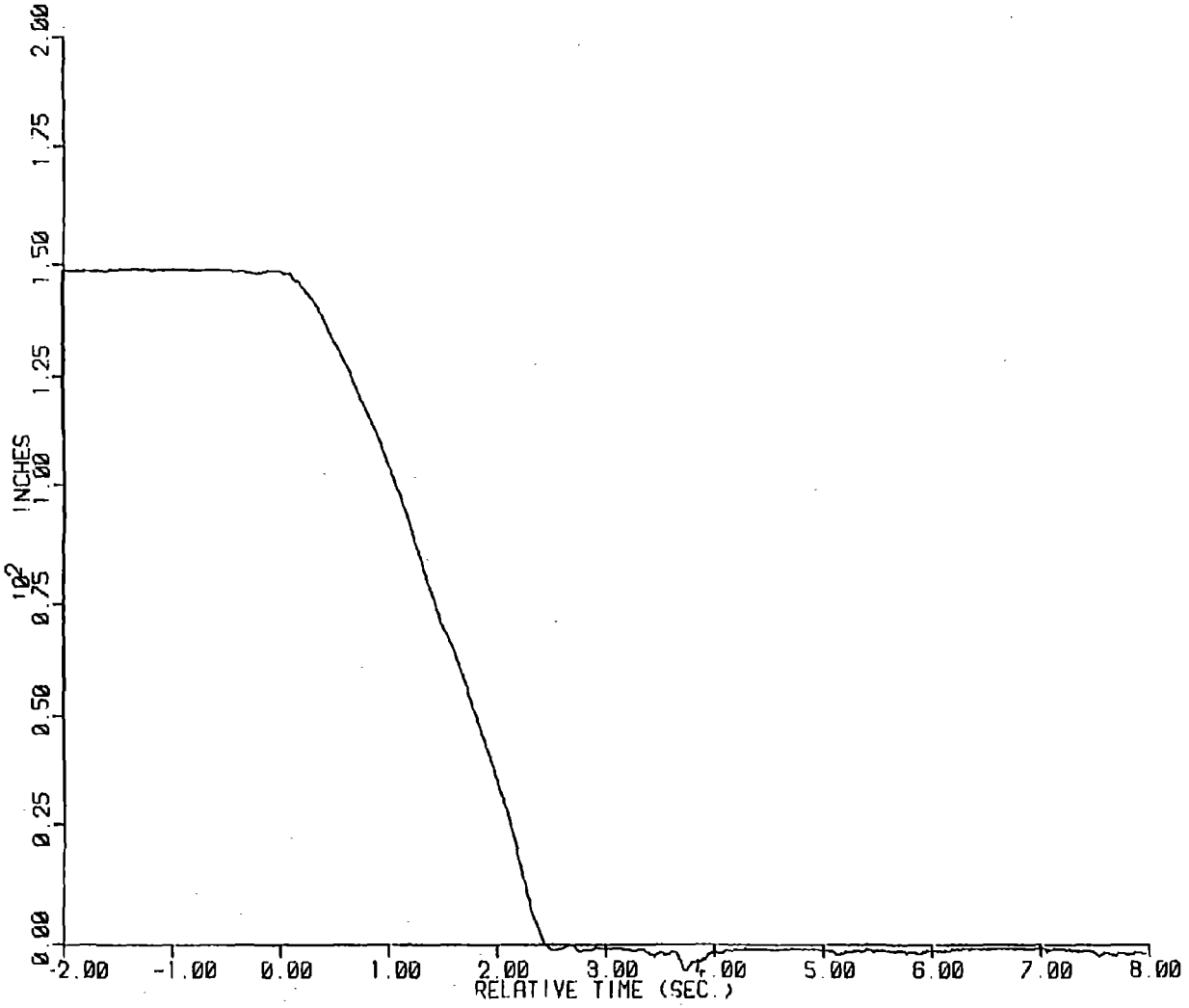

Figure 4-70. CEA Position - Part-Length CEA Drop - CEA P-24

Section 5

EXPERIMENTAL UNCERTAINTIES

The discussion given in Section 2 demonstrates that the largest source of measurement uncertainty in the neutron flux transients arises from uncertainty in the magnitude of the prompt component of the rhodium detector signal. Analysis of data taken at ANO-2 yields a best-estimate for the prompt component of the rhodium detector signals recorded during the reactor transient tests of 6.5 ± 0.5 percent (see Appendix). This translates into a total transient measurement error for the neutron flux data presented in this report of ± 5.6 percent (of the initial local flux*).

It should be pointed out that the transient measurement error quoted above includes only the experimental uncertainties discussed in Section 2 and the Appendix. It is possible that additional errors not accounted for in the above may also be present. In order to perform a comprehensive and rigorous evaluation of the uncertainty in the transient neutron flux measurements, further analyses of detector signal dynamics and detector signal processing beyond the scope of this report are required.

---

*Steady-state neutron flux measurements are accurate to ±7 percent. The steady-state error is not included in the transient measurement error.

Section 6

CONCLUSIONS

The results of the reactor transient tests at ANO-2 provide an important addition to the data base of the electric power industry for qualifying space-time reactor kinetics simulation codes. The in-core detector data recorded at ANO-2 cover a set of typical but diverse reactor transients, thus allowing code qualification in a more comprehensive manner than was possible with previously available data.

Further, the results of the simulated detector response experiments and the recorded data demonstrate that dynamically-compensated rhodium detector signals can be used to discern small variations in the time-dependent behavior of the local neutron flux. Thus, it is feasible to use rhodium self-powered neutron detectors to obtain data which may be used in the qualification of space-time core models. Although the present uncertainties in the neutron flux transients calculated from rhodium detector signals are somewhat larger than those typically desired for code qualification, the uncertainties are not so large as to preclude meaningful comparison with calculations made using space-time neutronics codes. The uncertainty in the neutron flux transient as derived from measured rhodium detector signals is determined for the most part by uncertainty in the prompt component of the rhodium detector response. Therefore, further studies, which are needed to increase the understanding of the rhodium detector response, would permit the reduction of uncertainty in the neutron flux transient to levels more compatible with those typically desired for code qualification.

In summary, the neutron flux transient data presented here are sufficiently accurate that qualitative comparisons with space-time neutronics code calculations can be made. Further, when additional information regarding transient rhodium response characteristics become available, neutron flux transient data with lower uncertainties can be generated, thus allowing more precise comparisons with calculations.

Section 7

REFERENCES

1. P. A. Gagne, ANO-2 NSS Design and Cycle One Operating History Data, EPRI NP-1707, Electric Power Research Institute, March, 1981.

2. D. P. Siska, NSSS Transient Tests at ANO-2, EPRI NP-1708, Electric Power Research Institute, May, 1981.

3. R. W. Bowring, J. W. Stewart, R. A. Shober and R. A. Sims, MEKIN: MIT-EPRI Nuclear Reactor Core Kinetics Code, Electric Power Research Institute, September, 1975.

4. P. E. Rohan, S. G. Wagner and S. E. Ritterbusch, HERMITE: A Multi-Dimensional Space - Time Kinetics Code for PWR Transients, Combustion Engineering, Inc., March, 1976.

5. A. Endler, K. Bohme and H. Stein, "Investigation of Signal Composition of SPND", IAEA-SM-226 (1978).

6. H. D. Warren and N. H. Sha, "Neutron and Gamma-Ray Effects on Self-Powered In-Core Radiation Detectors", Nuclear Science and Engineering 45, 395 (1974).

APPENDIX

IN-CORE NEUTRON DETECTORS

DETECTOR PHYSICS

The signal-producing mechanism of rhodium self-powered neutron detectors is governed by neutron-beta reactions within the rhodium emitter. Figure A-1 depicts the typical neutron capture reactions in rhodium. Note that there are two typical decay paths -- a 4.4 minute half-life rhodium isotope and a 42 second half-life rhodium isotope. The 42 second isotope predominates the reaction, contributing approximately 92 percent of the (n, β) signal. The remaining 8 percent of the (n, β) signal results from decay of the 4.4 minute isotope.

In addition to the signal generated from (n, β) reactions, a small but significant portion (approximately 6 percent) of the overall signal is generated by a (n, γ,e) reaction caused by capture gamma reactions in the rhodium emitter and external gamma flux reactions with the rhodium emitter and the detector sheath. The capture gamma and external gamma flux signals are prompt and provide useful prompt data.

In summary, the rhodium detector signal consists of three major time components, and only a small portion is prompt in nature. Figure A-2 shows a typical self-powered detector.

In order to utilize these detectors for fast transients such as a reactor scram or a dropped rod, compensation of the signal is required to reduce the lag time in the signal. Fortunately, both the magnitude and proportion of the three major signal components are measurable, thus allowing development of a compensation algorithm which can be used to calculate the incident neutron flux transient in real time (referred to herein as the compensated signal).

The total signal also includes a signal generated by a multitude of reactions with the signal cable itself. The primary reactions are capture gamma reactions (n, γ, e) of the detector cable material. This signal is not related to the rhodium pseudo-point source; rather, it is a signal integrated over the entire length of the cable. The exact models of this signal are quite complex. The cable signal represents less than

A. $^{103}_{45}Rh + ^{1}_{0}n \longrightarrow ^{104}_{45}Rh \xrightarrow[T1/2 = 42s]{} ^{104}_{46}Pd + ^{0}_{-1}\beta$

B. $^{103}_{45}Rh + ^{1}_{0}n \longrightarrow ^{104m}_{45}Rh \xrightarrow[T1/2 = 4.4M]{} ^{104}_{45}Rh + \gamma$

$^{104}_{45}Rh \xrightarrow{T1/2 = 42s} ^{104}_{46}Pd + ^{0}_{-1}\beta$

C. PROMPT REACTIONS (~6% OF TOTAL SIGNAL)

1. (n, γ, e) INELASTIC NEUTRON SCATTERING WHICH PRODUCES γ RADIATION AND HENCE $^{0}_{-1}\beta$ VIA COMPTON AND PHOTO-ELECTRIC REACTIONS
2. EXTERNAL γ REACTIONS WITH Rh AND DETECTOR SHEATH

Figure A-1. Rhodium SPND Nuclear Reactions

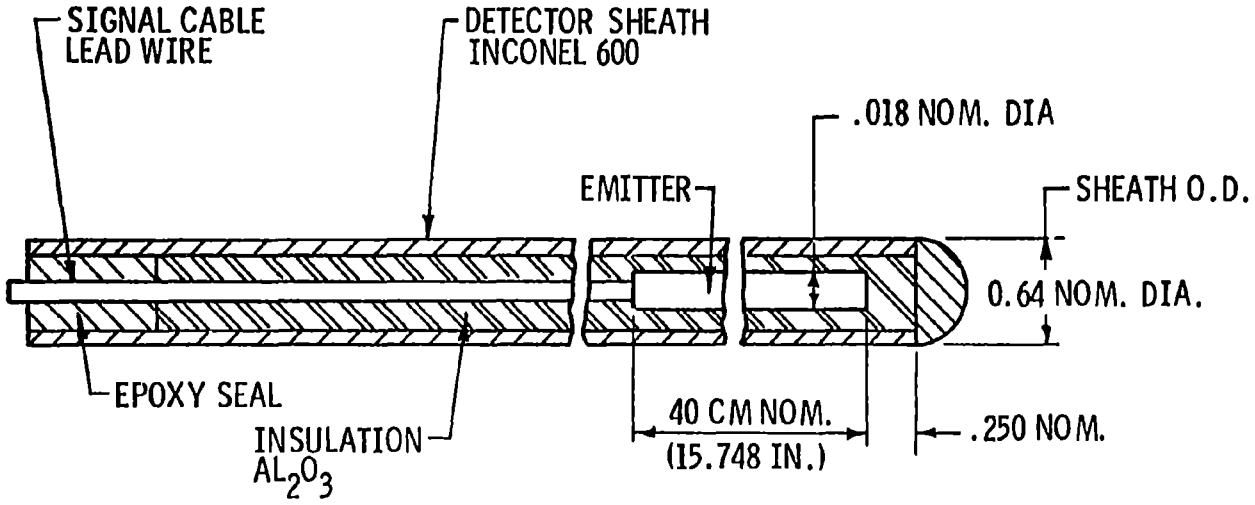

Figure A-2. Typical Self-Powered Neutron Detector Cross Section

3 percent of the overall detector signal; however, its effect on the dynamics of the overall signal can be significant. Techniques used to correct the total signal for cable-related reactions are discussed below.

DETECTOR SIGNAL CORRECTIONS AND DYNAMIC COMPENSATION

Raw in-core detector signal data require processing to derive the incident neutron flux transients, or compensated signals. This processing includes: subtraction of the background signal component, determination of the magnitude of the prompt signal component and dynamic compensation. The following sections discuss these processes in detail.

Background Correction Techniques

As described above, the total signal of the rhodium detector consists of a rhodium-related contribution and a cable-related contribution. The cable-related component is referred to as the "background" signal and must be accounted for in order to determine the true rhodium-related SPND response. Since the background signal is a function of the integrated flux over the cable length in the active core region, the background effect is greater for a level 1 detector (near the bottom of the core) than for a level 5 detector (near the top of the core). Although the steady-state background signal is small compared to the total SPND signal (on the order of 2 percent for a level 1 detector), it is important when dynamic flux changes are occurring. During fast neutron flux transients, the background signal (which is prompt) may be as large as 20 percent of the prompt response of the rhodium detectors. It is important, therefore to correct the SPND signal for background effects before dynamic compensation is performed.

The ANO-2 reactor has long and short background detectors at various radial locations in the core. The cable lengths of these detectors correspond to the level 1 and level 4 rhodium detectors, respectively. However, not all SPNDs have background detectors at the corresponding radial location. Therefore, both radial and axial correction methodologies must be developed to infer the background contribution to the total SPND signal at in-core detector locations where background signals are not available. The techniques used to correct the in-core rhodium detector signals for background in each of the three transient tests are detailed below.

Loss of Flow - For those detectors in the loss of flow for which a background signal is available at the same radial and axial location as the SPND, the background signal

can be subtracted directly from the SPND signal. For detectors at the same axial level as an available background detector but a different radial location, a known background signal is first multiplied by a Radial Correction Factor (RCF) before the subtraction is performed. The RCF is the ratio of the integrated flux for the appropriate axial level at the desired radial position to the corresponding quantity at the known radial position:

$$RCF(r_2 \rightarrow r_1)_{z_o} = \frac{\int_{z_o}^{150} \phi(r_1,z)\, dz}{\int_{z_o}^{150} \phi(r_2,z)\, dz} , \qquad (A\text{-}1)$$

where

r_1 = radial position of the unknown background signal ,
r_2 = radial location of known background signal ,
z_o = axial position of background signal ,
ϕ (r,z) = background-corrected flux at radial position r and axial position z.

The integrated flux at each radial and axial position is estimated using a 5-node axial flux distribution from plant computer data. Each flux value is weighted by the length of cable of a background detector in each node for the appropriate axial level. (Thus, the RCF depends on axial as well as radial position).

For detectors at axial levels other than those for which there is a background signal, the background contribution is inferred from the long background signals. A long (level 1) background signal is converted to a level 2, 3 or 5 background signal (level 4 corresponds to the short background) by first deleting from the signal a period of time corresponding to the time required for the CEAs to travel to level 1 from level 2, 3 or 5, respectively. The remaining portions of the signal before and after the deleted segment are then joined together by moving the "after portion" backward in time and decreasing the amplitude of the "before portion". A schematic diagram of this "axial correction" procedure is shown in Figure A-3. (Note that as a result of the "axial correction", the background signal for the loss of flow at any axial level is zero after the CEAs have passed that level). For detectors at the same radial location as an available background signal, the "axial-corrected" background signal is subtracted directly from the corresponding SPND signal. For detectors at radial positions where no background signal is available, an "axial-corrected" background

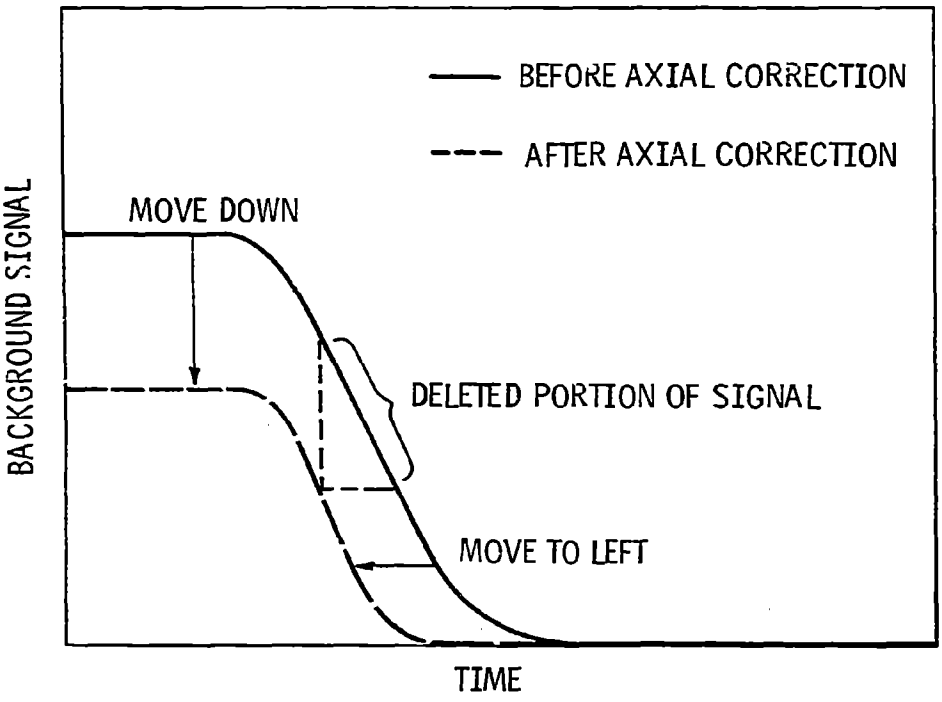

Figure A-3. Schematic of Axial Correction Procedure For Loss of Flow Background Signals

signal at another radial position is first multiplied by the corresponding RCF before the subtraction is performed.

In summary, then, the loss of flow data is corrected for background as follows:

Detector at radial position with background signal:

$$\phi(r_2,z_0) = f(S_D(r_2,z_0) - S_B(r_2,z_0)) \; ; \qquad \text{(A-2)}$$

Detector at radial position without background signal:

$$S_B(r_1,z_0) = S_B(r_2,z_0) \times RCF(r_2 \rightarrow r_1)_{z0} \; , \qquad \text{(A-3a)}$$

$$\phi(r_1,z_0) = f(S_D(r_1,z_0) - S_B(r_1, z_0)). \qquad \text{(A-3b)}$$

Here f( ) represents the dynamic compensation process and

$S_D(r,z)$ = rhodium in-core detector signal at radial position r and axial position z.

$S_B(r,z)$ = background detector signal at radial position r and axial position z.

Full-Length and Part-Length CEA Drops - Unlike the case for the loss of flow, the in-core flux for the full-length and part-length CEA drops does not go to zero when the CEA has dropped completely. Furthermore, since only a single CEA is dropped, the flux behavior near the dropped CEA is significantly different from the flux behavior far away from the dropped CEA. The background correction techniques for the CEA drops are therefore different than those for the loss of flow.

For those detectors in the full-length and part-length CEA drops for which a background signal is available at the same radial and axial location as the SPND, the background signal can be subtracted directly from the SNPD signal, as in the loss of flow case. For detectors at the same radial location as an available background signal but a different axial level, the long background signal can be "axially corrected", in a fashion similar to that shown in Figure A-3, to infer the background signal at levels 2, 3 and 5. However, since the background signal is not zero after the CEA has passed the appropriate axial level, an alternative method must be used to determine the correct background signal amplitude before subtraction from the SPND signal is performed. For levels 2 and 3, the background signal amplitude is cal-

culated by linear interpolating between the measured post-drop background signal values from the level 1 and level 4 background detectors, as shown in Figure A-4. For level 5, the background signal amplitude is sufficiently small (less than 0.1 percent of the SPND signal) that it can be neglected.

For detectors far away (more than several assemblies) from the dropped CEA and at a radial position with no background signal available, the background contribution is assumed to a constant fraction of the total detector signal. (Far away from the dropped CEA the flux does not change very much in time and the dynamic behavior of the background contribution is not very significant). For level 5, the background signal is less than 0.1 percent of the SPND signal, and is neglected. For levels 1, 2, 3 and 4, the SPND signal is corrected for background by multiplying the calibration factor used to convert the SPND signal voltage to flux units by 1 - MBF (measured background factor):

$$\phi(r_1,z_o) = f(S_D(r_1,z_o) \times (1 - MBF)) \ . \qquad (A\text{-}4)$$

The MBF is the background contribution to the total SPND signal at the appropriate radial and axial position prior to the CEA drop, and is calculated by comparing the voltage changes in the background and rhodium in-core detector signals during the loss of flow:

$$MBF = \frac{\text{Change in background signal voltage}}{\text{Change in SPND signal voltage}} \ . \qquad (A\text{-}5)$$

For detectors close to the dropped CEA, the dynamic behavior of the background contribution is important, and, at a radial position with no background signals available, more sophisticated background correction techniques must be applied. First, the changes in the long and short background signals at the desired radial position during the CEA drop are inferred by scaling the changes in measured long and short background signals at a neighboring radial position. The scaling factor is the ratio of the change in the uncorrected SPND signal due to the CEA drop at the desired radial position to the change in the uncorrected SPND signal due to the CEA drop at the neighboring radial position:

$$S_B(r_1,z_0)_{\text{pre-drop}} - S_B(r_1,z_0)_{\text{post-drop}}$$

$$= [S_B(r_2,z_0)_{\text{pre-drop}} - S_B(r_2,z_0)_{\text{post-drop}}] \times SF, \qquad (A\text{-}6)$$

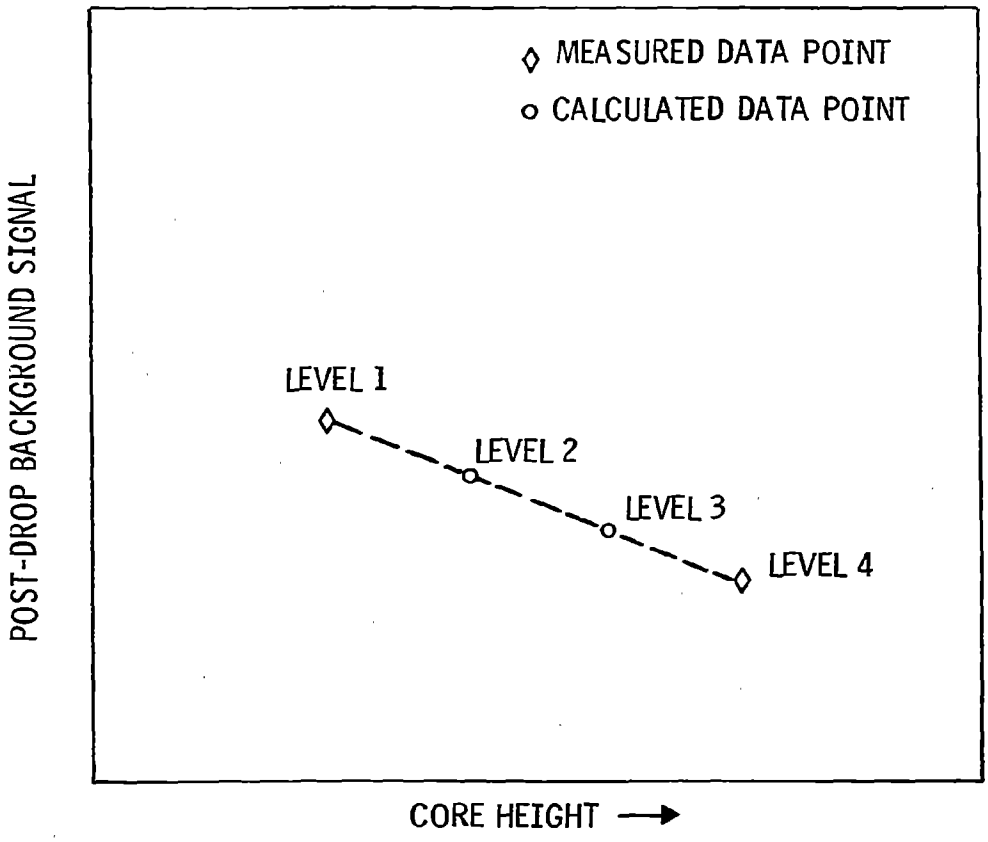

Figure A-4. Schematic of Amplitude Determination for CEA Drop Background Signals (Levels 2 and 3)

where

$$SF = \frac{S_D(r_1,z_0)_{\text{pre-drop}} - S_D(r_1,z_0)_{\text{post-drop}}}{S_D(r_2,z_0)_{\text{pre-drop}} - S_D(r_2,z_0)_{\text{post-drop}}} \quad . \tag{A-7}$$

Second, the amplitudes of the generated background signals are adjusted so that either the pre- or post-drop signal values are equal to the product of the pre- or post-drop values of the corresponding measured background signals and the appropriate radial correction factors:

$$S_B(r_1,z_o)_{\text{pre-drop (post-drop)}} = S_B(r_2,z_o)_{\text{pre-drop (post-drop)}} \times RCF(r_2 \div r_1)_{z_0} \quad . \tag{A-8}$$

Finally, having generated long and short background signals for the desired radial position, the background correction procedure can be carried out as for the case when measured background signals are available. For levels 1 and 4, respectively, the generated long and short background signals are subtracted directly from the corresponding SPND signals. For levels 2 and 3, the generated long background signal is axially corrected, as described above, before the subtraction is performed. For level 5, the background signal, being less than 0.1 percent of the SPND signal, is neglected.

Dynamic Compensation

As discussed previously, the rhodium detector signal consists of three major time components: (1) neutron-beta reactions characterized by a 42 second half-life, (2) neutron-beta reactions characterized by a 4.4 minute half-life and (3) prompt reactions. Accordingly, the detector step response is modeled as follows:

$$DSR(t) = p + (1 - p)\left[1 - (1 - C_1)\, e^{-t/\tau_1} - C_2\, e^{-t/\tau_2}\right] , \tag{A-9}$$

where

DSR = time-dependent detector response to a unit step increase in neutron flux,
p = fraction of detector output that is prompt (prompt component) ,
C_n = constant related to sensitivity ,
τ_n = nth decay time constant ,
t = time since activation.

The detector dynamic model yields an equation in the s domain of the form

$$\frac{\text{Detector Output}}{\text{Detector Input}} = H(s) = p + \frac{q}{\tau_1 s+1} + \frac{r}{(\tau_1 s+1)\ (\tau_2 s+1)}, \qquad \text{(A-10)}$$

where

$H(s)$ = detector transfer function
p = prompt component ,
q = component with single beta decay ,
r = component with two-stage decay ,
τ_1 = half-life of first component ,
τ_2 = half-life of second component .

The Laplace transform of the detector response to a unit step increase in neutron flux is then given by

$$H(s)\ \frac{1}{s} = \frac{p}{s} + \frac{q}{s(\tau_1 s+1)} + \frac{r}{s(\tau_1 s+1)\ (\tau_2 s+1)} \ . \qquad \text{(A-11)}$$

Simplifying and collecting terms yields

$$H(s)\ \frac{1}{s} = \frac{p}{s} + (1-p)\left[\frac{1}{s} - \frac{\tau_1 - \frac{r}{1-p}\ \frac{\tau_1\ \tau_2}{\tau_2 - \tau_1}}{(\tau_1 s+1)} - \frac{\frac{r}{1-p}\ \frac{\tau_2^{\,2}}{\tau_2 - \tau_1}}{(\tau_2 s+1)}\right]. \qquad \text{(A-12)}$$

The step response in the time domain is then the inverse Laplace transform of $H(s)\ \frac{1}{s}$. Hence,

$$DSR(t) = p + (1-p)\left[1 - \left(1 - \frac{r}{1-p}\ \frac{\tau_2}{\tau_2 - \tau_1}\right)\ e^{-t/\tau_1} - \left(\frac{r}{1-p}\ \frac{\tau_2}{\tau_2 - \tau_1}\right)\ e^{-t/\tau_2}\right]. \qquad \text{(A-13)}$$

This yields the exact form of the rhodium detector step response equation, and verifies that the detector model matches the observed detector step response.

The rhodium detector signal is digitally filtered to compensate for the detector dynamic response. This filter reconstructs the incident neutron flux transient by using the detector inverse transfer function. The filter is developed as shown below:

$$\frac{\text{Compensated Output}}{\text{Detector Output}} = G(s) = \frac{\text{Detector Input}}{\text{Detector Output}}$$

$$= \frac{1}{H(s)}$$

$$= \frac{1}{p + \frac{q}{\tau_1 s+1} + \frac{r}{(\tau_2 s+1)(\tau_1 s+1)}}$$

$$= \frac{s^2(\tau_1 \tau_2) + s(\tau_1 + \tau_2) + 1}{s^2(p\tau_1 \tau_2) + s(p\tau_1 + p\tau_2 + q\tau_2) + 1} \qquad \text{(A-14)}$$

The compensated output can then be represented by a backwards difference equation as follows:

$$CS(t) = J_1 \cdot CS(t-T) + J_2 \cdot CS(t-2T) + J_3 \cdot S(t) \qquad \text{(A-15)}$$

$$+ J_4 \cdot S(t-T) + J_5 \cdot S(t-2T) ,$$

where

CS(t)	= current compensated output ,
CS(t-T)	= first past value of compensated output ,
CS(t-2T)	= second past value of compensated output ,
S(T)	= current raw detector signal ,
S(t-T)	= first past value of raw detector signal ,
S(t-2T)	= second past value of raw detector signal ,
J_1 through J_5	= digital filter coefficients .

The filter coefficients are calculated by an iterative procedure to optimize the algorithm's ability to reproduce theroretical input functions (ramps and step changes).

IMPLEMENTATION OF COMPENSATION ALGORITHM

The digital in-core compensation algorithm discussed previously was implemented on a PDP-11/15 minicomputer system. The system is comprised of a 12-bit analog-to-digital converter, disk operating system and a FORTRAN compiler. Data recorded n a 14-track analog magnetic tape was reproduced, digitized by the computer system and stored on disk as discrete numerical sequences. The stored data was then processed by a FORTRAN program. The processing included the following steps:

- Conversion of 12-bit integers to floating point values expressed in units of neutron flux.

- Implementation of background detector corrections.

- Digital low-pass filtering.

- Processing by the in-core dynamic compensation algorithm.

- Output of reduced data to a digital incremental plotter as graphic time histories.

The entire process of the in-core detector, record/reproduce system and computer was treated as a sampled data system. As such, great attention was given to the dynamic characteristics of this process. Examination of test reactor and other PWR reactor in-core data revealed the need for a compensated SPND signal with a bandwidth of approximately 10 Hz. To achieve this and still obtain stable and relatively noise-free signals, low-pass filtering was implemented at several stages of the process.

A 4-pole Bessel filter with poles at about 10 Hz was used prior to tape recording to reduce 60 Hz powerline noise and permit full use of the dynamic range of the recording system. A Bessel filter was chosen to obtain optimum time-domain transient response.

A 4-pole RC filter with poles at 20 Hz was used between the taped data reproducer and the analog-to-digital converter. This anti-aliasing filter helped further reduce 60 Hz noise as well as noise products introduced by the tape recording system.

A 4-pole digital filter was introduced in the computer processing to reduce quantization noise in the compensated SPND signal. The filter has a recursive design patterned after a 10 Hz low-pass Bessel filter. Introduction of this filter is required for compensated SPND signal processing when the sampling rate is increased much above one sample per second. Normally, quantization noise is only a function of the resolution of the analog-to-digital converter (ADC). In this case the 12-bit analog to digital conversion has a signal to noise ratio (S/N) of about 1000. Increasing the sampling rate does not in itself change the S/N ratio. However, the compensation algorithm is a derivative rather than integral process. Therefore, it amplifies signal content more as frequency increases. Even though the S/N of the uncompensated signal stayed at 1000 as the sampling rate was increased, the compensated SPND signal noise would be greatly amplified without the use of a digital low-pass filter.

The compensation algorithm required implementation as a double precision operation to maintain acceptable accuracy and stability. On the PDP-11/15 this provides floating point numbers with a mantissa of 48 bits resolution.

DETERMINATION OF PROMPT COMPONENT

Previous experimental and calculational results show the prompt component of the rhodium self-powered neutron detector (SPND) signal to be 6 ± 2 percent of the total rhodium-related signal. This rather wide range of values is due to the fact that the magnitude of the prompt component is dependent on the flux environment in which the rhodium SPND is located. In particular, the magnitude of the prompt component is significantly influenced by the relative contribution of thermal and epithermal neutrons to the total neutron flux -- the larger the contribution of epithermal neutrons, the greater the value of the prompt component. (Therefore, the prompt component for a rhodium SPND located in a PWR will be larger than the prompt component for the same detector located in a test reactor). In addition, the neutron-to-gamma flux ratio can have a small but non-negligible effect on the magnitude of the prompt component.

The prompt component of the rhodium SPND signals at ANO-2 was determined by applying the dynamic compensation algorithm to detector data from the loss of flow test. First, dynamic compensation was applied to various background-corrected detector signals recorded during the loss of flow using assumed values of the prompt component ranging from 5 to 8 percent. Those values of the prompt component resulting in background-corrected, compensated detector signal which overshot the final detector signal reactor within a few seconds of value trip were deemed to be too small. This procedure establishes a greatest lower bound on the value of the prompt component.

Unfortunately, no procedure was able to be devised to determine a least upper bound on the value of prompt component from the recorded data. However, estimates of the prompt component could be made by comparing the initial rapid decrease of an uncompensated detector signal with the decrease in the corresponding compensated detector signal over the same time interval. This was done for a large number of detector locations, with emphasis focused on the upper level detectors (levels 4 and 5), where the initial rapid decrease is most clearly visible.

Based on the analyses described above, a best-estimate of 6.5 ± 0.5 percent for the prompt component was made. The error quoted includes the possibility that the prompt component may vary somewhat among the detectors (the analyses indicate that this indeed does occur) as well as the possibility that the prompt component of any detector may vary during the transient. These variations are due to changes in the neutron-

to-gamma flux which may occur (1) in different regions of the core and (2) during the transient. In addition, slight variations in the physical properties of the detectors may also be present. All data presented in this report have been compensated using a best-estimate value of 6.5 percent for the prompt component.